Jet Flow over Foredunes

Journal:	*Earth Surface Processes and Landforms*
Manuscript ID	ESP-15-0316.R2
Wiley - Manuscript type:	Paper
Date Submitted by the Author:	04-Feb-2016
Complete List of Authors:	Hesp, Patrick; Flinders University, Environment Smyth, Thomas; Flinders University, School of the Environment
Keywords:	jet, foredune, computational fluid dynamic model, flow dynamics

Jet Flow over Foredunes

Patrick A. Hesp and Thomas A.G. Smyth

Beach and Dune Systems (BEADS) Laboratory, School of the Environment,
Faculty of Science and Engineering, Flinders University, Bedford Park, South Australia 5042
Patrick.Hesp@flinders.edu.au; Thomas.Smyth@flinders.edu.au

Key Points

- Jet flow over a foredune is examined for a range of wind speeds/directions.
- Jets develop regardless of wind speed, best developed for perpendicular winds.
- Surface roughness affects jet development

Abstract

Jet flows, which are localized flows exhibiting a high speed maxima, are relatively common in nature, and in many devices. They have only been occasionally observed on dunes, and their dynamics are poorly known. This paper examines computational fluid dynamic (CFD) 2D modelling of jet flow over a foredune topography. Flow was simulated in 10° increments from onshore (0°) to highly oblique alongshore (70°) incident wind approach angles. CFD modelling reveals that the formation of a jet is not dependent on a critical wind speed, and an increase in incident wind velocity does not affect the magnitude of jet flow. A jet is first formed at ~1.0m seawards of the foredune crest on the Prince Edward Island foredune morphology example examined here. A jet is not developed when the incident wind is from an oblique approach angle greater than ~50° because there is significantly less flow acceleration across a much lower slope at this incident angle. The presence of a scarp does influence the structure of the crest jet, in that the jet is more pronounced where a scarp is present. Surface roughness affects the magnitude of jet expansion and jets are better developed on bare surfaces compared to vegetated ones.

Keywords: Foredune, jet, jet flow, computational fluid dynamics (CFD), flow dynamics; .

1. Introduction

Jet flows are relatively common in nature, and in many devices. A jet is a localized flow exhibiting a high-speed maxima according to Wei et al. (2013). The word comes from the French *jeter* and Latin *jactare* 'to throw', and by the 16th Century was used as a verb meaning 'to jut out' (http://www.oxforddictionaries.com/definition/english/jet), hence the observation that a jet has a well-defined 'nose' in the velocity profile (Wei et al., 2013; see e.g. http://www.eng.fsu.edu/~shih/succeed/jet/jet.htm). Jets may be formed where fluids are compressed and ejected from nozzles, pipes, taps, engines, exhausts (often as buoyant plumes) and similar objects or devices (Schlichting, 1955; Birkhoff and Zarontonello, 1957; Cala et al., 2006). One classic commonly cited example is the flow from a household tap. Jets are found, or occur in the atmosphere, for example, as low level jets during certain wind conditions (e.g. Kraus et al., 1985; Brook, 1985), as coastal phenomena associated with temperature gradients (e.g. Parish, 2000), in wakes behind bluff bodies (Bickley, 1939; Mattingly and Criminale, 1972), in various marine animals such as sponges and mollusks (Vogel, 1996), in tidal flows (e.g. Joshi, 1982), in river mouths and streams (e.g. Abramovich, 1963; Wright, 1977, Allen, 1982; Rowland et al., 2009), over stones in streams (Moth Iversen et al., 1989), in rip currents (e.g. Sonu, 1972, fig 9; Haller and Dalrymple, 2001), over steep slopes, scarps and cliff tops (Bowen and Lindley, 1977; Liu et al., 1999), and collimated jets are an important ingredient in the formation of stars (Bacciotti et al., 2003). Brook (1985) stated that "there are many types, their only common factor being a well-marked maximum in the boundary-layer wind speed profile" (Brook, 1985, p. 133).

In the near-surface terrestrial coastal zone, there have been only a few observations or studies of jets within incident flows in blowouts (Hesp and Hyde, 1996) and over dunes and ridges. Hsu (1977) measured the existence of a jet just above the surface over the crest of an ice ridge, and produced a general model indicating jet flow over similarly shaped dunes and ice ridges. Arens (1996), Arens et al. (1995), Petersen et al., (2011), and Hesp et al. (2013) have shown that under certain conditions jets occur on, or near the crests of scarps and foredunes. These studies demonstrate that sand may be transported across scarps and dune crests due to these locally accelerated flows (termed 'jettation' by Arens, (1996) for the suspended sand transport component; cf. Petersen et al., (2011)). The occurrence of jets may be related to incident wind speed, and/or incident wind direction, since in both the Arens (1996) and Hesp et al. (2013) studies, jets only appeared once the incident wind speeds had increased above a certain velocity, or approached from a certain wind direction.

In the aeolian/desert literature, jets have been shown to occur near or at the crests of various dune types, particularly transverse and barchan dunes, (although in some cases jets are observable in the velocity profiles but not discussed). Both Lancaster et al. (1996) and Omidyeganeh et al. (2013) have jets in some of their velocity profiles over terrestrial and subaqueous barchans respectively. Burkinshaw et al. (1993) encountered marked jets on occasions at 20-50cm high above the surface at the crest of a 7m high transverse dune. Walker and Shugar (2013, their figure 5a) appear to have a jet present in their dune crest velocity profile for a crest transverse flow. Jets have also been observed over small to large subaqueous dunes (e.g. Bridge and Best, 1988; van der Knaap et al., 1990; Bennett and Best, 1995; Kostaschuk and Villard, 1996).

Since jets are a specific, defined component of the flow field or regime, and may be critical to understanding the general flow behaviour over dunes and other topographies, it is important to recognise these phenomena as a distinct flow region, separate from other components of the flow (e.g. a speed-up region). It is critical to understand jet generation and behaviour over dunes since they may be prevalent more commonly than indicated by the few studies which encountered jets occurring over dunes, and they may be essential in assisting sediment transport up stoss slopes and/or generating onshore or offshore sediment transport downwind of the dune crest (Petersen et al., 2011; Hesp et al., 2013; Bauer et al., 2015). The same jets may be responsible for lifting and/or transporting sediment across vegetation canopies (Hesp et al., 2013), and perhaps in accelerating disturbance events (Hesp and Martinez, 2007). In addition, some models of wind flow over dunes do not consider or generate jets in their development (e.g. Van Boxel et al., 1999).

In the following, we model the development of jets over a foredune topographic profile from Prince Edward Island, Canada, (where jets have been recorded; see Hesp et al., 2009, 2013) via computational fluid dynamic (CFD) modelling, and then examine five principal questions regarding jets over foredunes:

1. Where and when does a jet form?
2. How does it change with incident flow speed?
3. How does it change with incident wind direction/slope?
4. How does it change over a scarped versus a non-scarped dune?
5. How is it affected by a change in surface roughness?

2. Methods

2.1 Dune Topography

The surface topography for this study is a foredune which has been studied for some years within the Greenwich Dunes unit of Prince Edward Island National Park on the north-east shore of Prince Edward Island (P.E.I.), Canada (see e.g. Davidson-Arnott et al., 2012; Hesp et al, 2009, 2013, Chapman et al, 2013; Walker et al., 2006, 2009; Bauer et al., 2012, 2015; Delgado-Fernandez and Davidson-Arnott, 2011).

The foredune crest is ~8 to 9 m above mean water level with a steep stoss slope (20°-25°) and an ENE-WSW crestline orientation. A low-gradient, microtidal (~1 m tidal range), moderate to high energy intermediate beach with a low-tide width of about 35 m is present on the seaward side of the dune. At the time of survey the foredune displayed a non-vegetated, 0.7 m high scarp, which later filled in with sand following a significant wind storm (see figure 6 in Hesp et al., 2009). The dune was vegetated by *Ammophila breviligulata,* with plant heights averaging 0.3 m and spatial density ranging from 2 – 45% based on visual assessments of percent cover on contiguous transects. The digital elevation model used to produce the dune surface within the computational domain was generated from 3666 RTK-DGPS points collected in a 100 m x 150 m area on the foredune at PEI.

Fig 1 here

2.2 Computational Fluid Dynamics (CFD) Methodology

Wind flow over the dune surface was simulated using computational fluid dynamics (CFD) CFD is a numerical method of solving fluid flow using the Navier-Stokes equations and has been successfully used to simulate flow over a number of coastal dune landforms (Wakes, 2013; Wakes et al., 2010; Smyth et al., 2012; 2013; Hesp et al., 2014; Jackson et al., 2011). The Navier-Stokes equations can also be solved linearly over dunes (Walmsley and Howard, 1985), with less computational cost than CFD, however this method is only appropriate where the windward slope is small and the wind flow not affected by near surface jets or flow separation. Wippermann and Gross (1985), also numerically modelled over a barchan dune using the mesoscale meteorological model, FITNAH (Flow over Irregular Terrain with Natural and Anthropogenic Heat Sources). FITNAH is however limited by its finest cell resolution of 2 m.). Simulations in this study were performed using the open source software OpenFOAM, which is capable of solving a range of complex fluid flows and also includes tools for meshing the surface topography and visualising the results. In this case, wind over the dune was calculated as an incompressible flow using a steady state solver, simpleFoam. Turbulence was modelled using the Renormalised group (RNG) κ-epsilon method (Yakhot et al., 1992). This is a turbulence model based on the Reynolds-averaged Navier-Stokes (RANS) equations, which focuses on the effects of turbulence on the average flow rather than resolving turbulence at every scale, as with direct numerical simulation (DNS) or at the larger scale such as a large eddy simulation (LES). The RNG model has been used to accurately simulate near surface flows over a transverse dune in a wind tunnel (Parsons et al., 2004), coastal dune complex (Wakes et al., 2010), a complex foredune blowout (Smyth et al., 2012; 2013), and flow over a foredune (Hesp et al., 2015). Joubert et al., (2012) also found that the original κ-epsilon turbulence model reproduced three-dimensional near surface patterns around a linear desert dune.

All simulations in this study were performed in two-dimensions. This approach was used because in three-dimensions, accurate representation of the change in the slope at the crest of the foredune in the mesh proved problematic as it became overly smoothed. In the two-dimensional simulations any change in slope was accurately recreated in the mesh using a polyline. Ideally flow modelling over the foredune would occur in three dimensions as wind is elliptic in nature as demonstrated by Hesp et al. (2015) who confirmed that incident winds which approach obliquely to the dune toe are deflected toward a more crest-normal orientation across the stoss slope of the foredune.

A mesh independence test was performed by calculating wind flow over 3 meshes of 0.5 m, 0.375 m and 0.25 m resolution. Between each case, wind flow at 30 points between 0.1 m and 3 m above the crest of the foredune changed by <1%. Due to the increased resolution of data points, the 0.25 m horizontal resolution mesh was employed for this study. The horizontal extent of each mesh ranged from 156 m for the 0° transect to 199 m for the 70° transect. In all cases the horizontal resolution of the mesh was 0.25 m and the vertical resolution progressed from 0.1 m at the surface to 1.63 m at the upper boundary located 64 m above the beach surface. Vertical cell size resolution of the mesh was restricted by the maximum dune surface roughness height (z_0) of 0.05 m. Each simulation was deemed complete when the residuals for each variable being solved (velocity, pressure, turbulent kinetic energy and energy dissipation) decreased by 4 orders of magnitude.

2.2.1 Computational Boundary conditions

In each simulation vertical profiles of wind speed (U), turbulent kinetic energy (k) and energy dissipation (ε) at the inlet boundary were defined assuming a constant shear velocity (u_*) value with height using equations 1, 2 and 3 (Richards and Hoxey, 1993 and Blocken et al., 2006):

$$U(z) = \frac{u_*}{k} \ln\left(\frac{z + z_0}{z_0}\right) \quad (1)$$

$$\kappa(z) = \frac{u_*}{\sqrt{C_\mu}} \quad (2)$$

$$\varepsilon(z) = \frac{u_*^3}{k(z+z_0)} \quad (3)$$

Where z is the height above the surface, k is the von Karman constant (0.42), z_0 is the surface roughness length and C_μ a constant of 0.09.

To examine how flow dynamics changed with wind speed, simulations were conducted using 4 values of u_* ranging from a minimum of 0.24 m s^{-1} to 0.60 m s^{-1} (Table 1). For each simulation a surface surrounding the dune was prescribed a surface roughness constant (z_0) of 0.0005 m, the equivalent of a sand surface (Bagnold, 1960). To test how jet dynamics change with roughness height, the foredune was prescribed roughness heights equivalent to that of bare sand (z_0 0.0005 m (Bagnold, 1954)), *Ammophila breviligulata* (z_0 0.01 m (Olson, 1958)), and thin grass 0.5 m high (z_0 0.05 m (Sutton, 1953)).

Table 1 here. Shear velocities (m s^{-1}) and equivalent wind speeds (m s^{-1}) at 1 m above the surface at the inlet of the computational domain for each simulation assuming a z_0 of 0.0005 m..

TABLE 1 HERE

3. Location of the Jet Formation

Because it is often the case that there are not enough instrumented masts in the field to adequately cover a foredune, it cannot be determined exactly where on the stoss face or near-crest region the jet flow is first formed. Thus, the CFD model was utilized to examine where the jet first forms on the foredune. Figure 2 illustrates seven locations across the upper stoss, crest and lee slope where velocity profiles were modelled in order to examine the first point of jet formation, and its downwind extension past the crest (if it occurs).

fig 2 here

In order to assess this, the wind velocity profiles were modelled at intervals of 0.25m across the P.E.I. foredune from upper stoss position over the crest, and down the lee slope to determine where the jet flow structure was initiated (Figure 2a). The transect utilized was the scarped profile, and a roughness height equivalent to *Ammophila breviligulata* (z_0 0.01 m) was applied to the foredune slope. Figure 2b demonstrates that the flow progressively accelerates up the stoss slope as observed in many similar dune and ridge studies (e.g. Arens et al., 1995; Finnigan, 2007; Walker et al., 2006, 2009; Bauer et al., 2013; Hesp et al., 2009, 2015). While there is some slight indication of jet formation at -1.5m, a clear jet is formed at 1.0m seawards of the crest. The flow becomes better defined as a more pronounced speed bulge (or nose) develops at around 50cm above the bed at -0.75 to -0.5mupslope, and is most pronounced at -0.25m seawards or downslope of the crest (Figure 2b). Note that the crest is itself quite convex and rounded (Figure 2a). The jet shifts upwards (to around 0.75m above the surface) and becomes more bulbous in the profile at 0.25m past the crest. It is likely that the very top of the crest is the point at which lee flow separation begins, and as this develops, the higher speed jet component of the flow is forced upwards over the separation envelope as observed in other studies (cf. Hsu, 1977). In addition, the flow tends to sweep upwards across the crest directed by the steep angle of the stoss slope, so the jet will tend to move upwards in the profile as it crosses the dune crest. Flow velocities are low near the surface in the lee of the dune crest due to flow separation development in this region.

The wind velocity profile with embedded jet at the dune crest displays a similar structure to that encountered in the field at P.E.I. (Hesp et al., 2009, 2013), and provides partial validation of the modelling. The vertical height above the bed at which the jet is most pronounced (the apex of the nose) in the modelling is lower by approximately 50cm (at the crest) to 25cm (just downwind of the crest) than that encountered in the field. This is likely due to the presence of vegetation in the field, whereas there is no vegetation present on the modelled surface.

4. Jet Structure and Incident Wind Speed

As noted in the introduction, observations of jets formed during different incident wind speeds have been made (e.g. Hsu, 1977; Arens et al., 1995; Hesp et al., 2009, 2013), but it is unclear if variations in incident wind speed actually produce changes in the jet formation or shape. Figure 3 shows wind velocity profiles simulated via CFD for four quite different incident wind velocities (5 m s^{-1} to 12.5m s^{-1} at 4m above the surface on the beach) for a directly onshore flow.

Fig 3 here

Jet flow was produced at the foredune crest for all four wind speeds tested (Figure 3) thereby indicating that once the flow velocity is above the threshold for sand transport, wind speed is not a factor determining whether a jet is present or not. Whilst it superficially appears as if the jet becomes more pronounced as wind speed increases (as in Hesp et al., 2013, their Figure 6)), when the results are made relative to the incident wind speed on the beach (at 4m height), all the four percent velocity profiles in Figure 3 virtually overlap, and there is only a very slight difference apparent indicating that incident wind speed has minimal effect on jet development.

5. Jet Development and Incident Wind Direction

Field observations of jets (e.g. Hesp et al., 2013) indicates that the jets vary according to incident wind direction. In order to test the influence of incident wind direction on jet development, a range of incident wind approach angles from 10° to 70° (almost perpendicular to almost dune crest parallel) were examined via the CFD model (Figure 4). Figure 1 illustrates the 2-D topographic profiles for the range of incident winds modelled. These show the relative slopes that the incident wind would encounter or "see" as it crosses the dune. Note how the slopes flatten considerably and elongate as the incident wind flow becomes increasingly oblique to the dune crest.

Fig 4 here

The incident wind angle/stoss slope has a significant impact on the production of a jet at the crest. As the incident angle becomes more oblique, making the slope less steep, the jet becomes slower and less defined until it is not discernable past 50° incident wind approach angle (Figure 4). In the field Hesp et al. (2013) found that a jet did not develop when the incident wind was from an angle >55°.

In three dimensions, the flow is topographically steered before reaching the dune crest (Walker et al., 2006; Hesp et al., 2015).This may cause the jet to form at more oblique incident angles than has been found here.

The jet is also more pronounced (i.e. more defined nose) in the vertical profile during winds that are perpendicular to the crest, likely because the stoss slope is steepest for these incident winds, and perhaps because of the presence of a more defined separation zone, which starts to limit the near surface wind speed near or at the crest.

Wind speed at the crest also decreases as incident wind direction becomes more oblique (cf. Walker et al., 2009; Hesp et al., 2015). The degree and magnitude of jet development for three incident directions (0°, 40° and 70°) may be seen in Figure59. The red zone indicates a high speed jet zone or region, and this is most pronounced in perpendicular flows. As the wind becomes increasingly oblique and the dune profile flattens and lengthens, the red zone decreases in size and the velocity declines. The degree of speedup also decreases as the incident flow becomes more oblique as indicated by the speed zones in Figure 5.

Fig 5 here

Figure 6 displays the maximum jet velocity developed at the foredune crest for each incident wind direction (Figure 6a), and the percent jet velocity relative to winds at 3m above the dune crest (Figure 6b). Figure 6c illustrates the log regressions of the vertical profiles of wind velocity up to 3 m height, and shows that as the incident wind becomes more oblique, the profile becomes more logarithmic. There are clear relationships between these such that the maximum jet speed declines as the incident wind direction becomes more oblique to highly oblique, relative jet velocities are highest compared to flow at 3 m above the foredune crest for directly onshore flow, and the velocity profiles progressively deviate from logarithmic as the incident flow becomes less oblique. The latter has clear implications for those wishing to determine shear stress at the bed from velocity profiles where jets are present. All plots have very high R^2 values.

Fig 6 here

6. Jet development for varying surface roughness

Figure 7 displays jet development for three surface roughness lengths based on data provided by Maun (2009) and for the same incident onshore wind velocity. It is apparent that the greatest jet development occurs for a bare sand surface with a very low roughness, and decreases with the presence of vegetation. There is less near surface turbulence and less drag where the surface is smooth (z_0 is close to zero in Figure 7), and therefore a greater degree of near surface flow acceleration upslope. However, there is little difference between a cover of *Ammophila breviligulata* and tall thin grass (as defined by Maun, 2009).

Fig 7 here

7. Scarped versus non-scarped foredune topography and jet development

Scarps are very commonly formed on foredunes since they occupy the seaward most position on the backshore (Carter et al., 1990; Hesp, 2002; Christiansen and Davidson-Arnott, 2004). In the discussion above, the CFD modelling (and previous field work) was conducted over the P.E.I. foredune which exhibited a small 0.7m high scarp. Since it is also common for jets to be formed over the crest of such scarps (Bowen and Lindley, 1977; Hesp et al., 2013), the presence of the scarp and attendant jet may have a downwind influence on the development of the foredune crest jet. A 2-D CFD comparison was conducted between the scarped profile and the same profile minus the scarp in order to determine if the scarp has a downwind effect on flow near the crest. Figure 8 demonstrates that the presence of the 0.7m high scarp does indeed influence the structure of the crest jet, in that the jet is more pronounced where the scarp is present. The highest velocities are also slightly closer to the bed. This may occur due to the scarp jet shedding higher velocity and more turbulent eddies downwind up the foredune stoss face compared to the situation where the scarp is not present.

Fig 8 here

The presence of the scarp at the dune toe leads to slightly greater development of the jet on the foredune ridge crest. The pressure fields were also examined for this comparison and show that (i) the high pressure zone which develops over the scarp region does not extend as far downwind across the foredune lower stoss slope compared to the non-scarped foredune, and, (ii) the low pressure zone over the dune crest is much higher (25%) for the scarped dune compared to the non-scarped dune.

8. Conclusions

The following conclusions can be derived from this study:

1. CFD modelling has successfully replicated jet flow development at a foredune crest region;

2. an increase in incident wind velocity does not affect the magnitude of jet flow;

3. a jet is first formed at ~1.0 m seawards of the foredune crest on the Prince Edward Island foredune morphology example examined here. The flow becomes better defined as a more pronounced nose develops at around 50 cm above the bed seawards of the crest, and is best developed at 0.25 m seawards of the dune crest. The jet shifts upwards and becomes slightly more bulbous in the profile just landwards or past the foredune crest and then disappears;

4. the jet is most pronounced and has the greatest aerial extent when winds are perpendicular to the foredune crest;

5. in the CFD modelling a jet did not develop a few degrees after an incident wind approach angle of 50° because there is significantly less flow acceleration across a much lower slope at an incident wind greater than ~55°;
6. the jet is higher in the vertical profile during winds that are more perpendicular to the dune crest in the 0° to 30° range of incident winds;
7. the degree of surface roughness influences the degree of jet development such that jets are better developed when the surface is bare compared to when vegetation is present;
8. the presence of a scarp at the dune toe does slightly influence the structure of the crest jet, in that the jet is more pronounced where a scarp is present.
9. jets are probably more common over dunes and similar topographies than believed or found due to (i) post data collection smoothing of velocity profiles (cf. Frank and Kocurek, 1996), or (ii) the fact that many field based wind profiling experiments do not have enough instruments stacked at closely spaced heights above the surface to be able to detect their presence.

Future research aims to examine the relationships between foredune morphology (particularly height and stoss slope gradient) and jet development, the nature of jet breakdown or dispersion, the nature of secondary circulation and instabilities in jets (see e.g. Ruith et al 2003; Cala et al 2006), and the dynamics and relationships between jet flow and reversing vortices within flow separation envelopes at, and past the foredune crest.

Acknowledgements

The authors thank the School of the Environment and Faculty of Science and Engineering, Flinders University for equipment grants to P. H. and post-doctoral funding to T.S., and support, the Flinders University supercomputer facility, the P.E.I. crew Robin, Ian, Bernie and Jeff, a grant (1024125) from NSF to P. Hesp, and Æolus for his continued ministry. The data in this paper are available by contacting the corresponding author.

References

Abramovich, G. N. (1963), *Theory of Turbulent Jets*, MIT Press, Cambridge.

Allen, J. R. L. (1982), Sedimentation from jets and separated flows, in Sedimentary Structures Their Character and Physical Basis: 133–171, Elsevier Scientific Publishing Company, Amsterdam.

Arens, S. M. (1996), Patterns of sand transport on vegetated foredunes, *Geomorphology*, *17*, 339–350.

Arens, S. M., H. M. E. Van Kaam-Peters, and J. H. Van Boxel (1995), Air flow over foredunes and implications for sand transport, *Earth Surface Processes and Landforms*, *20*(4), 315–332, doi:10.1002/esp.3290200403.

Bacciotti, F., T. P. Ray, J. Eisloffel, J. Woitas, J. Solf, R. Mundt, and C. . Davis (2003), Observations of Jet Diameter, Density and Dynamics, *Astrophysics and Space Science*, *287*, 3–13.

Bauer, B. O., Davidson-Arnott, R.G.D., Walker, I.J., Hesp, P.A., Ollerhead, J., 2012. Wind direction and complex sediment transport response across a beach-dune system, Earth Surface Processes and Landforms, 37(15), 1661–1677, doi:10.1002/esp.3306.

Bauer, B. O., Davidson-Arnott, R.G.D., Hesp, P.A., Namikas, S.L., . Ollerhead, J., Walker, I.J., 2009. Aeolian sediment transport on a beach: Surface moisture, wind fetch, and mean transport, Geomorphology, 105(1-2), 106–116, doi:10.1016/j.geomorph.2008.02.016.

Bauer, B.O., Hesp, P.A., Walker, I.J., Davidson-Arnott, R.G.D., 2015. Sediment (dis)continuity across a beach-dune profile during an offshore wind event. Geomorphology 245: 135-148.

Bauer, B. O., I. J. Walker, A. C. W. Baas, D. W. T. Jackson, C. M. Neuman, G. F. S. Wiggs, and P. A. Hesp (2013), Critical Reflections on the Coherent Flow Structures Paradigm in Aeolian Geomorphology, in *Coherent Flow Structures at Earth's Surface*, pp. 111–134, John Wiley & Sons, Ltd.

Bennett, S.J., Best, J.L., 1995. Mean flow and turbulence structure over fixed, two-dimensional dunes: implications for sediment transport and bedform stability. Sedimentology 42: 491-513.

Bickley, W. (1939), The Plane Jet, *Phil. Mag. Ser.*, *7*, 727–731.

Birkhoff, G., and E. Zarantonello (1957), *Jets, Wakes and Cavities*, Academic Press, New York.

Blocken, B., T. Stathopoulos, and J. Carmeliet (2007), CFD simulation of the atmospheric boundary layer : wall function problems, *Atmospheric Environment*, *41*(2), 238–252.

Bowen, A. J., and D. Lindley (1977), A wind-tunnel investigation of the wind speed and turbulence characteristics close to the ground over various enscarpment shapes, *Boundary-Layer Meteorology*, *12*(1977), 259–271.

Bridge, J.S., Best, J.L., 1988. Flow, sediment transport and bedform dynamics over the transition from dunes to upper-stage plane beds: implications for the formation of planar lamination. Sedimentology 35, 753-763.

Brook, R. A. (1985), The Koorin nocturnal low-level jet, *Boundary-Layer Meteorology*, *32*, 133–154.

Burkinshaw, J.R., Illenberger, W.K., Rust, I.C., 1993. Wind speed profiles over a reversing transverse dune. In: Pye, K. (ed.), The Dynamics and Environmental Context of Aeolian Sedimentary Systems. Geol. Soc. Spec. Publication No. 72: 25-36.

Cala, C. E., E. C. Fernandes, M. V Heitor, and S. I. Shtork (2006), Coherent structures in unsteady swirling jet flow, *Experiments in Fluids*, *40*(2), 267–276, doi:10.1007/s00348-005-0066-9.

Carter, R. W. G. (1988), *Coastal Environments. An Introduction to the Physical, Ecological and Cultural Systems of Coastlines*, Academic Press, London.

Carter, R. W. G., P. A. Hesp, and K. F. Nordstrom (1990), Geomorphology of erosional dune landscapes, in *Coastal Dunes: Processes and Morphology*, edited by K. F. Nordstrom, N. Psuty, and R. W. G. Carter, pp. 217–250, John Wiley & Sons, Ltd.

Chapman, C. A., I. J. Walker, P. A. Hesp, B. O. Bauer, and R. G. D. Davidson-Arnott (2011), Turbulent Reynolds stress and quadrant event activity in wind flow over a coastal foredune, *Geomorphology*, *151-152*, 1–12, doi:10.1016/j.geomorph.2011.11.015.

Chapman, C., I. J. Walker, P. a. Hesp, B. O. Bauer, R. G. D. Davidson-Arnott, and J. Ollerhead (2013), Reynolds stress and sand transport over a vegetated foredune, Earth Surface Processes and Landforms, 38(14), 1735–1747, doi:10.1002/esp.3428.

Christiansen, M. B., and R. Davidson-arnott (2004), Rates of Landward Sand Transport over the Foredune at Skallingen , Denmark and the Role of, *Danish Journal of Geography*, *104*(1), 31–43.

Davidson-Arnott, R. G. D., B. O. Bauer, I. J. Walker, P. A. Hesp, and J. Ollerhead (2009), Instantaneous and Mean Aeolian Sediment Transport Rate on Beaches : an Intercomparison of Measurements from Two Sensor Types, *Journal Of Coastal Research Special Issue*, (56), 297–301.

Davidson-Arnott, R. G. D., B. O. Bauer, I. J. Walker, P. a. Hesp, J. Ollerhead, and C. Chapman (2012), High-frequency sediment transport responses on a vegetated foredune, *Earth Surface Processes and Landforms*, *37*(11), 1227–1241, doi:10.1002/esp.3275.

Davidson-arnott, R. G. D., Y. Yang, J. Ollerhead, P. A. Hesp, and I. J. Walker (2008), The effects of surface moisture on aeolian sediment transport threshold and mass flux on a beach, *Earth Surface Processes an*, *33*, 55–74, doi:10.1002/esp.

Delgado-Fernandez, I., and R. Davidson-Arnott (2011), Meso-scale aeolian sediment input to coastal dunes: The nature of aeolian transport events, *Geomorphology*, *126*(1-2), 217–232, doi:10.1016/j.geomorph.2010.11.005.

Delgado-Fernandez, I., R. Davidson-Arnott, and J. Ollerhead (2009), Application of a Remote Sensing Technique to the Study of Coastal Dunes, *Journal of Coastal Research*, 1160–1167, doi:10.2112/09-1182.1.

Delgado-Fernandez, I., R. G. D. Davidson-Arnott, B. O. Bauer, I. J. Walker, and J. Ollerhead (2013), Evaluation of the optimal resolution for characterizing the effect of beach surface moisture derived from remote sensing on Aeolian transport and deposition, *Journal Of Coastal Research Special Issue*, (65), 1277–1282.

Finnigan, J. J. (2007), The turbulent wind in plant and forest canopies, in *Plant Disturbance Ecology: The Process and Response*, edited by E. A. Johnson and K. Miyanishi, pp. 15–58, Elsevier, Amsterdam.

Finnigan, J. J., and S. E. Belcher (2004), Flow over a hill covered with a plant canopy, *Quarterly Journal of the Royal Meteorological Society*, *130*(596), 1–29, doi:10.1256/qj.02.177.

Finnigan, J. J., and Y. Brunet (1995), Turbulent airflow in forests on flat and hilly terrain, in *Wind and Trees*, edited by M. P. Coutts and J. Grace, pp. 3–40, Cambridge University Press, Cambridge UK.

Frank A.J., Kocurek G. 1996. Airflow up the stoss slope of sand dunes: limitations of current understanding. Geomorphology 17: 47-54.

Haller, M. C., and R. A. Dalrymple (2001), Rip current instabilities, *J. Fluid Mech.*, *433*, 161–192.

Hesp, P.A. (2002), Foredunes and blowouts: initiation, geomorphology and dynamics, *Geomorphology*, *48*(1-3), 245–268, doi:10.1016/S0169-555X(02)00184-8.

Hesp, P. A., and I. J. Walker (2011), Three-dimensional æolian dynamics within a bowl blowout during offshore winds: Greenwich Dunes, Prince Edward Island, Canada, *Aeolian Research*, *3*, 389–399, doi:10.1016/j.aeolia.2011.09.002.

Hesp, P. A., and M. Martinez (2007), Disturbance in coastal dune ecosystems, in *Plant Disturbance Ecology: The Process and Response*, edited by E. A. Johnson and K. Miyanishi, pp. 215–247, Elsevier, Amsterdam.

Hesp, P. A., and R. Hyde (1996), Flow dynamics and geomorphology of a trough blowout, *Sedimentology*, *43*, 505–525.

Hesp, P. A., I. J. Walker, C. Chapman, R. Davidson-Arnott, and B. O. Bauer (2013), Aeolian dynamics over a coastal foredune, Prince Edward Island, Canada, *Earth Surface Processes and Landforms*, *38*(1), 1566–1575, doi:10.1002/esp.3444.

Hesp, P. A., I. J. Walker, S. L. Namikas, B. O. Bauer, J. Ollerhead, and M. Allison (2009), Storm Wind Flow over a Foredune , Prince Edward Island , Canada, *Journal of Coastal Research*, (SI 56), 312–316.

Hesp, P. A., R. Davidson-Arnott, I. J. Walker, and J. Ollerhead (2005), Flow dynamics over a foredune at Prince Edward Island, Canada, *Geomorphology*, *65*(1-2), 71–84, doi:10.1016/j.geomorph.2004.08.001.

Hesp, P. A., T. A. G. Smyth, P. Nielsen, I. J. Walker, B. O. Bauer, and R. Davidson-Arnott (2015), Flow deflection over a foredune, *Geomorphology*, *230*(0), 64–74, doi:http://dx.doi.org/10.1016/j.geomorph.2014.11.005.

Hsu, S. A. (1977), Boundary-layer Meteorological research in the coastal zone, *Geoscience and Man*, *XVIII*, 99–111.

Jackson, D. W. T., Beyers, J.H.M., Lynch, K., Cooper, J. A. G., Baas, A. C.W., Delgado-Fernandez, I., 2011. Investigation of three-dimensional wind flow behaviour over coastal dune morphology under offshore winds using computational fluid dynamics (CFD) and ultrasonic anemometry. Earth Surface Processes and Landforms 36, 1113–1124. doi:10.1002/esp.2139

Joshi, P. B. (1982), Hydromechanics of tidal jets, *Journal of the Waterway Port Coastal and Ocean Division*, *108*(3), 239–253.

Joubert, E.C., Harms, T.M., Muller, A., Hipondoka, M., Henschel, J.R., 2012. A CFD study of wind patterns over a desert dune and the effect on seed dispersion. Environmental Fluid Mechanics 12, 23–44. doi:10.1007/s10652-011-9230-3

Kostaschuk, R., and Villard, P., 1996. Flow and sediment transport over large subaqueous dunes: Fraser River, Canada. Sedimentology 43: 849-863.

Kraus, H., J. Malcher, and E. Schaller (1985), A nocturnal low level jet during PUKK, *Boundary-Layer Meteorology*, *31*(2), 187–195, doi:10.1007/BF00121177.

Lancaster N., Nickling W.G., McKenna Neuman C.K., Wyatt, V.E., 1996. Sediment flux and airflow on the stoss slope of a barchan dune. Geomorphology 17: 55-62.

Mattingly, G. E., and W. O. Criminale (1972), The stability of an incompressible two-dimensional wake, *Journal of Fluid Mechanics*, *51*, 233–272, doi:10.1017/S0022112072001193.

Maun, M. A. (2009), *The Biology of Coastal Sand Dunes*, Oxford University Press.

Moth Iversen, T.C., Lindegaard, K., Sand-Jensen, K., Thorup, J., 1989. Vandlobsokologi (Watercourse Ecology), Freshwater-Biological laboratory, Copenhagen University.

Ollerhead, J., R. Davidson-Arnott, I. J. Walker, and S. Mathew (2012), Annual to decadal morphodynamics of the foredune system at Greenwich Dunes, Prince Edward Island, Canada, *Earth Surface Processes and Landforms*, *38*(3), 284–298, doi:10.1002/esp.3327.

Olson, J.S., 1958. Lake Michigan dune development. 1. Wind-velocity profiles. J. Geology 66: 254-263.

Omidyeganeh, M., Piomelli, U., Christensen, K.T., Best, J.L., 2013. Large-eddy simulation of flow over barchans dunes. Proc. Marine and River Dune Dynamics – MARID IV, 15-16th April, 2013, Bruges, Belgium: 191-198.

Parish, T. R. (2000), Forcing of the Summertime Low-Level Jet along the California Coast., *Journal of Applied Meteorology*, *39*(12), 2421–2433.

Parsons, D. R., I. J. Walker, and G. F. S. Wiggs (2004), Numerical modelling of flow structures over idealized transverse aeolian dunes of varying geometry, *Geomorphology*, *59*(1-4), 149–164, doi:10.1016/j.geomorph.2003.09.012.

Pattanapol, W., S. J. Wakes, M. J. Hilton, and K. J. M. Dickinson (2007), Modeling of Surface Roughness for Flow Over a Complex Vegetated Surface, *Proceedings of world academy of science, Engineering and*, *26*, 273–281.

Petersen, P. S., M. J. Hilton, and S. J. Wakes (2011), Evidence of aeolian sediment transport across an Ammophila arenaria-dominated foredune, Mason Bay, Stewart Island, *New Zealand Geographer*, *67*(3), 174–189, doi:10.1111/j.1745-7939.2011.01210.x.

Rasmussen, K. R. (1989), Some aspects of flow over coastal dunes, *Proceedings of the Royal Society of Edinburgh Section B: Biological Sciences*, *96*, 129–147.

Rowland, J. C., M. T. Stacey, and W. E. Dietrich (2009), Turbulent characteristics of a shallow wall-bounded plane jet: experimental implications for river mouth hydrodynamics. *Journal of Fluid Mechanics*, *627*, 423–449.

Ruith, M. R., P. Chen, E. Meiburg, and T. Maxworthy (2003), Three-dimensional vortex breakdown in swirling jets and wakes: direct numerical simulation, *Journal of Fluid Mechanics*, *486*, 331–378. doi:10.1017/S0022112003004749.

Schlichting, H. (1955), *Boundary-layer Theory*, 7th 1979 ed., McGraw-Hill, New York.

Smyth, T. A. G., D. W. T. Jackson, and J. A. G. Cooper (2012), Geomorphology High resolution measured and modelled three-dimensional airflow over a coastal bowl blowout, *Geomorphology*, *177-178*, 62–73, doi:10.1016/j.geomorph.2012.07.014.

Smyth, T. A. G., D. W. T. Jackson, and J. A. G. Cooper (2013), Three dimensional airflow patterns within a coastal trough – bowl blowout during fresh breeze to hurricane force winds, *Aeolian Research*, *9*, 111–123.

Sonu, C. J. (1972), Field observation of nearshore circulation and meandering currents, *Journal of Geophysical Research*, *77*(18), 3232–3247, doi:10.1029/JC077i018p03232.

Sutton, O. G. (1953), Micrometeorology: a study of physical processes in the lowest layers of the earth's atmosphere. New York: McGraw-Hill.

Van Boxel, J. H., S. M. Arens, and P. M. Van Dijk (1999), Aeolian processes across transverse dunes. I: Modelling the air flow, *Earth Surface Processes and Landforms*, *24*, 255–270.

van der Knaap, F.C.M., van Mierlo, M.C.L.M., Officier, M.J., 1991. Measurements and computations of the turbulent flow field above fixed bed-forms. In: Soulsby, R. and Bettess, R., (Eds.), Sand Transport in Rivers, Estuaries and the Sea. Proc. Euromech 262

Colloquim on sand transport in Rivers, Estuaries and the Sea, Wallingford, 26-29 june, 1990: 179-185. A.A. Balkema, Rotterdam.

Vogel, S. (1996), *Life in Moving Fluids. The Physical Biology of Flow*, Princeton University Press, New Jersey.

Wakes, S. (2013), Three-dimensional Computational Fluid Dynamic experiments over a complex dune topography, *Journal of Coastal Research*, (S I65), 1337–1342, doi:10.2112/SI65-226.1.

Wakes, S. J., T. Maegli, K. J. Dickinson, and M. J. Hilton (2010), Numerical modelling of wind flow over a complex topography, *Environmental Modelling & Software*, *25*(2), 237–247, doi:10.1016/j.envsoft.2009.08.003.

Walker, I. J. (2005), Physical and logistical considerations of using ultrasonic anemometers in aeolian sediment transport research, *Geomorphology*, *68*(1-2), 57–76, doi:10.1016/j.geomorph.2004.09.031.

Walker, I. J., P. A. Hesp, B. O. Bauer, J. Ollerhead, and M. Allison (2009a), Mean Flow and Turbulence Responses in Airflow over Foredunes : New Insights from Recent Research. *Journal of Coastal Research*, (SI 56), 366–370.

Walker, I. J., P. A. Hesp, R. G. D. Davidson-Arnott, and J. Ollerhead (2006), Topographic Steering of Alongshore Airflow over a Vegetated Foredune: Greenwich Dunes, Prince Edward Island, Canada, *Journal of Coastal Research*, *22*(5), 1278–1291, doi:10.2112/06A-0010.1.

Walker, I. J., P. A. Hesp, R. G. D. Davidson-Arnott, B. O. Bauer, S. L. Namikas, and J. Ollerhead (2009b), Responses of three-dimensional flow to variations in the angle of incident wind and profile form of dunes: Greenwich Dunes, Prince Edward Island, Canada, *Geomorphology*, *105* (1-2), 127–138, doi:10.1016/j.geomorph.2007.12.019.

Walker, I. J., & Shugar, D. H. (2013). Secondary flow deflection in the lee of transverse dunes with implications for dune morphodynamics and migration.*Earth Surface Processes and Landforms*, *38*(14), 1642-1654.

Walmsley, J.L., Howard, A.D., 1985. Application of a boundary-layer model to flow over an eolian dune. Journal of Geophysical Research 90, 631–640.

Wei, W., B. G. Wu, X. X. Ye, H. X. Wang, and H. S. Zhang (2013), Characteristics and Mechanisms of Low-Level Jets in the Yangtze River Delta of China, *Boundary-Layer Meteorology*, *149* (3), 403–424, doi:10.1007/s10546-013-9852-8.Wolfe, S. A., and W. G. Nickling (1996), Shear stress partitioning in sparsely vegetated desert canopies, *Earth Surface Processes and Landforms*, *21*, 607–619.

Wipperman, F.K., Gross, G., 1986. The wind-induced shaping and migration of an isolated dune: A numerical experiment. Boundary-Layer Meteorology 36, 319–334.

Wright, L. D. (1977), Sediment transport and deposition at river mouths: A synthesis, *Geological Society of America Bulletin*, *88*(6), 859–868.

Xianwan, L., L. Sen, and S. Jianyou (1999), Wind tunnel simulation experiment of mountain dunes, *Journal of Arid Environments*, *42*(1), 49–59. doi:http://dx.doi.org/10.1006/jare.1998.0488.

Yakhot, V., S. A. Orszag, S. Thangam, T. B. Gatski, and C. G. Speziale (1992), Development of turbulence models for shear flows by a double expansion technique *Phys. Fluids A*, *7*(May), 1510–1520, doi:10.1063/1.858424.

Figure CAPTIONS

Figure 1. Digital elevation model of the P.E.I. foredune. Orientation of two topographic profile lines relative to the dune crestline used in the CFD modelling are indicated. Topographic profiles over the P.E.I. foredune from 0° (onshore) to 70° (obliquely alongshore). Note that the profile flattens and broadens considerably as the incident flow swings from perpendicular to highly oblique.

Figure 2a. Location of the seven points on the upper stoss slope, crest and lee slope sampled for CFD velocity profiles. The vertical height (m) of each location is labelled. Distance indicated by the x axis is relative to the dune crest (at 0 m).

Figure 2b. Wind velocity profiles from the upper stoss slope starting at – 1.5m upwind (down-slope) of the crest (the red line, at 0m) (locations in 2a) and down the upper lee slope for a 0° incident wind (i.e. perpendicular to the dune crest). The velocity profiles indicate progressive acceleration up the stoss slope and the jet flow appears at ~1m seawards of the dune crest. Ref wind speed refers to wind speed 4 m above the surface at the inlet.

Figure 3. Percent wind velocity profiles at the crest of the foredune for a directly onshore flow. Jets were produced for a range of shear velocities (u_* 0.23 – 0.58) equivalent to incident wind speeds of 5.0 to 12.5ms^{-1} at 4 m height on the beach upwind of the foredune. Ref wind speed refers to wind speed 4 m above the surface at the inlet.

Figure 4. Comparison of the foredune crest percent wind velocity profiles for a range of incident wind directions. Zero (0°) indicates directly onshore winds. Jet development is not present at an incident approach direction of 60° but is present by 50°, and is most pronounced for onshore to low angle oblique winds. Ref wind speed refers to wind speed 4 m above the surface at the inlet.

Figure 5. The degree and magnitude of jet development for three incident directions (0° - directly onshore, 40° and 70°). The jet is most pronounced and has the greatest aerial extent when winds are perpendicular to the foredune crest.

Figure 6. Maximum jet velocity developed at the foredune crest for each incident wind direction (a), the percent jet velocity relative to winds at 3m above the dune crest (b) and the log regressions of the vertical profiles of wind velocity up to 3 m height (c).

Figure 7. Wind velocity profiles and jet development for three different surface roughness lengths (left side), and isovels over the dune topography and varying surface roughness (right side). The presence of vegetation retards the degree of jet development. Ref wind speed refers to wind speed 4 m above the surface at the inlet.

Figure 8. Wind velocity profiles measured at the foredune crest for an onshore 2-D flow for the scarped (0.7m high) and non-scarped morphology. The jet is marginally faster (5%) at the crest where the scarp is present. Ref wind speed refers to wind speed 4 m above the surface at the inlet.

Shear Velocity (m s^{-1})	Wind Speed 4 m above surface (m s^{-1})
0.23	5
0.35	7.5
0.47	10
0.58	12.5

TABLE CAPTION

Table 1. Shear velocities (m s^{-1}) and equivalent wind speeds (m s^{-1}) at 1 m above the surface at the inlet of the computational domain for each simulation assuming a z_0 of 0.0005 m.

Jet Flow over Foredunes

Patrick A. Hesp and Thomas A.G. Smyth

School of the Environment, Faculty of Science and Engineering, Flinders University, Bedford Park, South Australia 5042
Patrick.Hesp@flinders.edu.au; Thomas.Smyth@flinders.edu.au

Key Points

- Jet flow over a foredune is examined for a range of wind speeds/directions.
- Jets develop regardless of wind speed, best developed for perpendicular winds.
- Surface roughness affects jet development

Abstract

Jet flows, which are localized flows exhibiting a high speed maxima, are relatively common in nature, and in many devices. They have only been occasionally observed on dunes, and their dynamics are poorly known. This paper examines computational fluid dynamic (CFD) 2D modelling of jet flow over a foredune topography. Flow was simulated in 10° increments from onshore (0°) to highly oblique alongshore (70°) incident wind approach angles. CFD modelling reveals that the formation of a jet is not dependent on a critical wind speed, and an increase in incident wind velocity does not affect the magnitude of jet flow. A jet is first formed at ~1.0m seawards of the foredune crest on the Prince Edward Island foredune morphology example examined here. A jet is not developed when the incident wind is from an oblique approach angle greater than ~50° because there is significantly less flow acceleration across a much lower slope at this incident angle. The presence of a scarp does influence the structure of the crest jet, in that the jet is more pronounced where a scarp is present. Surface roughness affects the magnitude of jet expansion and jets are better developed on bare surfaces compared to vegetated ones.

Keywords: Foredune, jet, jet flow, computational fluid dynamics (CFD), flow dynamics; .

1. Introduction

Jet flows are relatively common in nature, and in many devices. A jet is a localized flow exhibiting a high-speed maxima according to Wei et al. [(2013]). The word comes from the French *jeter* and Latin *jactare* 'to throw', and by the 16th Century was used as a verb meaning 'to jut out' (http://www.oxforddictionaries.com/definition/english/jet), hence the observation that a jet has a well-defined 'nose' in the velocity profile (Wei et al., {(2013}); see e.g. http://www.eng.fsu.edu/~shih/succeed/jet/jet.htm). Jets may be formed where fluids are compressed and ejected from nozzles, pipes, taps, engines, exhausts (often as buoyant plumes) and similar objects or devices {(Schlichting, 1955; Birkhoff and Zarontonello, 1957; Cala et al., 2006}). One classic commonly cited example is the flow from a household tap. Jets are found, or occur in the atmosphere, for example, as low level jets during certain wind conditions {(e.g. Kraus et al., 1985; Brook, 1985}), as coastal phenomena associated with temperature gradients {(e.g. Parish, 2000}), in wakes behind bluff bodies {(Bickley, 1939; Mattingly and Criminale, 1972}), in various marine animals such as sponges and mollusks {(Vogel, 1996}), in tidal flows {(e.g. Joshi, 1982}), in river mouths and streams {(e.g. Abramovich, 1963; Wright, 1977, Allen, 1982; Rowland et al., 2009}), over stones in streams (Moth Iversen et al., 1989), in rip currents {(e.g. Sonu, 1972, fig 9; Haller and Dalrymple, 2001}), over steep slopes, scarps and cliff tops {(Bowen and Lindley, 1977; Liu et al., 1999}), and collimated jets are an important ingredient in the formation of stars {(Bacciotti et al., 2003}). Brook {(1985}) stated that "there are many types, their only common factor being a well-marked maximum in the boundary-layer wind speed profile" {(Brook, 1985, p. 133}).

In the near-surface terrestrial coastal zone, there have been only a few observations or studies of jets within incident flows in blowouts {(Hesp and Hyde, 1996}) and over dunes and ridges. Hsu {(1977}) measured the existence of a jet just above the surface over the crest of an ice ridge, and produced a general model indicating jet flow over similarly shaped dunes and ice ridges. Arens {(1996}), Arens et al. {(1995}), Petersen et al., {(2011}), and Hesp et al. {(2013}) have shown that under certain conditions jets occur on, or near the crests of scarps and foredunes. These studies demonstrate that sand may be transported across scarps and dune crests due to these locally accelerated flows (termed 'jettation' by Arens, {(1996}) for the suspended sand transport component; cf. Petersen et al., {(2011})). The occurrence of jets may be related to incident wind speed, and/or incident wind direction, since in both the Arens {(1996}) and Hesp et al. {(2013}) studies, jets only appeared once the incident wind speeds had increased above a certain velocity, or approached from a certain wind direction.

In the aeolian/desert literature, jets have been shown to occur near or at the crests of various dune types, particularly transverse and barchan dunes, (although in some cases jets are observable in the velocity profiles but not discussed). Both Lancaster et al. (1996) and Omidyeganeh et al. (2013) have jets in some of their velocity profiles over terrestrial and subaqueous barchans respectively. Burkinshaw et al. (1993) encountered marked jets on occasions at 20-50cm high above the surface at the crest of a 7m high transverse dune. Walker and Shugar (2013, their figure 5a) appear to have a jet present in their dune crest velocity profile for a crest transverse flow. Jets have also been observed over small to large subaqueous dunes (e.g. Bridge and Best, 1988; van der Knaap et al., 1990; Bennett and Best, 1995; Kostaschuk and Villard, 1996).

Since jets are a specific, defined component of the flow field or regime, and may be critical to understanding the general flow behaviour over dunes and other topographies, it is important to recognise these phenomena as a distinct flow region, separate from other components of the flow (e.g. a speed-up region). It is critical to understand jet generation and behaviour over dunes since they may be prevalent more commonly than indicated by the few studies which encountered jets occurring them in studies over dunes, and they may be essential in assisting sediment transport up stoss slopes and/or generating onshore or offshore sediment transport downwind of the dune crest [(Petersen et al., 2011; Hesp et al., 2013; Bauer et al., 2015]). The same jets may be responsible for lifting and/or transporting sediment across vegetation canopies [(Hesp et al., 2013]), and perhaps in accelerating disturbance events [(Hesp and Martinez, 2007]). In addition, some models of wind flow over dunes do not consider or generate jets in their development [(e.g. Van Boxel et al., 1999]).

In the following, we model the development of jets over a foredune topographic profile from Prince Edward Island, Canada, (where jets have been recorded; see Hesp et al., 2009, 2013) via computational fluid dynamic (CFD) modelling, and then examine five principal questions regarding jets over foredunes:

1. Where and when does a jet form?
2. How does it change with incident flow speed?
3. How does it change with incident wind direction/slope?
4. How does it change over a scarped versus a non-scarped dune?
5. How is it affected by a change in surface roughness?

2. Methods

2.1 Dune Topography

The surface topography for this study is a foredune which has been studied for some years within the Greenwich Dunes unit of Prince Edward Island National Park on the north-east shore of Prince Edward Island (P.E.I.), Canada (see e.g. Davidson-Arnott et al., 2012; Hesp et al, 2009, 2013, Chapman et al, 2013; Walker et al., 2006, 2009; Bauer et al., 2012, 2015; Delgado-Fernandez and Davidson-Arnott, 2011).

The foredune crest is ~8 to 9 m above mean water level with a steep stoss slope (20°-25°) and an ENE-WSW crestline orientation. A low-gradient, microtidal (~1 m tidal range), moderate to high energy intermediate beach with a low-tide width of about 35 m is present on the seaward side of the dune. At the time of survey the foredune displayed a non-vegetated, 0.7 m high scarp, which later filled in with sand following a significant wind storm [(see figure 6 in Hesp et al., 2009]). The dune was vegetated by *Ammophila breviligulata,* with plant heights averaging 0.3 m and spatial density ranging from 2 – 45% based on visual assessments of percent cover on contiguous transects. The digital elevation model used to produce the dune surface within the computational domain was generated from 3666 RTK-DGPS points collected in a 100 m x 150 m area on the foredune at PEI.

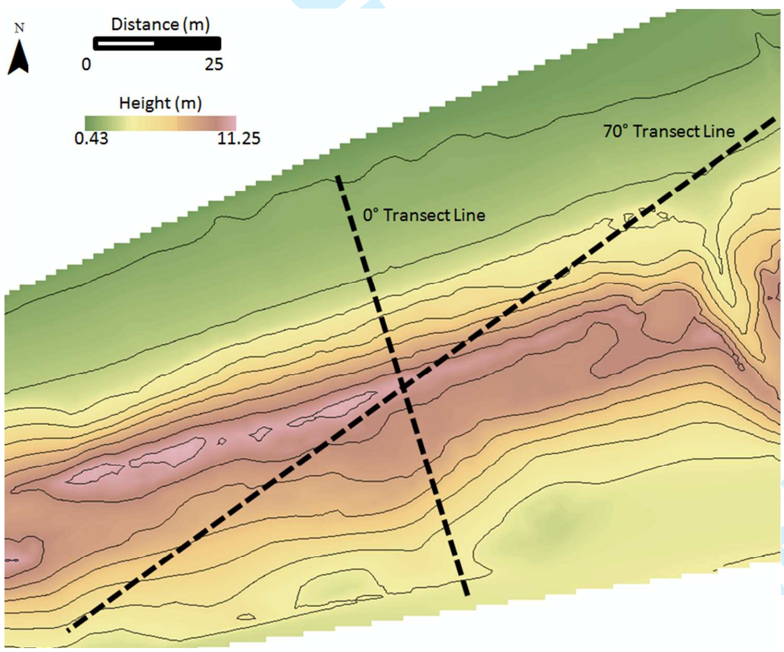

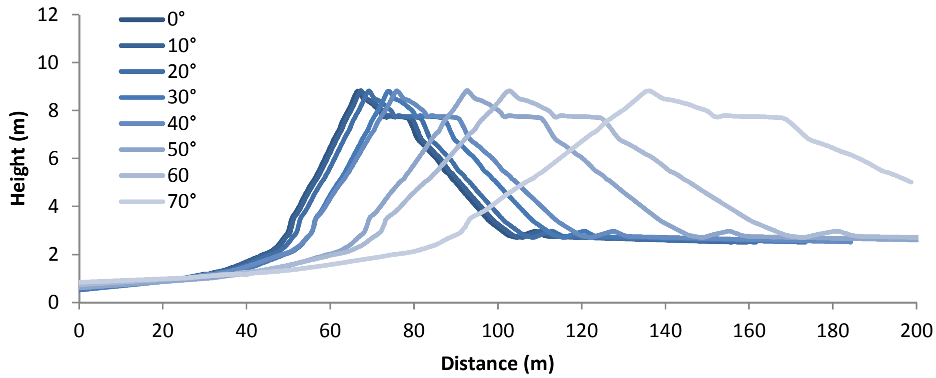

Figure 1. Digital elevation model of the P.E.I. foredune. Orientation of two topographic profile lines relative to the dune crestline used in the CFD modelling are indicated. Topographic profiles over the P.E.I. foredune from 0° (onshore) to 70° (obliquely alongshore). Note that the profile flattens and broadens considerably as the incident flow swings from perpendicular to highly oblique.

2.2 Computational Fluid Dynamics (CFD) Methodology

Wind flow over the dune surface was simulated using computational fluid dynamics (CFD) CFD is a numerical method of solving fluid flow using the Navier-Stokes equations and . ~~CFD~~ has been successfully used to simulate flow over a number of coastal dune landforms [(Wakes, 2013; Wakes et al., 2010; Smyth et al., 2012; 2013; Hesp et al., 2014; Jackson et al., 2011). The Navier-Stokes equations can also be solved linearly over dunes (Walmsley and Howard, 1985), with less computational cost than CFD, however this method is only appropriate where the windward slope is small and the wind flow not affected by near surface jets or flow separation. Wippermann and Gross (1985), also numerically modelled over a barchan dune using the mesoscale meteorological model, FITNAH (Flow over Irregular Terrain with Natural and Anthropogenic Heat Sources). FITNAH is however limited by its finest cell resolution of 2 m.]). Simulations in this study were performed using the open source software OpenFOAM, which is capable of solving a range of complex fluid flows and also includes tools for meshing the surface topography and visualising the results. In this case, wind over the dune was calculated as an incompressible flow using a steady state solver, simpleFoam. Turbulence was modelled using the Renormalised group (RNG) κ-epsilon method [(Yakhot et al., 1992]). This is a turbulence model based on the Reynolds-averaged Navier-Stokes (RANS) equations, which focuses on the effects of turbulence on the average flow rather than resolving turbulence at every scale, as with direct numerical simulation (DNS) or at the larger scale such as a large eddy simulation (LES). The RNG model has been used to accurately simulate near surface flows over a transverse dune in a wind tunnel [(Parsons et al., 2004]), coastal dune complex [(Wakes et al., 2010]), a complex foredune blowout [(Smyth et al., 2012; 2013]), and flow over a foredune [(Hesp et al., 2015]). Joubert et al., (2012) also found that the original κ-epsilon turbulence model reproduced three-dimensional near surface patterns around a linear desert dune.

Formatted: Font: (Default) Times New Roman, 12 pt

Formatted: Font: (Default) Times New Roman, 12 pt

Formatted: Font: (Default) Times New Roman, 12 pt

Formatted: Font: (Default) Times New Roman, 12 pt

All simulations in this study were performed in two-dimensions. This approach was used because in three-dimensions, accurate representation of the change in the slope at the crest of the foredune in the mesh proved problematic as it became overly smoothed. In the two-dimensional simulations any change in slope was accurately recreated in the mesh using a polyline. Ideally flow modelling over the foredune would occur in three dimensions as wind is elliptic in nature as demonstrated by Hesp et al. (2015) who confirmed that incident winds which approach obliquely to the dune toe are deflected toward a more crest-normal orientation across the stoss slope of the foredune.

A mesh independence test was performed by calculating wind flow over 3 meshes of 0.5 m, 0.375 m and 0.25 m resolution. Between each case, wind flow at 30 points between 0.1 m and 3 m above the crest of the foredune changed by <1%. Due to the increased resolution of data points, the 0.25 m horizontal resolution mesh was employed for this study. The horizontal extent of each mesh ranged from 156 m for the 0° transect to 199 m for the 70° transect. In all cases the horizontal resolution of the mesh was 0.25 m and the vertical resolution progressed from 0.1 m at the surface to 1.63 m at the upper boundary located 64 m above the beach surface. Vertical cell size resolution of the mesh was restricted by the maximum dune surface roughness height (z_0) of 0.05 m. Each simulation was deemed complete when the residuals for each variable being solved (velocity, pressure, turbulent kinetic energy and energy dissipation) decreased by 4 orders of magnitude.

2.2.1 Computational Boundary conditions

In each simulation vertical profiles of wind speed (U), turbulent kinetic energy (k) and energy dissipation (ε) at the inlet boundary were defined assuming a constant shear velocity (u_*) value with height using equations 1, 2 and 3 (Richards and Hoxey, 1993 and Blocken et al., 2006):

$$U(z) = \frac{u_*}{k} \ln\left(\frac{z + z_0}{z_0}\right) \quad (1)$$

$$\kappa(z) = \frac{u_*}{\sqrt{C_\mu}} \quad (2)$$

$$\varepsilon(z) = \frac{u_*^3}{k(z+z_0)} \quad (3)$$

Where z is the height above the surface, k is the von Karman constant (0.42), z_0 is the surface roughness length and C_μ a constant of 0.09.

To examine how flow dynamics changed with wind speed, simulations were conducted using 4 values of u_* ranging from a minimum of 0.24 m s^{-1} to 0.60 m s^{-1} (Table 1). For each simulation a surface surrounding the dune was prescribed a surface roughness constant (z_0) of 0.0005 m, the equivalent of a sand surface (Bagnold, 1960). To test how jet dynamics change with roughness height, the foredune was prescribed roughness heights equivalent to that of bare sand (z_0 0.0005 m (Bagnold, 1954)), *Ammophila breviligulata* (z_0 0.01 m (Olson, 1958)), and thin grass 0.5 m high (z_0 0.05 m (Sutton, 1953)).

Table 1. Shear velocities (m s^{-1}) and equivalent wind speeds (m s^{-1}) at 1 m above the surface at the inlet of the computational domain for each simulation assuming a z_0 of 0.0005 m.

Shear Velocity (m s^{-1})	Wind Speed 4 m above surface (m s^{-1})
0.23	5.0
0.35	7.5
0.47	10
0.58	12.5

.

3. Location of the Jet Formation

Because it is often the case that there are not enough instrumented masts in the field to adequately cover a foredune, it cannot be determined exactly where on the stoss face or near-crest region the jet flow is first formed. Thus, the CFD model was utilized to examine where the jet first forms on the foredune. Figure 2 illustrates seven locations across the upper stoss, crest and lee slope where velocity profiles were modelled in order to examine the first point of jet formation, and its downwind extension past the crest (if it occurs).

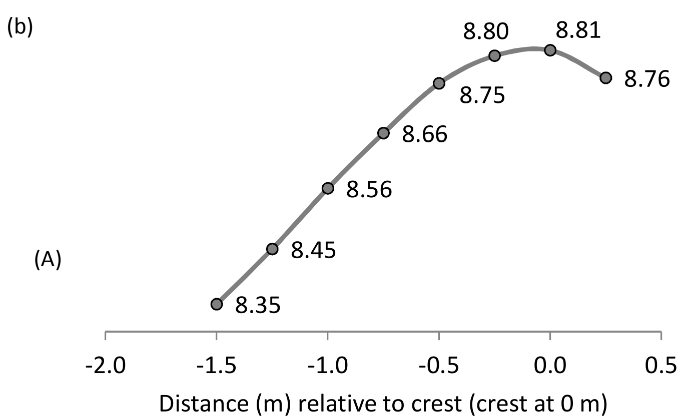

Figure 2a. Location of the seven points on the upper stoss slope, crest and lee slope sampled for CFD velocity profiles. The vertical height (m) of each location is labelled. Distance indicated by the x axis is relative to the dune crest (at 0 m).

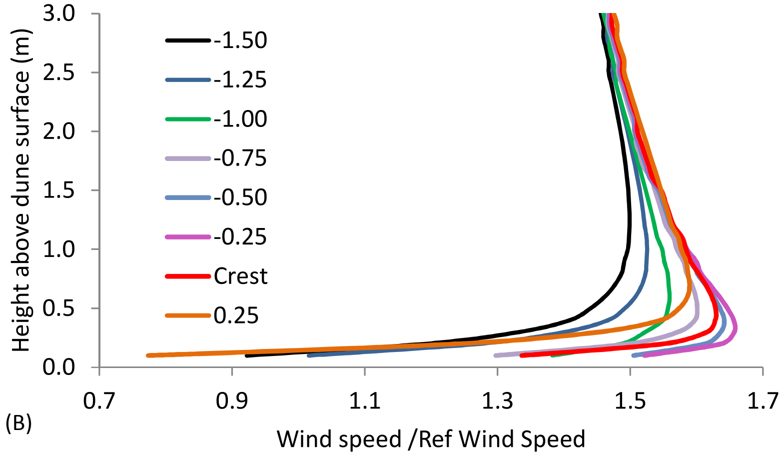

Figure 2b. Wind velocity profiles from the upper stoss slope starting at – 1.5m upwind (down-slope) of the crest (the red line, at 0m) (locations in 2a) -and down the upper lee slope for a 0° incident wind (i.e. perpendicular to the dune crest). The velocity profiles indicate progressive acceleration up the stoss slope and the jet flow appears at ~1m seawards of the dune crest. Ref wind speed refers to wind speed 4 m above the surface at the inlet.

In order to assess this, the wind velocity profiles were modelled at intervals of 0.25m across the P.E.I. -foredune from upper stoss position over the crest, and down the lee slope to determine where the jet flow structure was initiated (Figure 2a). The transect utilized was the scarped profile, and a roughness height equivalent to *Ammophila breviligulata* (z_0 0.01 m) was applied to the foredune slope. Figure 2b demonstrates that the flow progressively accelerates up the stoss slope as observed in many similar dune and ridge studies [(e.g. Arens et al., 1995; Finnigan, 2007; Walker et al., 2006, 2009; Bauer et al., 2013; Hesp et al., 2009, 20154]). While there is some slight indication of jet formation at -1.5m, a clear jet is formed at 1.0m seawards of the crest. The flow becomes better defined as a more pronounced speed bulge (or nose) develops at around 50cm above the bed at -0.75 to -0.5m~~in the next 50cm horizontal distance downwind (or ~~upslope~~)~~, and is most pronounced at -0.25m seawards or downslope of the crest (Figure 2b). Note that the crest is itself quite convex and rounded (Figure 2a). The jet shifts upwards (to around 0.75m above the surface) and becomes more bulbous in the profile at 0.25m past the crest. It is likely that the very top of the crest is the point at which lee flow separation begins, and as this develops, the higher speed jet component of the flow is forced upwards over the separation envelope as observed in other studies [(cf. Hsu, 1977]). In addition, the flow tends to sweep upwards across the crest directed by the steep angle of the stoss slope, so the jet will tend to move upwards in the profile as it crosses the dune crest. Flow velocities are low near the surface in the lee of the dune crest due to flow separation development in this region.

The wind velocity profile with embedded jet at the dune crest displays a similar structure to that encountered in the field at P.E.I. (Hesp et al., 2009, 2013), and provides partial validation of the modelling. The vertical height above the bed at which the jet is most pronounced (the apex of the nose) in the modelling is lower by approximately 50cm (at the crest) to 25cm (just downwind of the crest) than that encountered in the field. This is likely due to the presence of vegetation in the field, whereas there is no vegetation present on the modelled surface.

4. Jet Structure and Incident Wind Speed

As noted in the introduction, observations of jets formed during different incident wind speeds have been made [(e.g. Hsu, 1977; Arens et al., 1995; Hesp et al., 2009, 2013]), but it is unclear if variations in incident wind speed actually produce changes in the jet formation or shape. Figure 3 shows wind velocity profiles simulated via CFD for four quite different incident wind velocities (5 m s^{-1} to 12.5m s^{-1} at 4m above the surface on the beach) for a directly onshore flow.

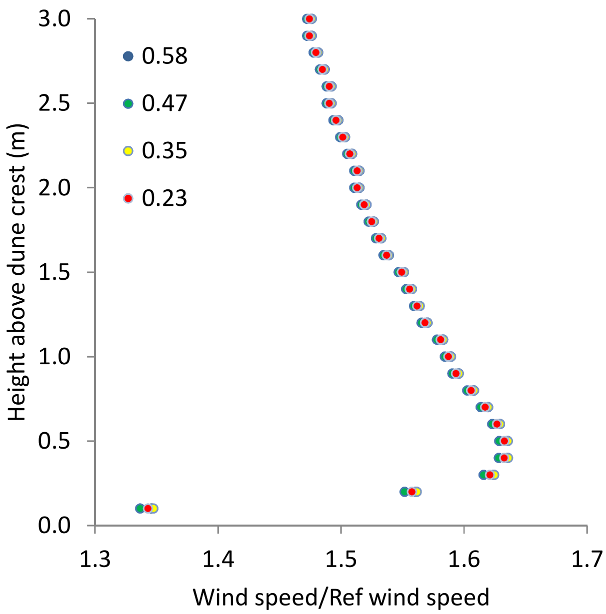

Figure 3. Percent wind velocity profiles at the crest of the foredune for a directly onshore flow. Jets were produced for a range of shear velocities (u_* 0.23 – 0.58) equivalent to incident wind speeds of 5.0 to 12.5ms^{-1} at 4 m height on the beach upwind of the foredune. Ref wind speed refers to wind speed 4 m above the surface at the inlet.

Jet flow was produced at the foredune crest for all four wind speeds tested (Figure 3) thereby indicating that once the flow velocity is above the threshold for sand transport, wind speed is not a factor determining whether a jet is present or not. Whilst it superficially appears as if the jet becomes more pronounced as wind speed increases (as in Hesp et al., 2013, their Figure 6)), when the results are made relative to the incident wind speed on the beach (at 4m height), all the four percent velocity profiles in Figure 3 virtually overlap, and there is only a very slight difference apparent indicating that incident wind speed has minimal effect on jet development.

5. Jet Development and Incident Wind Direction

Field observations of jets (e.g. Hesp et al., 2013) indicates that the jets vary according to incident wind direction. In order to test the influence of incident wind direction on jet development, a range of incident wind approach angles from 10° to 70° (almost perpendicular to almost dune crest parallel) were examined via the CFD model (Figure 4). Figure 1 illustrates the 2-D topographic profiles for the range of incident winds modelled. These show the relative slopes that the incident wind would encounter or "see" as it crosses the dune. Note how the slopes flatten considerably and elongate as the incident wind flow becomes increasingly oblique to the dune crest.

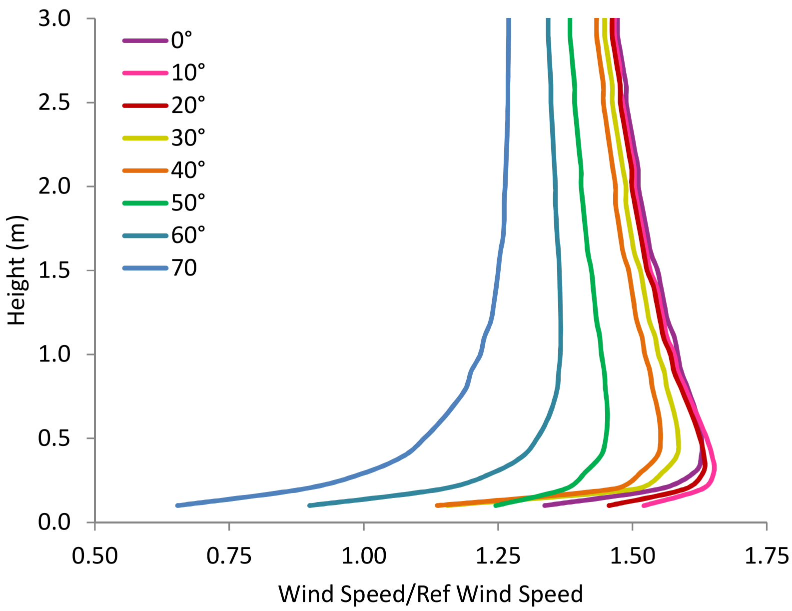

Figure 4. Comparison of the foredune crest percent wind velocity profiles for a range of incident wind directions. Zero (0°) indicates directly onshore winds. Jet development is not present at an incident approach direction of 60° but is present by 50°, and is most pronounced for onshore to low angle oblique winds. Ref wind speed refers to wind speed 4 m above the surface at the inlet.

The incident wind angle/stoss slope has a significant impact on the production of a jet at the crest. As the incident angle becomes more oblique, making the slope less steep, the jet becomes slower and less defined until it is not discernable past 50° incident wind approach angle (Figure 4). In the field Hesp et al. (2013) found that a jet did not develop when the incident wind was from an angle >55°.

In three dimensions, the flow is topographically steered before reaching the dune crest (Walker et al., 2006; Hesp et al., 2015).This may cause the jet to form at more oblique incident angles than has been found here.

The jet is also more pronounced (i.e. more defined nose) in the vertical profile during winds that are perpendicular to the crest, likely because the stoss slope is steepest for these incident winds, and perhaps because of the presence of a more defined separation zone, which starts to limit the near surface wind speed near or at the crest.

Wind speed at the crest also decreases as incident wind direction becomes more oblique ~~[~~(cf. Walker et al., 2009; Hesp et al., 2015~~]~~). The degree and magnitude of jet development for three incident directions (0°, 40° and 70°) may be seen in Figure59. The red zone indicates a high speed jet zone or region, and this is most pronounced in perpendicular flows. As ~~the dune profile flattens and lengthens and~~ the wind becomes increasingly oblique and the dune profile flattens and lengthens, the red zone decreases in size and the velocity declines. The degree of speedup also decreases as the incident flow becomes more oblique as indicated by the speed zones in Figure 5.

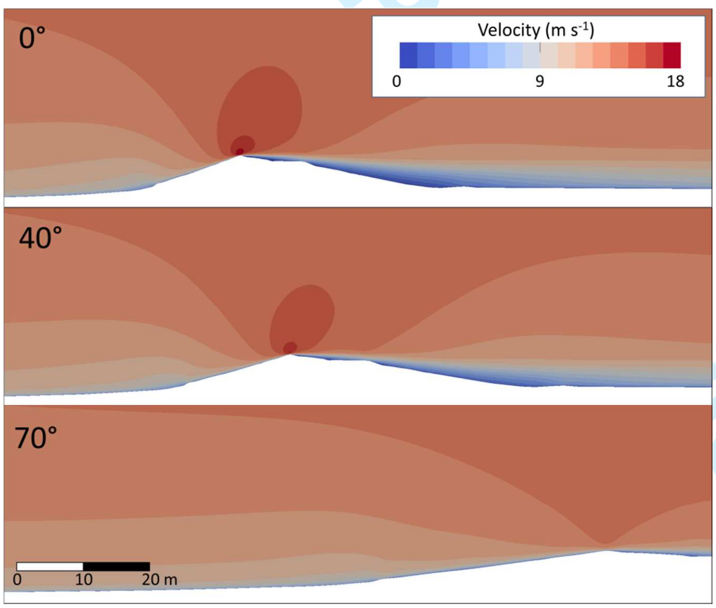

Figure 5. The degree and magnitude of jet development for three incident directions (0° - directly onshore, 40° and 70°). The jet is most pronounced and has the greatest aerial extent when winds are perpendicular to the foredune crest.

Figure 6 displays the maximum jet velocity developed at the foredune crest for each incident wind direction (Figure 6a), and the percent jet velocity relative to winds at 3m above the dune crest (Figure 6b). Figure 6c illustrates the log regressions of the vertical profiles of wind velocity up to 3 m height, and shows that as the incident wind becomes more oblique, the profile becomes more logarithmic. There are clear relationships between these such that the maximum jet speed declines as the incident wind direction becomes more oblique to highly oblique, relative jet velocities are highest compared to flow at 3 m above the foredune crest for directly onshore flow, and the velocity profiles progressively deviate from logarithmic as the incident flow becomes less oblique. The latter has clear implications for those wishing to determine shear stress at the bed from velocity profiles where jets are present. All plots have very high R^2 values.

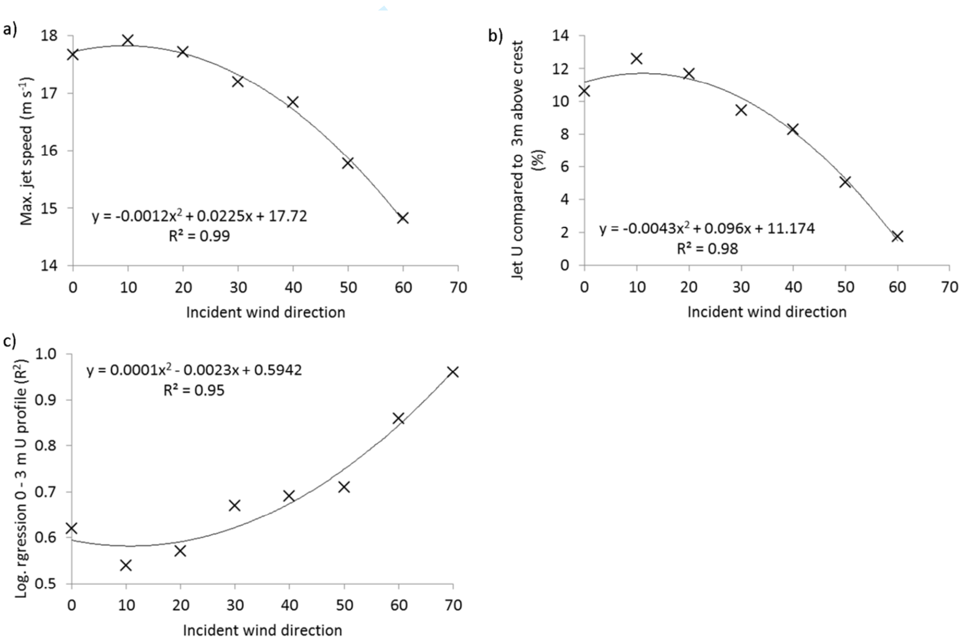

Figure 6. Maximum jet velocity developed at the foredune crest for each incident wind direction (a), the percent jet velocity relative to winds at 3m above the dune crest (b) and the log regressions of the vertical profiles of wind velocity up to 3 m height (c).

6. Jet development for varying surface roughness

Figure 7 displays jet development for three surface roughness lengths based on data provided by Maun (2009) and for the same incident onshore wind velocity. It is apparent that the greatest jet development occurs for a bare sand surface with a very low roughness, and decreases with the presence of vegetation. However, there is little difference between a cover of *Ammophila Breviligulata* and thick grass (as defined by Maun, (2009)).

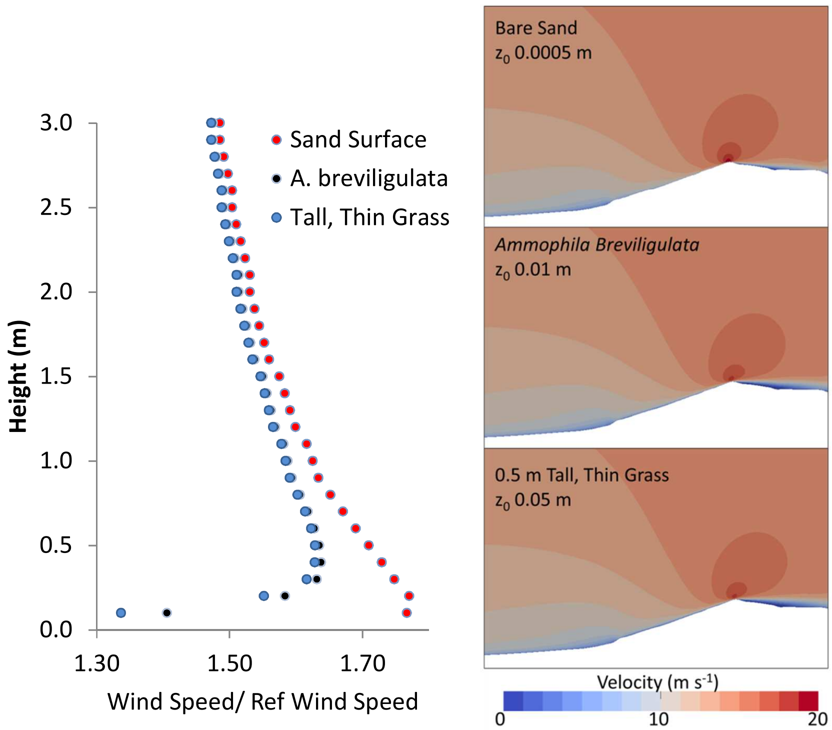

Figure 7. Jet development for three different surface roughness lengths. The presence of vegetation retards the degree of jet development. Ref wind speed refers to wind speed 4 m above the surface at the inlet.

7. Scarped versus non-scarped foredune topography and jet development

Scarps are very commonly formed on foredunes since they occupy the seaward most position on the backshore ~~[~~(Carter et al., 1990; Hesp, 2002; Christiansen and Davidson-Arnott, 2004~~]~~). In the discussion above, the CFD modelling (and previous field work) was conducted over the P.E.I. foredune which exhibited a small 0.7m high scarp. Since it is also common for jets to be formed over the crest of such scarps ~~[~~(Bowen and Lindley, 1977; Hesp et al., 2013~~]~~), the presence of the scarp and attendant jet may have a downwind influence on the development of the foredune crest jet. A 2-D CFD comparison was conducted between the scarped profile and the same profile minus the scarp in order to determine if the scarp has a downwind effect on flow near the crest. Figure 8 demonstrates that the presence of the 0.7m high scarp does indeed influence the structure of the crest jet, in that the jet is more pronounced where the scarp is present. The highest velocities are also slightly closer to the bed. This may occur due to the scarp jet shedding higher velocity and more turbulent eddies downwind up the foredune stoss face compared to the situation where the scarp is not present.

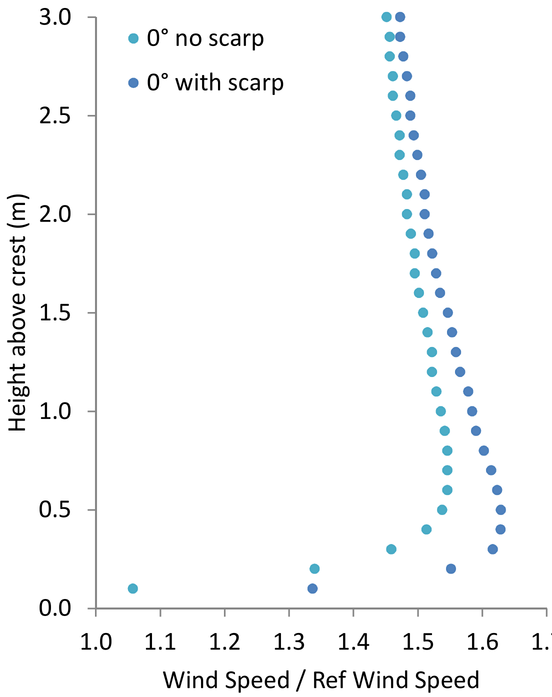

Figure 8. Wind velocity profiles measured at the foredune crest for an onshore 2-D flow for the scarped (0.7m high) and non-scarped morphology. The jet is marginally faster (5%) at the crest where the scarp is present. Ref wind speed refers to wind speed 4 m above the surface at the inlet.

The presence of the scarp at the dune toe leads to slightly greater development of the jet on the foredune ridge crest. The pressure fields were also examined for this comparison and show that (i) the high pressure zone which develops over the scarp region does not extend as far downwind across the foredune lower stoss slope compared to the non-scarped foredune, and, (ii) the low pressure zone over the dune crest is much higher (25%) for the scarped dune compared to the non-scarped dune.

8. Conclusions

The following conclusions can be derived from this study:

1. CFD modelling has successfully replicated jet flow development at a foredune crest region;

2. an increase in incident wind velocity does not affect the magnitude of jet flow;

3. a jet is first formed at ~1.0 m seawards of the foredune crest on the Prince Edward Island foredune morphology example examined here. The flow becomes better defined as a more pronounced nose develops at around 50 cm above the bed upslope, and is best developed at 0.25 m seawards of the dune crest. The jet shifts upwards and becomes slightly more bulbous in the profile just landwards or past the foredune crest and then disappears;

4. the jet is most pronounced and has the greatest aerial extent when winds are perpendicular to the foredune crest;

5. in the CFD modelling a jet did not develop a few degrees after an incident wind approach angle of 50° because there is significantly less flow acceleration across a much lower slope at anincident wind greater than ~55°;

6. the jet is higher in the vertical profile during winds that are more perpendicular to the dune crest in the 0° to 30° range of incident winds;

7. the degree of surface roughness influences the degree of jet development such that jets are better developed when the surface is bare compared to when vegetation is present;

8. the presence of a scarp at the dune toe does slightly influence the structure of the crest jet, in that the jet is more pronounced where a scarp is present.

9. jets are probably more common over dunes and similar topographies than believed or found due to (i) post data collection smoothing of velocity profiles (cf. Frank and Kocurek, 1996), or (ii) the fact that many field based wind profiling experiments do not have enough instruments stacked at closely spaced heights above the surface to be able to detect their presence.

Future research aims to examine the relationships between foredune morphology (particularly height and stoss slope gradient) and jet development, the nature of jet breakdown or dispersion, the nature of secondary circulation and instabilities in jets [(see e.g. Ruith et al 2003; Cala et al 2006]), and the dynamics and relationships between jet flow and reversing vortices within flow separation envelopes at, and past the foredune crest.

Acknowledgements

The authors thank the School of the Environment and Faculty of Science and Engineering, Flinders University for equipment grants to P. H. and post-doctoral funding to T.S., and support, the Flinders University supercomputer facility, the P.E.I. aeolianistas, Robin, Ian, Bernie and Jeff, a grant (1024125) from NSF to P. Hesp, and Æolus for his continued ministry. The data in this paper are available by contacting the corresponding author.

References

Abramovich, G. N. (1963), *Theory of Turbulent Jets*, MIT Press, Cambridge.

Allen, J. R. L. (1982), Sedimentation from jets and separated flows, in Sedimentary Structures Their Character and Physical Basis: 133–171, Elsevier Scientific Publishing Company, Amsterdam.

Arens, S. M. (1996), Patterns of sand transport on vegetated foredunes, *Geomorphology*, *17*, 339–350.

Arens, S. M., H. M. E. Van Kaam-Peters, and J. H. Van Boxel (1995), Air flow over foredunes and implications for sand transport, *Earth Surface Processes and Landforms*, *20*(4), 315–332, doi:10.1002/esp.3290200403.

Bacciotti, F., T. P. Ray, J. Eisloffel, J. Woitas, J. Solf, R. Mundt, and C. . Davis (2003), Observations of Jet Diameter, Density and Dynamics, *Astrophysics and Space Science*, *287*, 3–13.

Bauer, B. O., Davidson-Arnott, R.G.D., Walker, I.J., Hesp, P.A., Ollerhead, J., 2012. Wind direction and complex sediment transport response across a beach-dune system, Earth Surface Processes and Landforms, 37(15), 1661–1677, doi:10.1002/esp.3306.

Bauer, B. O., Davidson-Arnott, R.G.D., Hesp, P.A., Namikas, S.L., . Ollerhead, J., Walker, I.J., 2009. Aeolian sediment transport on a beach: Surface moisture, wind fetch, and mean transport, Geomorphology, 105(1-2), 106–116, doi:10.1016/j.geomorph.2008.02.016.

Bauer, B.O., Hesp, P.A., Walker, I.J., Davidson-Arnott, R.G.D., 2015. Sediment (dis)continuity across a beach-dune profile during an offshore wind event. Geomorphology 245: 135-148.

Bauer, B. O., I. J. Walker, A. C. W. Baas, D. W. T. Jackson, C. M. Neuman, G. F. S. Wiggs, and P. A. Hesp (2013), Critical Reflections on the Coherent Flow Structures Paradigm in Aeolian Geomorphology, in *Coherent Flow Structures at Earth's Surface*, pp. 111–134, John Wiley & Sons, Ltd.

Bennett, S.J., Best, J.L., 1995. Mean flow and turbulence structure over fixed, two-dimensional dunes: implications for sediment transport and bedform stability. Sedimentology 42: 491-513.

Bickley, W. (1939), The Plane Jet, *Phil. Mag. Ser.*, *7*, 727–731.

Birkhoff, G., and E. Zarantonello (1957), *Jets, Wakes and Cavities*, Academic Press, New York.

Blocken, B., T. Stathopoulos, and J. Carmeliet (2007), CFD simulation of the atmospheric boundary layer : wall function problems, *Atmospheric Environment*, *41*(2), 238–252.

Bowen, A. J., and D. Lindley (1977), A wind-tunnel investigation of the wind speed and turbulence characteristics close to the ground over various enscarpment shapes, *Boundary-Layer Meteorology*, *12*(1977), 259–271.

Bridge, J.S., Best, J.L., 1988. Flow, sediment transport and bedform dynamics over the transition from dunes to upper-stage plane beds: implications for the formation of planar lamination. Sedimentology 35, 753-763.

Brook, R. A. (1985), The Koorin nocturnal low-level jet, *Boundary-Layer Meteorology*, *32*, 133–154.

Burkinshaw, J.R., Illenberger, W.K., Rust, I.C., 1993. Wind speed profiles over a reversing transverse dune. In: Pye, K. (ed.), The Dynamics and Environmental Context of Aeolian Sedimentary Systems. Geol. Soc. Spec. Publication No. 72: 25-36.

Cala, C. E., E. C. Fernandes, M. V Heitor, and S. I. Shtork (2006), Coherent structures in unsteady swirling jet flow, *Experiments in Fluids*, *40*(2), 267–276, doi:10.1007/s00348-005-0066-9.

Carter, R. W. G. (1988), *Coastal Environments. An Introduction to the Physical, Ecological and Cultural Systems of Coastlines*, Academic Press, London.

Carter, R. W. G., P. A. Hesp, and K. F. Nordstrom (1990), Geomorphology of erosional dune landscapes, in *Coastal Dunes: Processes and Morphology*, edited by K. F. Nordstrom, N. Psuty, and R. W. G. Carter, pp. 217–250, John Wiley & Sons, Ltd.

Chapman, C. A., I. J. Walker, P. A. Hesp, B. O. Bauer, and R. G. D. Davidson-Arnott (2011), Turbulent Reynolds stress and quadrant event activity in wind flow over a coastal foredune, *Geomorphology*, *151-152*, 1–12, doi:10.1016/j.geomorph.2011.11.015.

Chapman, C., I. J. Walker, P. a. Hesp, B. O. Bauer, R. G. D. Davidson-Arnott, and J. Ollerhead (2013), Reynolds stress and sand transport over a vegetated foredune, Earth Surface Processes and Landforms, 38(14), 1735–1747, doi:10.1002/esp.3428.

Formatted: Font: (Default) Times New Roman, 12 pt, Not Italic

Christiansen, M. B., and R. Davidson-arnott (2004), Rates of Landward Sand Transport over the Foredune at Skallingen , Denmark and the Role of, *Danish Journal of Geography*, *104*(1), 31–43.

Davidson-Arnott, R. G. D., B. O. Bauer, I. J. Walker, P. A. Hesp, and J. Ollerhead (2009), Instantaneous and Mean Aeolian Sediment Transport Rate on Beaches : an Intercomparison of Measurements from Two Sensor Types, *Journal Of Coastal Research Special Issue*, (56), 297–301.

Davidson-Arnott, R. G. D., B. O. Bauer, I. J. Walker, P. a. Hesp, J. Ollerhead, and C. Chapman (2012), High-frequency sediment transport responses on a vegetated foredune, *Earth Surface Processes and Landforms*, *37*(11), 1227–1241, doi:10.1002/esp.3275.

Davidson-arnott, R. G. D., Y. Yang, J. Ollerhead, P. A. Hesp, and I. J. Walker (2008), The effects of surface moisture on aeolian sediment transport threshold and mass flux on a beach, *Earth Surface Processes an*, *33*, 55–74, doi:10.1002/esp.

Delgado-Fernandez, I., and R. Davidson-Arnott (2011), Meso-scale aeolian sediment input to coastal dunes: The nature of aeolian transport events, *Geomorphology*, *126*(1-2), 217–232, doi:10.1016/j.geomorph.2010.11.005.

Delgado-Fernandez, I., R. Davidson-Arnott, and J. Ollerhead (2009), Application of a Remote Sensing Technique to the Study of Coastal Dunes, *Journal of Coastal Research*, 1160–1167, doi:10.2112/09-1182.1.

Delgado-Fernandez, I., R. G. D. Davidson-Arnott, B. O. Bauer, I. J. Walker, and J. Ollerhead (2013), Evaluation of the optimal resolution for characterizing the effect of beach surface moisture derived from remote sensing on Aeolian transport and deposition, *Journal Of Coastal Research Special Issue*, (65), 1277–1282.

Finnigan, J. J. (2007), The turbulent wind in plant and forest canopies, in *Plant Disturbance Ecology: The Process and Response*, edited by E. A. Johnson and K. Miyanishi, pp. 15–58, Elsevier, Amsterdam.

Finnigan, J. J., and S. E. Belcher (2004), Flow over a hill covered with a plant canopy, *Quarterly Journal of the Royal Meteorological Society*, *130*(596), 1–29, doi:10.1256/qj.02.177.

Finnigan, J. J., and Y. Brunet (1995), Turbulent airflow in forests on flat and hilly terrain, in *Wind and Trees*, edited by M. P. Coutts and J. Grace, pp. 3–40, Cambridge University Press, Cambridge UK.

Frank A.J., Kocurek G. 1996. Airflow up the stoss slope of sand dunes: limitations of current understanding. Geomorphology 17: 47-54.

Haller, M. C., and R. A. Dalrymple (2001), Rip current instabilities, *J. Fluid Mech.*, *433*, 161–192.

Hesp, P.A. (2002), Foredunes and blowouts: initiation, geomorphology and dynamics, *Geomorphology*, *48*(1-3), 245–268, doi:10.1016/S0169-555X(02)00184-8.

Hesp, P. A., and I. J. Walker (2011), Three-dimensional æolian dynamics within a bowl blowout during offshore winds: Greenwich Dunes, Prince Edward Island, Canada, *Aeolian Research*, *3*, 389–399, doi:10.1016/j.aeolia.2011.09.002.

Hesp, P. A., and M. Martinez (2007), Disturbance in coastal dune ecosystems, in *Plant Disturbance Ecology: The Process and Response*, edited by E. A. Johnson and K. Miyanishi, pp. 215–247, Elsevier, Amsterdam.

Hesp, P. A., and R. Hyde (1996), Flow dynamics and geomorphology of a trough blowout, *Sedimentology*, *43*, 505–525.

Hesp, P. A., I. J. Walker, C. Chapman, R. Davidson-Arnott, and B. O. Bauer (2013), Aeolian dynamics over a coastal foredune, Prince Edward Island, Canada, *Earth Surface Processes and Landforms*, *38*(1), 1566–1575, doi:10.1002/esp.3444.

Hesp, P. A., I. J. Walker, S. L. Namikas, B. O. Bauer, J. Ollerhead, and M. Allison (2009), Storm Wind Flow over a Foredune , Prince Edward Island , Canada, *Journal of Coastal Research*, (SI 56), 312–316.

Hesp, P. A., R. Davidson-Arnott, I. J. Walker, and J. Ollerhead (2005), Flow dynamics over a foredune at Prince Edward Island, Canada, *Geomorphology*, *65*(1-2), 71–84, doi:10.1016/j.geomorph.2004.08.001.

Hesp, P. A., T. A. G. Smyth, P. Nielsen, I. J. Walker, B. O. Bauer, and R. Davidson-Arnott (2015), Flow deflection over a foredune, *Geomorphology*, *230*(0), 64–74, doi:http://dx.doi.org/10.1016/j.geomorph.2014.11.005.

Hsu, S. A. (1977), Boundary-layer Meteorological research in the coastal zone, *Geoscience and Man*, *XVIII*, 99–111.

Jackson, D. W. T., Beyers, J.H.M., Lynch, K., Cooper, J. A. G., Baas, A. C.W., Delgado-Fernandez, I., 2011. Investigation of three-dimensional wind flow behaviour over coastal dune morphology under offshore winds using computational fluid dynamics (CFD) and ultrasonic anemometry. Earth Surface Processes and Landforms 36, 1113–1124. doi:10.1002/esp.2139

Joshi, P. B. (1982), Hydromechanics of tidal jets, *Journal of the Waterway Port Coastal and Ocean Division*, *108*(3), 239–253.

Joubert, E.C., Harms, T.M., Muller, A., Hipondoka, M., Henschel, J.R., 2012. A CFD study of wind patterns over a desert dune and the effect on seed dispersion. Environmental Fluid Mechanics 12, 23–44. doi:10.1007/s10652-011-9230-3

Kostaschuk, R., and Villard, P., 1996. Flow and sediment transport over large subaqueous dunes: Fraser River, Canada. Sedimentology 43: 849-863.

Kraus, H., J. Malcher, and E. Schaller (1985), A nocturnal low level jet during PUKK, *Boundary-Layer Meteorology*, *31*(2), 187–195, doi:10.1007/BF00121177.

Formatted: Font: (Default) Times New Roman, 12 pt

Formatted: Font: (Default) Times New Roman, 12 pt

Lancaster N., Nickling W.G., McKenna Neuman C.K., Wyatt, V.E., 1996. Sediment flux and airflow on the stoss slope of a barchan dune. Geomorphology 17: 55-62.

Mattingly, G. E., and W. O. Criminale (1972), The stability of an incompressible two-dimensional wake, *Journal of Fluid Mechanics*, *51*, 233–272, doi:10.1017/S0022112072001193.

Maun, M. A. (2009), *The Biology of Coastal Sand Dunes*, Oxford University Press.

Moth Iversen, T.C., Lindegaard, K., Sand-Jensen, K., Thorup, J., 1989. Vandlobsokologi (Watercourse Ecology), Freshwater-Biological laboratory, Copenhagen University.

Ollerhead, J., R. Davidson-Arnott, I. J. Walker, and S. Mathew (2012), Annual to decadal morphodynamics of the foredune system at Greenwich Dunes, Prince Edward Island, Canada, *Earth Surface Processes and Landforms*, *38*(3), 284–298, doi:10.1002/esp.3327.

Olson, J.S., 1958. Lake Michigan dune development. 1. Wind-velocity profiles. J. Geology 66: 254-263.

Omidyeganeh, M., Piomelli, U., Christensen, K.T., Best, J.L., 2013. Large-eddy simulation of flow over barchans dunes. Proc. Marine and River Dune Dynamics – MARID IV, 15-16th April, 2013, Bruges, Belgium: 191-198.

Parish, T. R. (2000), Forcing of the Summertime Low-Level Jet along the California Coast., *Journal of Applied Meteorology*, *39*(12), 2421–2433.

Parsons, D. R., I. J. Walker, and G. F. S. Wiggs (2004), Numerical modelling of flow structures over idealized transverse aeolian dunes of varying geometry, *Geomorphology*, *59*(1-4), 149–164, doi:10.1016/j.geomorph.2003.09.012.

Pattanapol, W., S. J. Wakes, M. J. Hilton, and K. J. M. Dickinson (2007), Modeling of Surface Roughness for Flow Over a Complex Vegetated Surface, *Proceedings of world academy of science, Engineering and*, *26*, 273–281.

Petersen, P. S., M. J. Hilton, and S. J. Wakes (2011), Evidence of aeolian sediment transport across an Ammophila arenaria-dominated foredune, Mason Bay, Stewart Island, *New Zealand Geographer*, *67*(3), 174–189, doi:10.1111/j.1745-7939.2011.01210.x.

Rasmussen, K. R. (1989), Some aspects of flow over coastal dunes, *Proceedings of the Royal Society of Edinburgh Section B: Biological Sciences*, *96*, 129–147.

Rowland, J. C., M. T. Stacey, and W. E. Dietrich (2009), Turbulent characteristics of a shallow wall-bounded plane jet: experimental implications for river mouth hydrodynamics. *Journal of Fluid Mechanics*, *627*, 423–449.

Ruith, M. R., P. Chen, E. Meiburg, and T. Maxworthy (2003), Three-dimensional vortex breakdown in swirling jets and wakes: direct numerical simulation, *Journal of Fluid Mechanics*, *486*, 331–378. doi:10.1017/S0022112003004749.

Schlichting, H. (1955), *Boundary-layer Theory*, 7th 1979 ed., McGraw-Hill, New York.

Smyth, T. A. G., D. W. T. Jackson, and J. A. G. Cooper (2012), Geomorphology High resolution measured and modelled three-dimensional airflow over a coastal bowl blowout, *Geomorphology*, *177-178*, 62–73, doi:10.1016/j.geomorph.2012.07.014.

Smyth, T. A. G., D. W. T. Jackson, and J. A. G. Cooper (2013), Three dimensional airflow patterns within a coastal trough – bowl blowout during fresh breeze to hurricane force winds, *Aeolian Research*, *9*, 111–123.

Sonu, C. J. (1972), Field observation of nearshore circulation and meandering currents, *Journal of Geophysical Research*, *77*(18), 3232–3247, doi:10.1029/JC077i018p03232.

Sutton, O. G. (1953), Micrometeorology: a study of physical processes in the lowest layers of the earth's atmosphere. New York: McGraw-Hill.

Van Boxel, J. H., S. M. Arens, and P. M. Van Dijk (1999), Aeolian processes across transverse dunes. I: Modelling the air flow, *Earth Surface Processes and Landforms*, *24*, 255–270.

van der Knaap, F.C.M., van Mierlo, M.C.L.M., Officier, M.J., 1991. Measurements and computations of the turbulent flow field above fixed bed-forms. In: Soulsby, R. and Bettess, R., (Eds.), Sand Transport in Rivers, Estuaries and the Sea. Proc. Euromech 262 Colloquim on sand transport in Rivers, Estuaries and the Sea, Wallingford, 26-29 june, 1990: 179-185. A.A. Balkema, Rotterdam.

Vogel, S. (1996), *Life in Moving Fluids. The Physical Biology of Flow*, Princeton University Press, New Jersey.

Wakes, S. (2013), Three-dimensional Computational Fluid Dynamic experiments over a complex dune topography, *Journal of Coastal Research*, (S I65), 1337–1342, doi:10.2112/SI65-226.1.

Wakes, S. J., T. Maegli, K. J. Dickinson, and M. J. Hilton (2010), Numerical modelling of wind flow over a complex topography, *Environmental Modelling & Software*, *25*(2), 237–247, doi:10.1016/j.envsoft.2009.08.003.

Walker, I. J. (2005), Physical and logistical considerations of using ultrasonic anemometers in aeolian sediment transport research, *Geomorphology*, *68*(1-2), 57–76, doi:10.1016/j.geomorph.2004.09.031.

Walker, I. J., P. A. Hesp, B. O. Bauer, J. Ollerhead, and M. Allison (2009a), Mean Flow and Turbulence Responses in Airflow over Foredunes : New Insights from Recent Research. *Journal of Coastal Research*, (SI 56), 366–370.

Walker, I. J., P. A. Hesp, R. G. D. Davidson-Arnott, and J. Ollerhead (2006), Topographic Steering of Alongshore Airflow over a Vegetated Foredune: Greenwich Dunes, Prince Edward Island, Canada, *Journal of Coastal Research*, *22*(5), 1278–1291, doi:10.2112/06A-0010.1.

Walker, I. J., P. A. Hesp, R. G. D. Davidson-Arnott, B. O. Bauer, S. L. Namikas, and J. Ollerhead (2009b), Responses of three-dimensional flow to variations in the angle of incident wind and profile form of dunes: Greenwich Dunes, Prince Edward Island, Canada, *Geomorphology*, *105* (1-2), 127–138, doi:10.1016/j.geomorph.2007.12.019.

Walker, I. J., & Shugar, D. H. (2013). Secondary flow deflection in the lee of transverse dunes with implications for dune morphodynamics and migration.*Earth Surface Processes and Landforms*, *38*(14), 1642-1654.

Walmsley, J.L., Howard, A.D., 1985. Application of a boundary-layer model to flow over an eolian dune. Journal of Geophysical Research 90, 631–640.

Wei, W., B. G. Wu, X. X. Ye, H. X. Wang, and H. S. Zhang (2013), Characteristics and Mechanisms of Low-Level Jets in the Yangtze River Delta of China, *Boundary-Layer Meteorology*, *149* (3), 403–424, doi:10.1007/s10546-013-9852-8.Wolfe, S. A., and W. G. Nickling (1996), Shear stress partitioning in sparsely vegetated desert canopies, *Earth Surface Processes and Landforms*, *21*, 607–619.

Wipperman, F.K., Gross, G., 1986. The wind-induced shaping and migration of an isolated dune: A numerical experiment. Boundary-Layer Meteorology 36, 319–334.

Wright, L. D. (1977), Sediment transport and deposition at river mouths: A synthesis, *Geological Society of America Bulletin*, *88*(6), 859–868.

Xianwan, L., L. Sen, and S. Jianyou (1999), Wind tunnel simulation experiment of mountain dunes, *Journal of Arid Environments*, *42*(1), 49–59. doi:http://dx.doi.org/10.1006/jare.1998.0488.

Yakhot, V., S. A. Orszag, S. Thangam, T. B. Gatski, and C. G. Speziale (1992), Development of turbulence models for shear flows by a double expansion technique *Phys. Fluids A*, *7*(May), 1510–1520, doi:10.1063/1.858424.

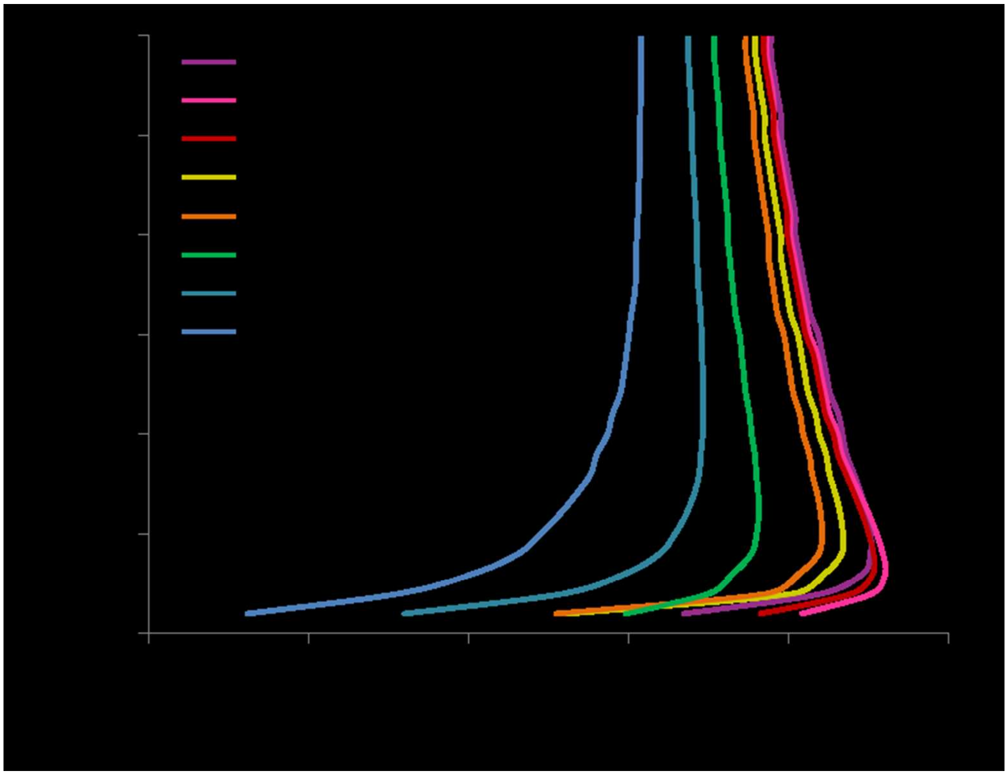

Figure 4. Comparison of the foredune crest percent wind velocity profiles for a range of incident wind directions. Zero (0°) indicates directly onshore winds. Jet development is not present at an incident approach direction of 60° but is present by 50°, and is most pronounced for onshore to low angle oblique winds. Ref wind speed refers to wind speed 4 m above the surface at the inlet.
136x104mm (150 x 150 DPI)

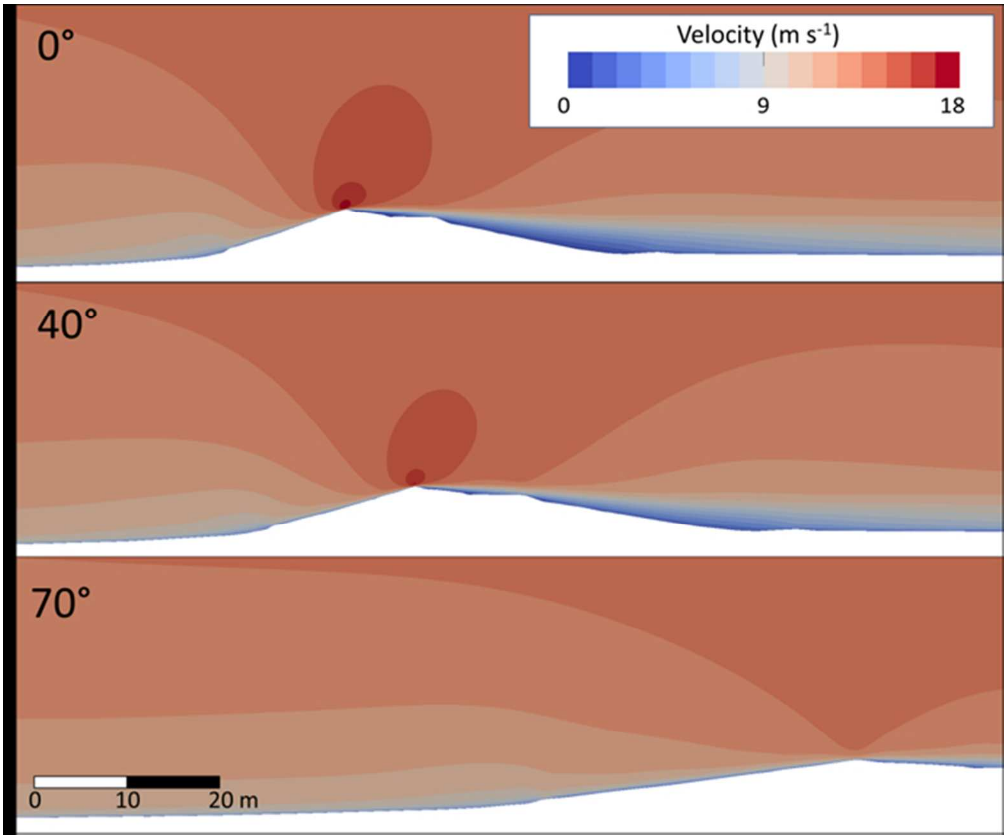

Figure 5. The degree and magnitude of jet development for three incident directions (0° - directly onshore, 40° and 70°). The jet is most pronounced and has the greatest aerial extent when winds are perpendicular to the foredune crest.
116x96mm (150 x 150 DPI)

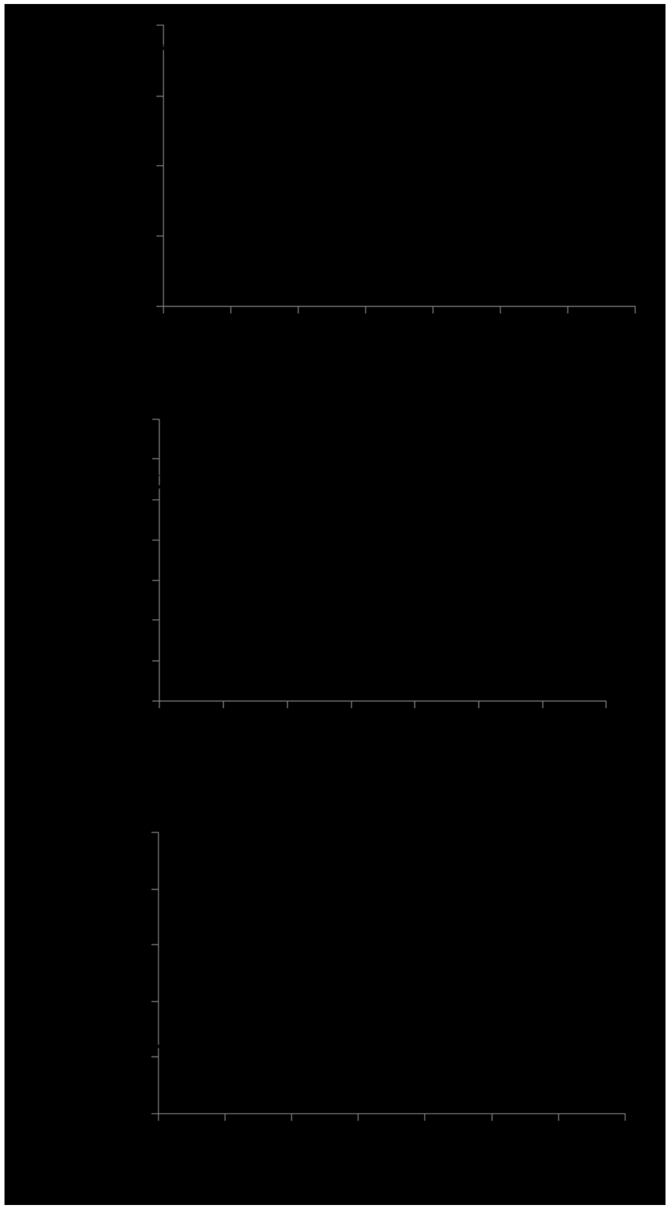

Figure 6. Maximum jet velocity developed at the foredune crest for each incident wind direction (a), the percent jet velocity relative to winds at 3m above the dune crest (b) and the log regressions of the vertical profiles of wind velocity up to 3 m height (c).
134x244mm (150 x 150 DPI)

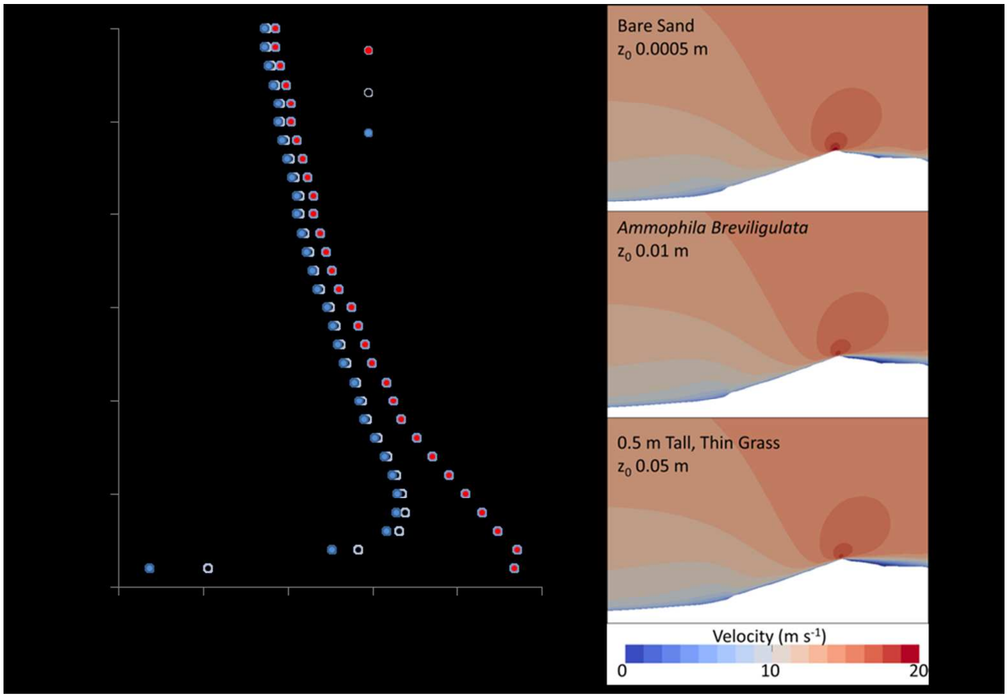

Figure 7. Wind velocity profiles and jet development for three different surface roughness lengths (left side), and isovels over the dune topography and varying surface roughness (right side). The presence of vegetation retards the degree of jet development. Ref wind speed refers to wind speed 4 m above the surface at the inlet.
173x120mm (150 x 150 DPI)

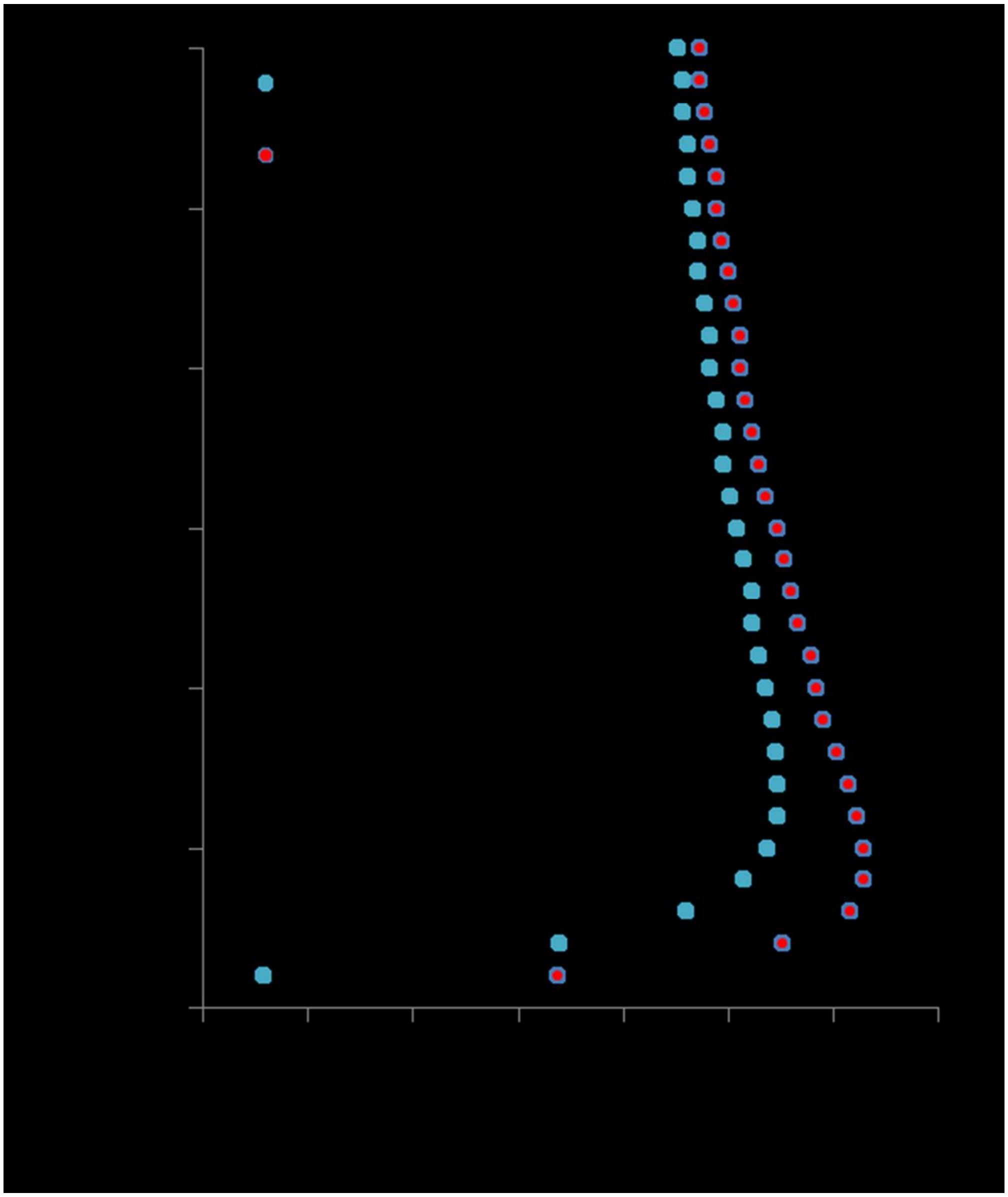

Figure 8. Wind velocity profiles measured at the foredune crest for an onshore 2-D flow for the scarped (0.7m high) and non-scarped morphology. The jet is marginally faster (5%) at the crest where the scarp is present. Ref wind speed refers to wind speed 4 m above the surface at the inlet.
100x118mm (150 x 150 DPI)

0.13	#REF!	
0.55	#REF!	13.83
1.05	#REF!	16.26
1.87	#REF!	15.68
3	#REF!	16.34

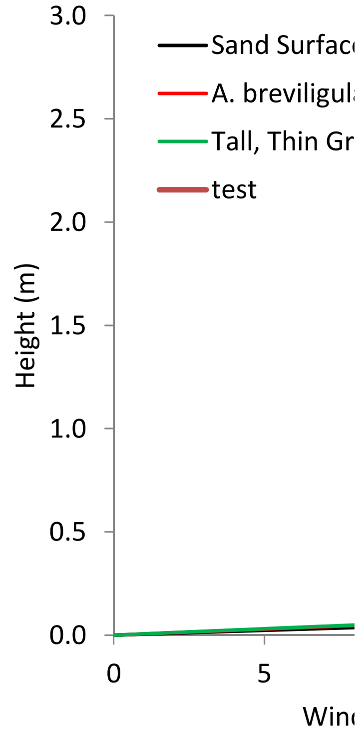

Sand Surface						*A. brevilig*	
	u	v	w	wind speed	rel ws		u
0.001				0		0.001	
0.1	19.1691	0	-0.27924	19.17	1.77	0.1	15.2454
0.2	19.2069	-2.53E-20	0.208724	19.21	1.77	0.2	17.1472
0.3	18.9578	9.63E-18	0.565233	18.97	1.75	0.3	17.6398
0.4	18.7478	7.70E-18	0.749554	18.76	1.73	0.4	17.6938
0.5	18.5283	-6.77E-18	0.899252	18.55	1.71	0.5	17.6533
0.6	18.3087	-1.99E-19	1.01951	18.34	1.69	0.6	17.5641
0.7	18.0935	-3.88E-20	1.11475	18.13	1.67	0.7	17.4492
0.8	17.8849	-3.40E-20	1.18882	17.92	1.65	0.8	17.3214
0.9	17.6837	0	1.24504	17.73	1.63	0.9	17.1876
1	17.5859	4.58E-24	1.26738	17.63	1.63	1	17.1197

1.1	17.4899	0	1.28628	17.54	1.62	1.1	17.0517
1.2	17.3036	-4.75E-20	1.31495	17.35	1.60	1.2	16.9158
1.3	17.2132	-2.88E-18	1.32522	17.26	1.59	1.3	16.8482
1.4	17.1245	2.76E-18	1.33307	17.18	1.58	1.4	16.7811
1.5	17.0377	4.03E-20	1.3387	17.09	1.58	1.5	16.7144
1.6	16.8692	0	1.34403	16.92	1.56	1.6	16.5829
1.7	16.7876	2.17E-18	1.34404	16.84	1.55	1.7	16.5181
1.8	16.7078	-4.17E-18	1.34247	16.76	1.54	1.8	16.4541
1.9	16.6296	2.01E-18	1.33944	16.68	1.54	1.9	16.391
2	16.5533	1.91E-18	1.33507	16.61	1.53	2	16.3287
2.1	16.5533	1.91E-18	1.33507	16.61	1.53	2.1	16.3287
2.2	16.4786	-4.87E-20	1.32946	16.53	1.52	2.2	16.2674
2.3	16.4057	-9.89E-20	1.32271	16.46	1.52	2.3	16.207
2.4	16.3345	-1.63E-18	1.3149	16.39	1.51	2.4	16.1477
2.5	16.265	-1.46E-18	1.30611	16.32	1.50	2.5	16.0894
2.6	16.265	-1.46E-18	1.30611	16.32	1.50	2.6	16.0894
2.7	16.1972	1.42E-18	1.29641	16.25	1.50	2.7	16.0321
2.8	16.1311	8.57E-20	1.28586	16.18	1.49	2.8	15.976
2.9	16.0666	8.12E-20	1.27453	16.12	1.49	2.9	15.921
3	16.0666	8.12E-20	1.27453	16.12	1.49	3	15.921

ulata

v	w	wind speed	rel ws
		0	
0	0.463806	15.25	1.41
-2.50E-20	1.08785	17.18	1.58
9.54E-18	1.48325	17.70	1.63
7.48E-18	1.6502	17.77	1.64
-6.36E-18	1.76292	17.74	1.64
-1.56E-19	1.83631	17.66	1.63
-3.54E-20	1.88102	17.55	1.62
-3.10E-20	1.90449	17.43	1.61
0	1.912	17.29	1.59
3.32E-22	1.91101	17.23	1.59

Tall, Thin Grass

	u	v	w
0.001	19.3835	0	0.577089
0.1	14.5024	0	0.223012
0.2	16.8136	-2.61E-20	0.867937
0.3	17.4856	1.01E-17	1.30734
0.4	17.6023	7.94E-18	1.50223
0.5	17.596	-6.74E-18	1.6391
0.6	17.5238	-1.69E-19	1.73242
0.7	17.4165	-3.69E-20	1.79335
0.8	17.2913	-3.19E-20	1.83014
0.9	17.1579	0	1.84877
1	17.0899	2.77E-22	1.8527

0	1.90737	17.16	1.58	1.1	17.0217	0	1.85363
-4.41E-20	1.89338	17.02	1.57	1.2	16.8854	-4.45E-20	1.84788
-2.67E-18	1.88354	16.95	1.56	1.3	16.8177	-2.69E-18	1.84179
2.55E-18	1.87207	16.89	1.56	1.4	16.7505	2.57E-18	1.83385
3.77E-20	1.85916	16.82	1.55	1.5	16.6838	3.78E-20	1.82428
0	1.82962	16.68	1.54	1.6	16.5525	0	1.80086
2.03E-18	1.81323	16.62	1.53	1.7	16.4879	2.03E-18	1.7873
-3.92E-18	1.79591	16.55	1.53	1.8	16.4242	-3.91E-18	1.77266
1.89E-18	1.77776	16.49	1.52	1.9	16.3614	1.88E-18	1.75704
1.81E-18	1.75885	16.42	1.51	2	16.2995	1.80E-18	1.74054
1.81E-18	1.75885	16.42	1.51	2.1	16.2995	1.80E-18	1.74054
-4.26E-20	1.73927	16.36	1.51	2.2	16.2386	-4.27E-20	1.72324
-9.01E-20	1.71908	16.30	1.50	2.3	16.1786	-9.00E-20	1.70521
-1.55E-18	1.69834	16.24	1.50	2.4	16.1198	-1.54E-18	1.68652
-1.39E-18	1.6771	16.18	1.49	2.5	16.062	-1.39E-18	1.66723
-1.39E-18	1.6771	16.18	1.49	2.6	16.062	-1.39E-18	1.66723
1.36E-18	1.65541	16.12	1.49	2.7	16.0053	1.35E-18	1.64738
8.18E-20	1.63332	16.06	1.48	2.8	15.9497	8.14E-20	1.62704
7.78E-20	1.61086	16.00	1.47	2.9	15.8952	7.73E-20	1.60624
7.78E-20	1.61086	16.00	1.47	3	15.8952	7.73E-20	1.60624

wind speed	rel ws
0.00	
14.50	1.34
16.84	1.55
17.53	1.62
17.67	1.63
17.67	1.63
17.61	1.62
17.51	1.61
17.39	1.60
17.26	1.59
17.19	1.58

17.12	1.58
16.99	1.57
16.92	1.56
16.85	1.55
16.78	1.55
16.65	1.53
16.58	1.53
16.52	1.52
16.46	1.52
16.39	1.51
16.39	1.51
16.33	1.51
16.27	1.50
16.21	1.49
16.15	1.49
16.15	1.49
16.09	1.48
16.03	1.48
15.98	1.47
15.98	1.47

	spd0	spd1	spd2	spd3
0.1	1.25	1.24	1.25	1.25
0.2	1.45	1.44	1.45	1.45
0.3	1.51	1.50	1.51	1.51
0.4	1.52	1.51	1.52	1.52
0.5	1.52	1.51	1.52	1.52
0.6	1.51	1.51	1.51	1.51
0.7	1.50	1.50	1.50	1.50
0.8	1.49	1.49	1.49	1.49
0.9	1.48	1.48	1.48	1.48
1	1.48	1.47	1.48	1.48
1.1	1.47	1.47	1.47	1.47
1.2	1.46	1.45	1.46	1.46
1.3	1.45	1.45	1.45	1.45
1.4	1.45	1.44	1.45	1.45
1.5	1.44	1.44	1.44	1.44
1.6	1.43	1.43	1.43	1.43
1.7	1.42	1.42	1.42	1.42
1.8	1.42	1.41	1.42	1.42
1.9	1.41	1.41	1.41	1.41
2	1.41	1.40	1.41	1.41
2.1	1.41	1.40	1.41	1.41
2.2	1.40	1.40	1.40	1.40
2.3	1.40	1.39	1.40	1.40
2.4	1.39	1.39	1.39	1.39
2.5	1.39	1.38	1.38	1.39
2.6	1.39	1.38	1.38	1.39
2.7	1.38	1.38	1.38	1.38
2.8	1.38	1.37	1.37	1.38
2.9	1.37	1.37	1.37	1.37
3	1.37	1.37	1.37	1.37
	19.0588			

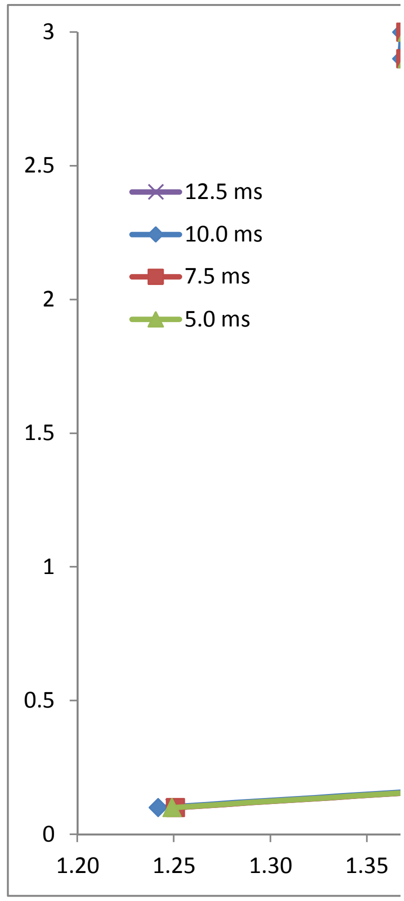

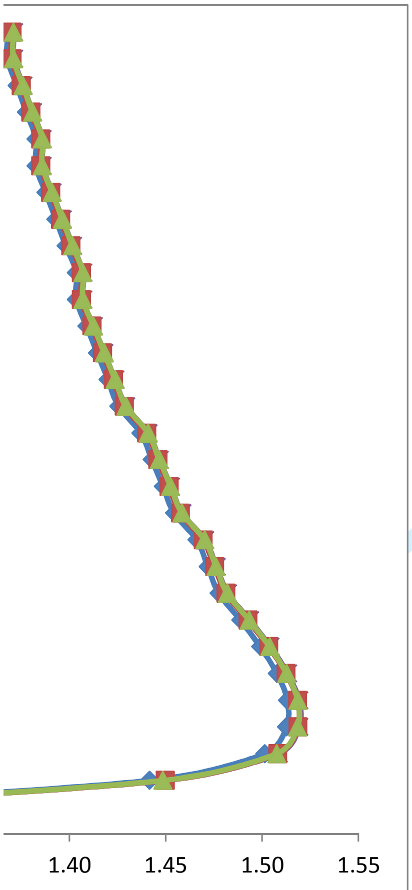

Height	12.5 ms		10.0 ms	
0.1	17.38	1.35	14.50	1.34
0.2	20.15	1.56	16.84	1.55
0.3	20.97	1.62	17.53	1.62
0.4	21.12	1.64	17.67	1.63
0.5	21.1[illegible]	[illegible]	[illegible]	[illegible]
0.6	21.0[illegible]	[illegible]	[illegible]	[illegible]
0.7	20.9[illegible]	[illegible]	[illegible]	[illegible]
0.8	20.7[illegible]	[illegible]	[illegible]	[illegible]
0.9	20.6[illegible]	[illegible]	[illegible]	[illegible]
1.0	20.5[illegible]	[illegible]	[illegible]	[illegible]
1.1	20.4[illegible]	[illegible]	[illegible]	[illegible]
1.2	20.2[illegible]	[illegible]	[illegible]	[illegible]
1.3	20.1[illegible]	[illegible]	[illegible]	[illegible]
1.4	20.1[illegible]	[illegible]	[illegible]	[illegible]
1.5	20.0[illegible]	[illegible]	[illegible]	[illegible]
1.6	19.8[illegible]	[illegible]	[illegible]	[illegible]
1.7	19.7[illegible]	[illegible]	[illegible]	[illegible]
1.8	19.7[illegible]	[illegible]	[illegible]	[illegible]
1.9	19.6[illegible]	[illegible]	[illegible]	[illegible]
2.0	19.5[illegible]	[illegible]	[illegible]	[illegible]
2.1	19.5[illegible]	[illegible]	[illegible]	[illegible]
2.2	19.4[illegible]	[illegible]	[illegible]	[illegible]
2.3	19.4[illegible]	[illegible]	[illegible]	[illegible]
2.4	19.34	1.50	16.21	1.49
2.5	19.27	1.49	16.15	1.49
2.6	19.27	1.49	16.15	1.49
2.7	19.20	1.49	16.09	1.48
2.8	19.13	1.48	16.03	1.48
2.9	19.06	1.48	15.98	1.47
3.0	19.06	1.48	15.98	1.47

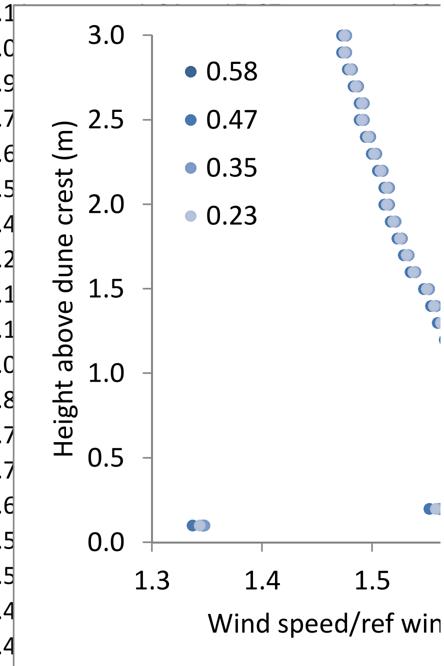

7.5 ms		5.0 ms	
10.44	1.35	6.94	1.34
12.10	1.56	8.05	1.56
12.59	1.62	8.38	1.62
12.68	1.64	8.44	1.63
	1.64	8.44	1.63
	1.63	8.41	1.63
	1.62	8.36	1.62
	1.61	8.30	1.61
	1.60	8.24	1.59
	1.59	8.21	
	1.58	8.17	
	1.57	8.11	
	1.56	8.08	
	1.56	8.04	
	1.55	8.01	
	1.54	7.95	
	1.53	7.92	
	1.53	7.88	
	1.52	7.85	
	1.51	7.82	
	1.51	7.82	
	1.51	7.79	
	1.50	7.76	
11.61	1.50	7.73	
11.56	1.49	7.71	
11.56	1.49	7.71	
11.52	1.49	7.68	
11.48	1.48	7.65	1.48
11.44	1.48	7.62	1.47
11.44	1.48	7.62	1.47

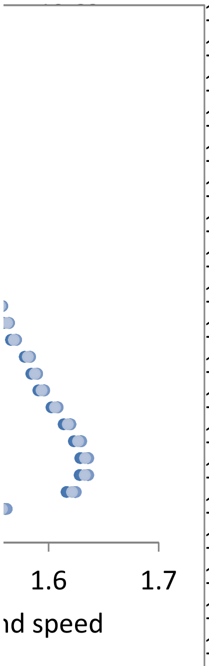

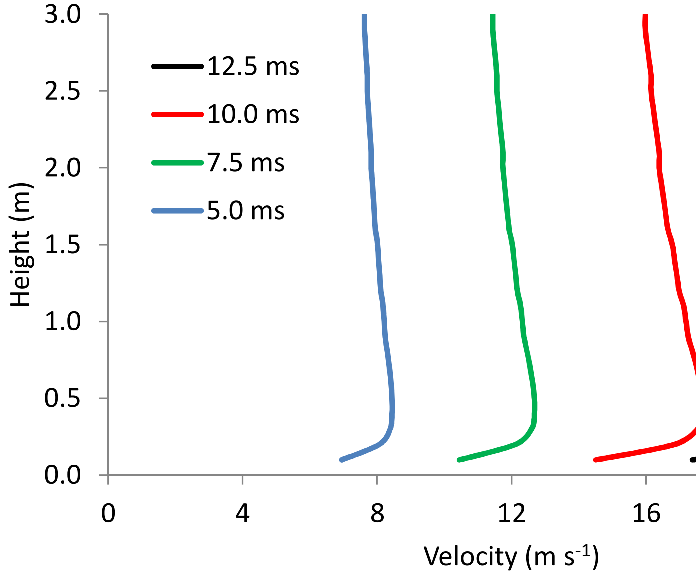


20
24

conv -3

0.001				0.00		0	0.13	0.00
0.1	17.3765	0	0.259494	17.38	1.25		0.55	20.15
0.2	20.1234	-3.11E-20	1.02663	20.15	1.45		1.05	21.12
0.3	20.9098	1.20E-17	1.54846	20.97	1.51		1.87	20.91
0.4	21.0401	9.36E-18	1.77963	21.12	1.52		3	20.27
0.5	21.0254	-7.90E-18	1.94195	21.11	1.52			
0.6	20.9335	-1.98E-19	2.05275	21.03	1.51			
0.7	20.8007	-4.30E-20	2.12525	20.91	1.50			
0.8	20.6474	-3.71E-20	2.16919	20.76	1.49			
0.9	20.4849	0	2.19164	20.60	1.48			
1	20.4024	3.24E-22	2.19648	20.52	1.48			
1.1	20.3196	0	2.19776	20.44	1.47			
1.2	20.1546	-5.15E-20	2.1913	20.27	1.46			
1.3	20.0728	-3.11E-18	2.18424	20.19	1.45			
1.4	19.9917	2.97E-18	2.17499	20.11	1.45			
1.5	19.9113	4.36E-20	2.1638	20.03	1.44			
1.6	19.7532	0	2.13633	19.87	1.43			
1.7	19.6755	2.34E-18	2.12038	19.79	1.42			
1.8	19.5989	-4.51E-18	2.10315	19.71	1.42			
1.9	19.5233	2.17E-18	2.08475	19.63	1.41			
2	19.4489	2.08E-18	2.0653	19.56	1.41			
2.1	19.4489	2.08E-18	2.0653	19.56	1.41			
2.2	19.3756	-4.92E-20	2.04488	19.48	1.40			
2.3	19.3036	-1.04E-19	2.02359	19.41	1.40			
2.4	19.2329	-1.78E-18	2.0015	19.34	1.39			
2.5	19.1634	-1.59E-18	1.97869	19.27	1.39			
2.6	19.1634	-1.59E-18	1.97869	19.27	1.39			
2.7	19.0953	1.55E-18	1.95522	19.20	1.38			
2.8	19.0286	9.36E-20	1.93114	19.13	1.38			
2.9	18.9632	8.88E-20	1.90651	19.06	1.37			
3	18.9632	8.88E-20	1.90651	19.06	1.37			
				% jet	10.8			
				R2	0.07			

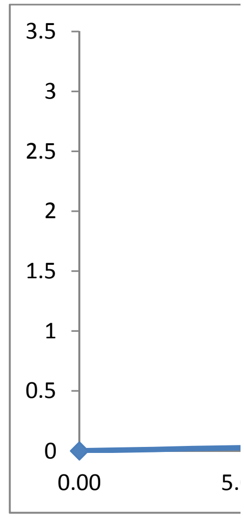

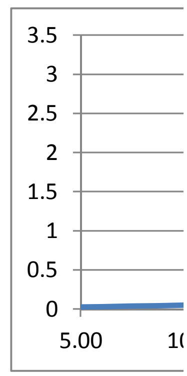

13.83
16.26
15.68
16.34

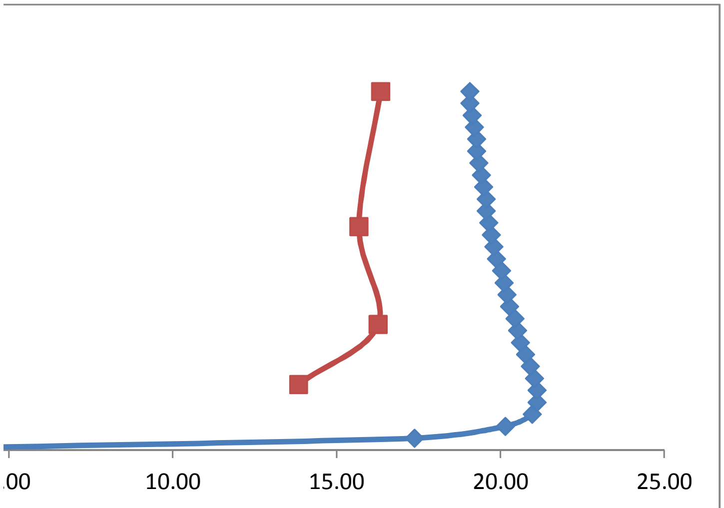

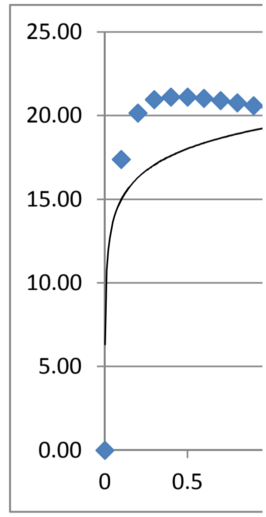

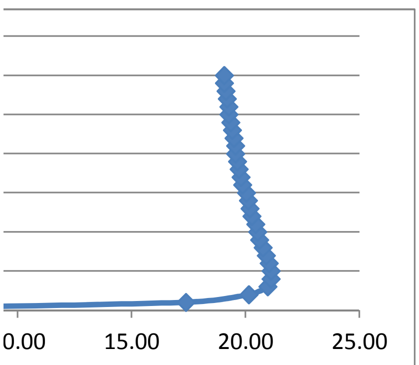

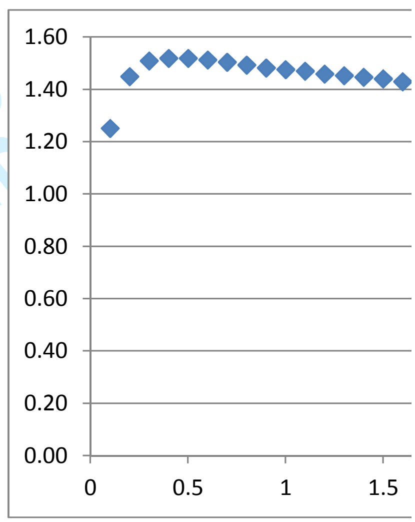

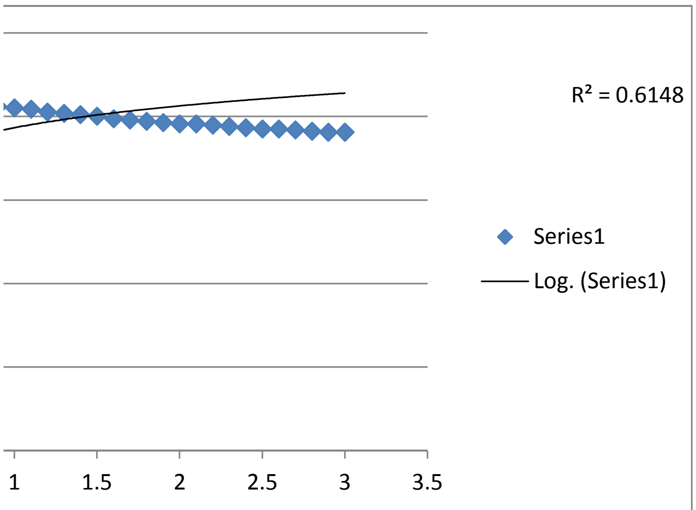
R² = 0.6148
Series1
Log. (Series1)
1
1.5
2
2.5
3
3.5

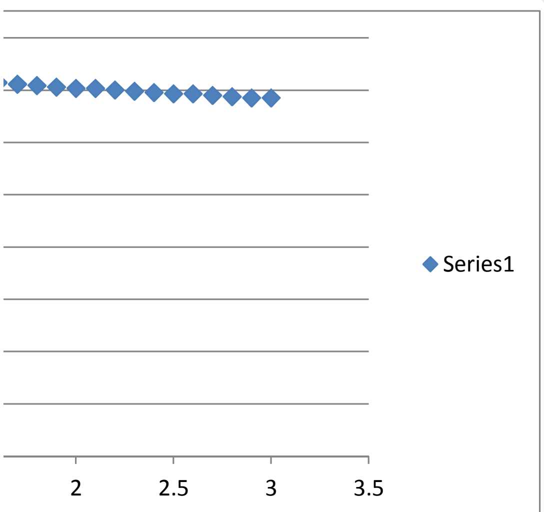
Series1
2
2.5
3
3.5

conv -4

0.001				0.00	
0.1	14.5024	0	0.223012	14.50	1.24
0.2	16.8136	-2.61E-20	0.867937	16.84	1.44
0.3	17.4856	1.01E-17	1.30734	17.53	1.50
0.4	17.6023	7.94E-18	1.50223	17.67	1.51
0.5	17.596	-6.74E-18	1.6391	17.67	1.51
0.6	17.5238	-1.69E-19	1.73242	17.61	1.51
0.7	17.4165	-3.69E-20	1.79335	17.51	1.50
0.8	17.2913	-3.19E-20	1.83014	17.39	1.49
0.9	17.1579	0	1.84877	17.26	1.48
1	17.0899	2.77E-22	1.8527	17.19	1.47
1.1	17.0217	0	1.85363	17.12	1.47
1.2	16.8854	-4.45E-20	1.84788	16.99	1.45
1.3	16.8177	-2.69E-18	1.84179	16.92	1.45
1.4	16.7505	2.57E-18	1.83385	16.85	1.44
1.5	16.6838	3.78E-20	1.82428	16.78	1.44
1.6	16.5525	0	1.80086	16.65	1.43
1.7	16.4879	2.03E-18	1.7873	16.58	1.42
1.8	16.4242	-3.91E-18	1.77266	16.52	1.41
1.9	16.3614	1.88E-18	1.75704	16.46	1.41
2	16.2995	1.80E-18	1.74054	16.39	1.40
2.1	16.2995	1.80E-18	1.74054	16.39	1.40
2.2	16.2386	-4.27E-20	1.72324	16.33	1.40
2.3	16.1786	-9.00E-20	1.70521	16.27	1.39
2.4	16.1198	-1.54E-18	1.68652	16.21	1.39
2.5	16.062	-1.39E-18	1.66723	16.15	1.38
2.6	16.062	-1.39E-18	1.66723	16.15	1.38
2.7	16.0053	1.35E-18	1.64738	16.09	1.38
2.8	15.9497	8.14E-20	1.62704	16.03	1.37
2.9	15.8952	7.73E-20	1.60624	15.98	1.37
3	15.8952	7.73E-20	1.60624	15.98	1.37

% jet	10.6
R2	0.06

0.13	0.00
0.55	16.84
1.05	17.67
1.87	17.51
3	16.99

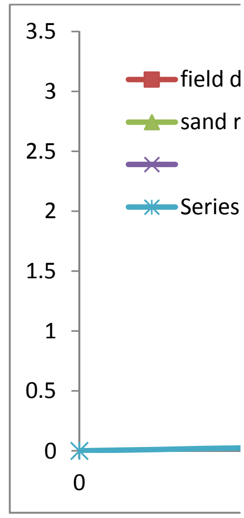

13.83
16.26
15.68
16.34

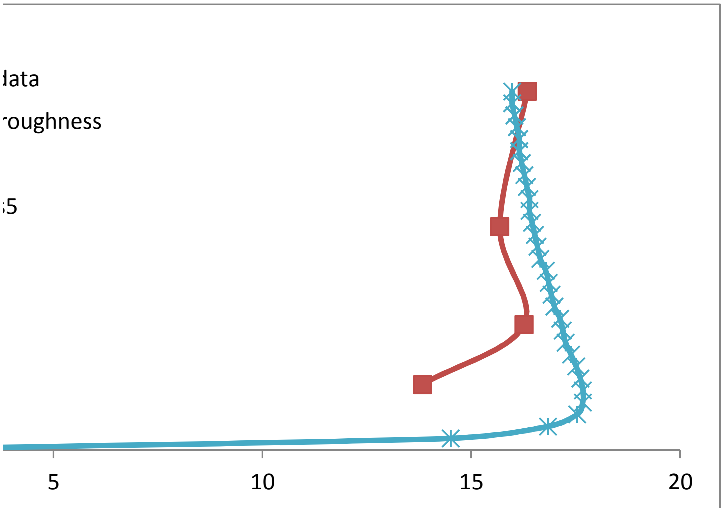

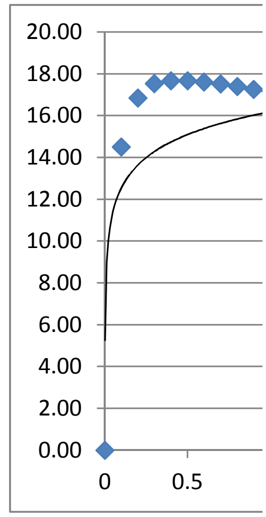

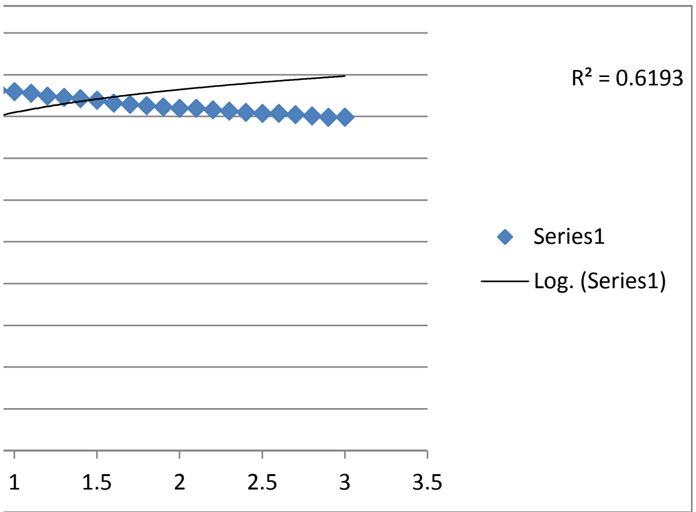
R² = 0.6193
Series1
Log. (Series1)
1
1.5
2
2.5
3
3.5

conv

						0.13	0.00	
0.001				0.00				
0.1	10.4422	0	0.154469	10.44	1.25	0.55	12.10	13.83
0.2	12.0885	-1.87E-20	0.6144	12.10	1.45	1.05	12.68	16.26
0.3	12.5574	7.16E-18	0.927084	12.59	1.51	1.87	12.55	15.68
0.4	12.634	5.59E-18	1.06555	12.68	1.52	3	12.17	16.34
0.5	12.624	-4.71E-18	1.16279	12.68	1.52			
0.6	12.568	-1.18E-19	1.22921	12.63	1.51			
0.7	12.4878	-2.56E-20	1.27272	12.55	1.50			
0.8	12.3954	-2.21E-20	1.29914	12.46	1.49			
0.9	12.2976	0	1.3127	12.37	1.48			
1	12.2479	1.93E-22	1.31565	12.32	1.48			
1.1	12.1981	0	1.31647	12.27	1.47			
1.2	12.0989	-3.06E-20	1.31271	12.17	1.46			
1.3	12.0498	-1.84E-18	1.30853	12.12	1.45			
1.4	12.001	1.76E-18	1.30304	12.07	1.45			
1.5	11.9528	2.59E-20	1.29639	12.02	1.44			
1.6	11.8577	0	1.28002	11.93	1.43			
1.7	11.811	1.39E-18	1.27051	11.88	1.42			
1.8	11.765	-2.68E-18	1.26023	11.83	1.42			
1.9	11.7195	1.29E-18	1.24925	11.79	1.41			
2	11.6748	1.23E-18	1.23763	11.74	1.41			
2.1	11.6748	1.23E-18	1.23763	11.74	1.41			
2.2	11.6307	-2.93E-20	1.22543	11.70	1.40			
2.3	11.5874	-6.15E-20	1.2127	11.65	1.40			
2.4	11.5448	-1.05E-18	1.1995	11.61	1.39			
2.5	11.503	-9.45E-19	1.18585	11.56	1.38			
2.6	11.503	-9.45E-19	1.18585	11.56	1.38			
2.7	11.4619	9.21E-19	1.17181	11.52	1.38			
2.8	11.4216	5.55E-20	1.1574	11.48	1.37			
2.9	11.3821	5.27E-20	1.14265	11.44	1.37			
3	11.3821	5.27E-20	1.14265	11.44	1.37			

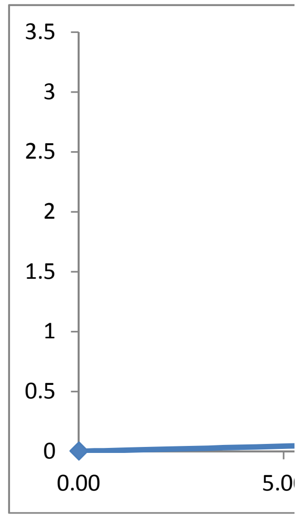

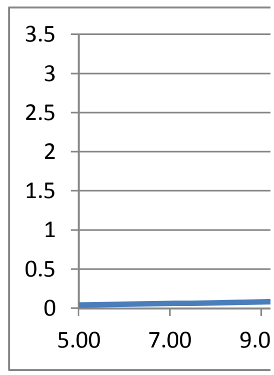

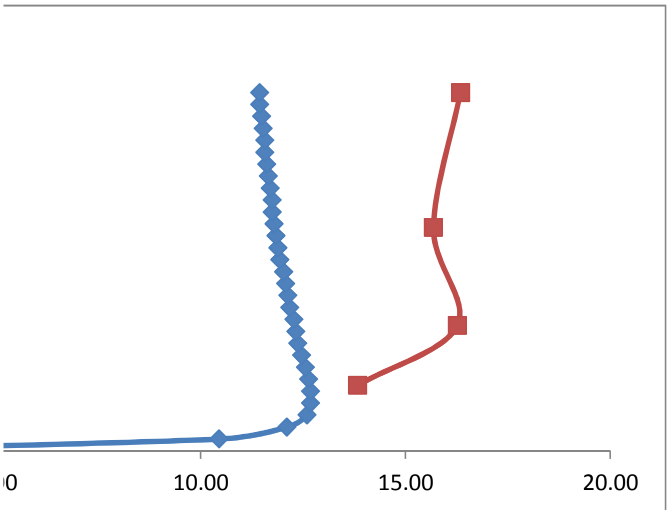
10.00
15.00
20.00

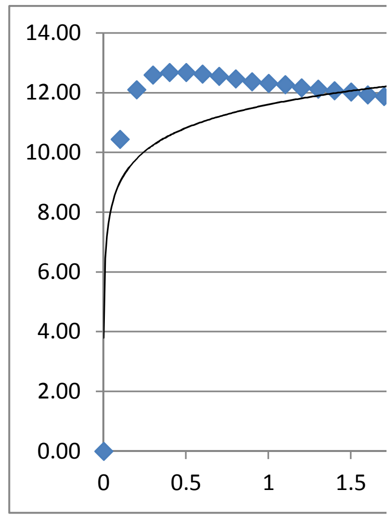
14.00
12.00
10.00
8.00
6.00
4.00
2.00
0.00
0
0.5
1
1.5

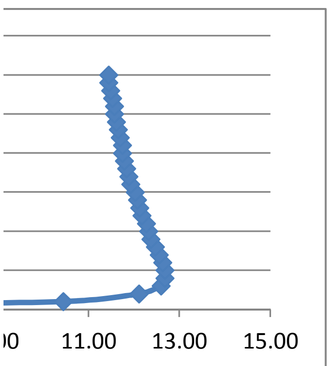
11.00
13.00
15.00

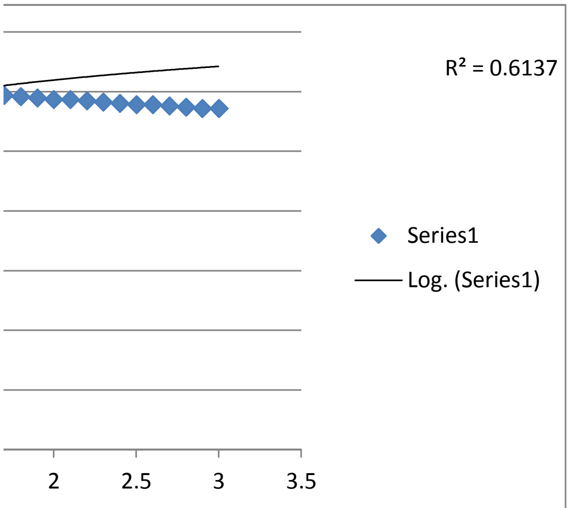
R² = 0.6137
Series1
Log. (Series1)
2
2.5
3
3.5

conv

						0.13	0.00	
0.001				0.00				
0.1	6.9428	0	0.104462	6.94	1.25	0.55	8.05	13.83
0.2	8.04247	-1.25E-20	0.411542	8.05	1.45	1.05	8.44	16.26
0.3	8.35833	4.79E-18	0.620513	8.38	1.51	1.87	8.36	15.68
0.4	8.41133	3.75E-18	0.713124	8.44	1.52	3	8.11	16.34
0.5	8.40621	-3.17E-18	0.778175	8.44	1.52			
0.6	8.37011	-7.94E-20	0.822589	8.41	1.51			
0.7	8.31756	-1.73E-20	0.851666	8.36	1.50			
0.8	8.25671	-1.49E-20	0.869299	8.30	1.49			
0.9	8.19213	0	0.878323	8.24	1.48			
1	8.15929	1.30E-22	0.880278	8.21	1.48			
1.1	8.12633	0	0.880808	8.17	1.47			
1.2	8.06061	-2.07E-20	0.878256	8.11	1.46			
1.3	8.028	-1.25E-18	0.875446	8.08	1.45			
1.4	7.99564	1.19E-18	0.871763	8.04	1.45			
1.5	7.96357	1.75E-20	0.867299	8.01	1.44			
1.6	7.9004	0	0.856338	7.95	1.43			
1.7	7.86936	9.42E-19	0.849973	7.92	1.42			
1.8	7.83872	-1.81E-18	0.843093	7.88	1.42			
1.9	7.8085	8.72E-19	0.835746	7.85	1.41			
2	7.77871	8.34E-19	0.827976	7.82	1.41			
2.1	7.77871	8.34E-19	0.827976	7.82	1.41			
2.2	7.74938	-1.97E-20	0.819821	7.79	1.40			
2.3	7.72052	-4.16E-20	0.811317	7.76	1.40			
2.4	7.69215	-7.13E-19	0.802494	7.73	1.39			
2.5	7.66429	-6.40E-19	0.793381	7.71	1.39			
2.6	7.66429	-6.40E-19	0.793381	7.71	1.39			
2.7	7.63694	6.24E-19	0.784002	7.68	1.38			
2.8	7.61012	3.76E-20	0.774381	7.65	1.38			
2.9	7.58382	3.57E-20	0.764538	7.62	1.37			
3	7.58382	3.57E-20	0.764538	7.62	1.37			

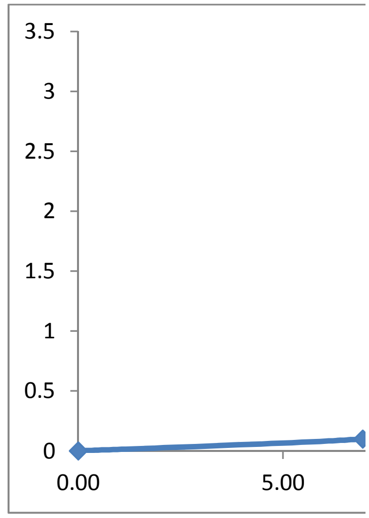

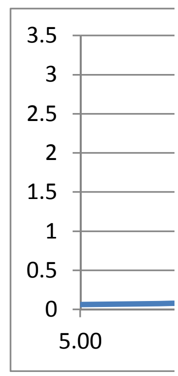

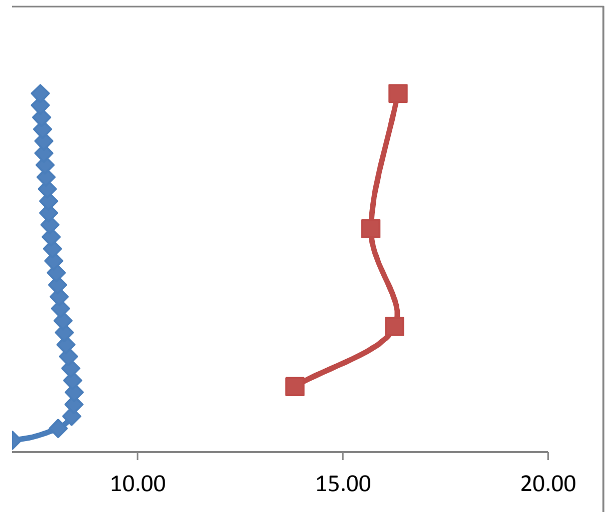
10.00
15.00
20.00

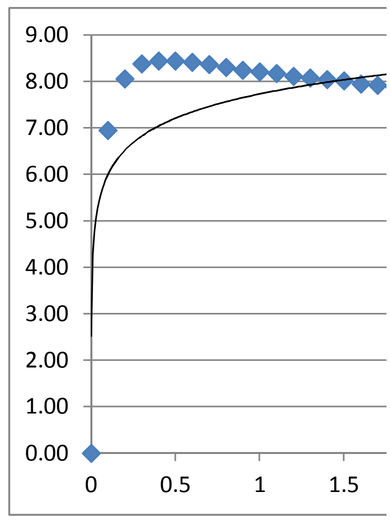
9.00
8.00
7.00
6.00
5.00
4.00
3.00
2.00
1.00
0.00
0
0.5
1
1.5

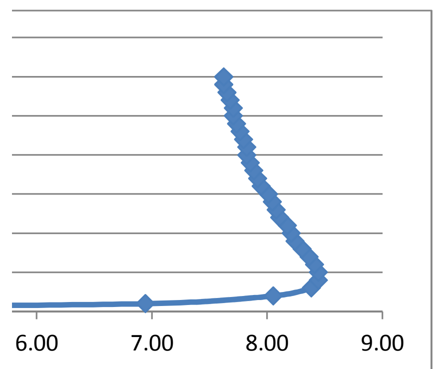
6.00
7.00
8.00
9.00

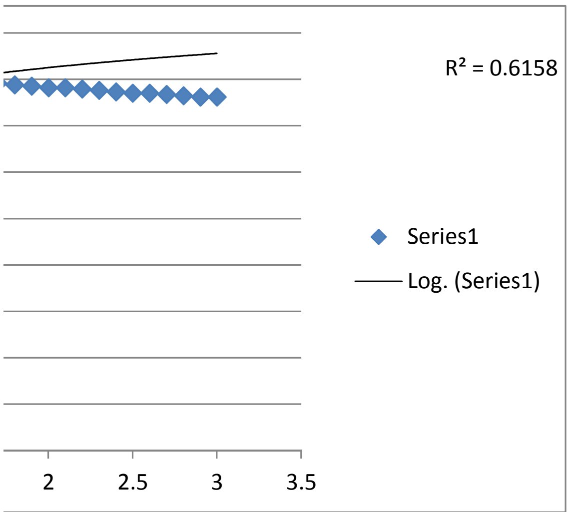
R² = 0.6158
Series1
Log. (Series1)
2
2.5
3
3.5

0° no scarp						0° with scarp	
0.001	0	0.00E+00	0	0.00		0.001	
0.1	11.3695	-1.92E-20	1.57838	11.48	1.06	0.1	14.50
0.2	14.3897	-2.66E-19	2.06935	14.54	1.34	0.2	16.81
0.3	15.6444	-3.14E-18	2.41928	15.83	1.46	0.3	17.49
0.4	16.2107	3.24E-18	2.6333	16.42	1.51	0.4	17.60
0.5	16.46	-1.67E-19	2.72962	16.68	1.54	0.5	17.596
0.6	16.545	-2.43E-18	2.7566	16.77	1.55	0.6	17.5238
0.7	16.545	-2.43E-18	2.7566	16.77	1.55	0.7	17.4165
0.8	16.5459	2.25E-18	2.74448	16.77	1.55	0.8	17.2913
0.9	16.5062	1.82E-18	2.7109	16.73	1.54	0.9	17.1579
1	16.448	-1.59E-18	2.66657	16.66	1.54	1	17.0899
1.1	16.3821	0	2.61732	16.59	1.53	1.1	17.0217
1.2	16.3137	0	2.56643	16.51	1.52	1.2	16.8854
1.3	16.3137	0	2.56643	16.51	1.52	1.3	16.8177
1.4	16.2452	-7.89E-20	2.51552	16.44	1.52	1.4	16.7505
1.5	16.178	-7.10E-20	2.4654	16.36	1.51	1.5	16.6838
1.6	16.1126	-6.70E-20	2.41645	16.29	1.50	1.6	16.5525
1.7	16.0493	-1.24E-19	2.36881	16.22	1.50	1.7	16.4879
1.8	16.0493	-1.24E-19	2.36881	16.22	1.50	1.8	16.4242
1.9	15.9881	2.08E-21	2.32252	16.16	1.49	1.9	16.3614
2	15.9292	-9.54E-19	2.27755	16.09	1.48	2	16.2995
2.1	15.9292	-9.54E-19	2.27755	16.09	1.48	2.1	16.2995
2.2	15.8725	9.17E-19	2.23385	16.03	1.48	2.2	16.2386
2.3	15.8178	-9.39E-20	2.19135	15.97	1.47	2.3	16.1786
2.4	15.8178	-9.39E-20	2.19135	15.97	1.47	2.4	16.1198
2.5	15.7653	0	2.14999	15.91	1.47	2.5	16.062
2.6	15.7147	8.46E-20	2.1097	15.86	1.46	2.6	16.062
2.7	15.7147	8.46E-20	2.1097	15.86	1.46	2.7	16.0053
2.8	15.6661	-7.99E-20	2.07041	15.80	1.46	2.8	15.9497
2.9	15.6661	-7.99E-20	2.07041	15.80	1.46	2.9	15.8952
3	15.6193	-1.07E-21	2.03207	15.75	1.45	3	15.8952
				% jet	4.3		
				R2	0.21		

		0.00	
0	0.223012	14.50	1.34
-2.6E-20	0.867937	16.84	1.55
1.01E-17	1.30734	17.53	1.62
7.94E-18	1.50223	17.67	1.63
-6.7E-18	1.6391	17.67	1.63
-1.7E-19	1.73242	17.61	1.62
-3.7E-20	1.79335	17.51	1.61
-3.2E-20	1.83014	17.39	1.60
0	1.84877	17.26	1.59
2.77E-22	1.8527	17.19	1.58
0	1.85363	17.12	1.58
-4.5E-20	1.84788	16.99	1.57
-2.7E-18	1.84179	16.92	1.56
2.57E-18	1.83385	16.85	1.55
3.78E-20	1.82428	16.78	1.55
0	1.80086	16.65	1.53
2.03E-18	1.7873	16.58	1.53
-3.9E-18	1.77266	16.52	1.52
1.88E-18	1.75704	16.46	1.52
1.8E-18	1.74054	16.39	1.51
1.8E-18	1.74054	16.39	1.51
-4.3E-20	1.72324	16.33	1.51
-9E-20	1.70521	16.27	1.50
-1.5E-18	1.68652	16.21	1.49
-1.4E-18	1.66723	16.15	1.49
-1.4E-18	1.66723	16.15	1.49
1.35E-18	1.64738	16.09	1.48
8.14E-20	1.62704	16.03	1.48
7.73E-20	1.60624	15.98	1.47
7.73E-20	1.60624	15.98	1.47

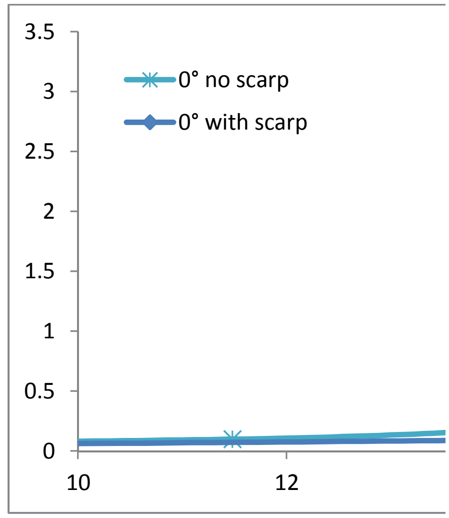

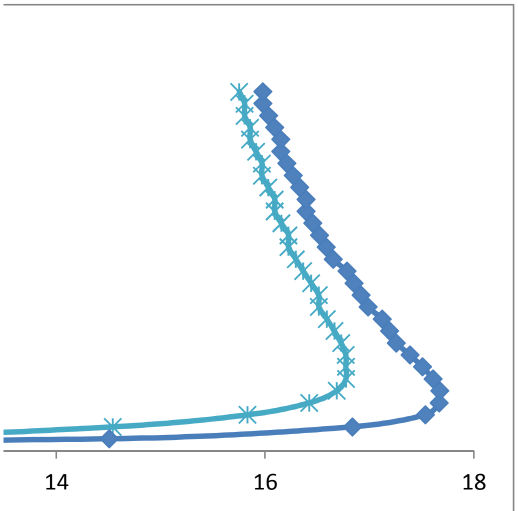
14
16
18

conv

0.001				0.00
0.1	16.3281	-4.77E-20	2.42237	16.507
0.2	17.4815	-1.65E-17	2.70576	17.690
0.3	17.7058	-4.38E-20	2.75281	17.919
0.4	17.6698	1.90E-17	2.72715	17.879
0.5	17.5705	3.09E-20	2.67905	17.774
0.6	17.4421	-6.64E-18	2.61923	17.638
0.7	17.3023	-4.37E-20	2.55383	17.490
0.8	17.1602	-4.82E-18	2.48624	17.339
0.9	17.0196	-3.20E-20	2.41824	17.191
1	16.9505	0	2.38437	17.117
1.1	16.8151	0	2.31716	16.974
1.2	16.7488	3.18E-18	2.28385	16.904
1.3	16.6834	-3.02E-18	2.25075	16.835
1.4	16.6189	0	2.21786	16.766
1.5	16.4926	-3.99E-20	2.15269	16.632
1.6	16.4308	-3.78E-20	2.1204	16.567
1.7	16.3699	-3.59E-20	2.0883	16.503
1.8	16.3098	3.40E-20	2.05639	16.439
1.9	16.2507	0	2.02466	16.376
2	16.1926	-5.51E-22	1.99312	16.315
2.1	16.1926	-5.51E-22	1.99312	16.315
2.2	16.1353	0	1.96176	16.254
2.3	16.0791	0	1.93057	16.195
2.4	16.0238	-1.66E-18	1.89956	16.136
2.5	15.9696	3.30E-18	1.86872	16.079
2.6	15.9164	-1.54E-18	1.83804	16.022
2.7	15.9164	-1.54E-18	1.83804	16.022
2.8	15.8642	-4.48E-20	1.80752	15.967
2.9	15.813	1.70E-19	1.77716	15.913
3	15.813	1.70E-19	1.77716	15.913

0.13	16.33	
0.55	17.77	13.83
1.05	17.88	16.26
1.87	16.38	15.68
3	16.90	16.34

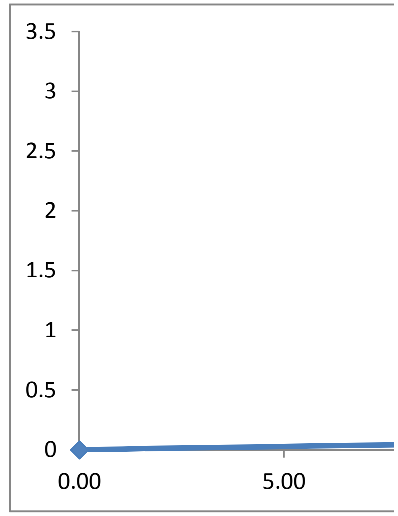

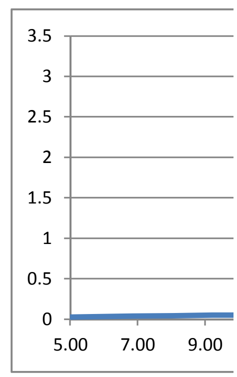

% jet 12.6

R2 0.59

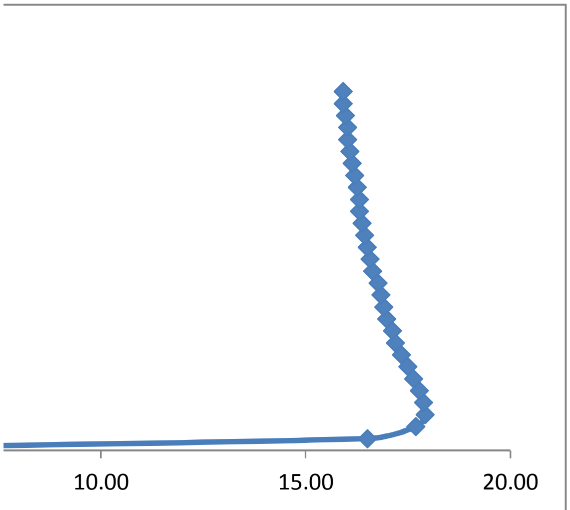
10.00
15.00
20.00

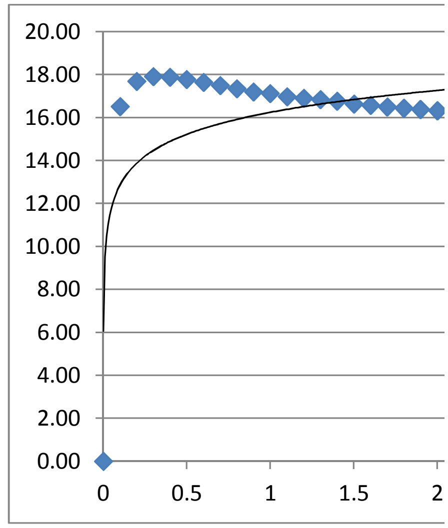
20.00
18.00
16.00
14.00
12.00
10.00
8.00
6.00
4.00
2.00
0.00
0
0.5
1
1.5
2

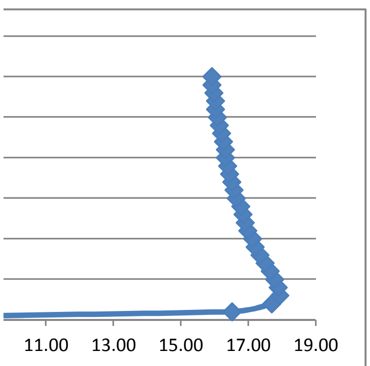
11.00
13.00
15.00
17.00
19.00

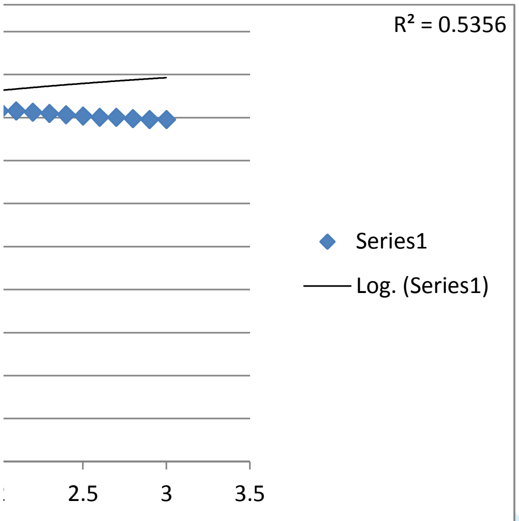
R² = 0.5356
Series1
Log. (Series1)
2.5
3
3.5

conv

0.001				0.00
0.1	15.7445	5.39E-18	1.35007	15.80
0.2	17.2517	-3.77E-18	1.82425	17.35
0.3	17.5888	5.36E-18	2.04344	17.71
0.4	17.5898	0	2.11143	17.72
0.5	17.5124	-2.78E-20	2.14117	17.64
0.6	17.3967	-3.00E-18	2.14566	17.53
0.7	17.264	0	2.13339	17.40
0.8	17.1254	1.07E-18	2.10993	17.25
0.9	16.9865	3.01E-20	2.07897	17.11
1	16.9178	0	2.06147	17.04
1.1	16.7827	0	2.02354	16.90
1.2	16.7164	0	2.00341	16.84
1.3	16.6509	-4.40E-20	1.98267	16.77
1.4	16.5864	4.16E-20	1.96141	16.70
1.5	16.4601	-3.91E-22	1.91758	16.57
1.6	16.3982	0	1.89514	16.51
1.7	16.3373	5.68E-19	1.87239	16.44
1.8	16.2773	-1.03E-18	1.84938	16.38
1.9	16.2182	4.93E-19	1.82613	16.32
2	16.16	1.16E-19	1.80267	16.26
2.1	16.16	1.16E-19	1.80267	16.26
2.2	16.1027	5.53E-20	1.77903	16.20
2.3	16.0465	0	1.75522	16.14
2.4	15.9912	0	1.73127	16.08
2.5	15.937	4.74E-20	1.70718	16.03
2.6	15.937	4.74E-20	1.70718	16.03
2.7	15.8838	-3.54E-19	1.68297	15.97
2.8	15.8316	8.55E-21	1.65865	15.92
2.9	15.7805	8.17E-21	1.63423	15.86
3	15.7805	8.17E-21	1.63423	15.86

0.13	0.00	
0.55	17.53	13.83
1.05	16.90	16.26
1.87	16.32	15.68
3	16.84	16.34

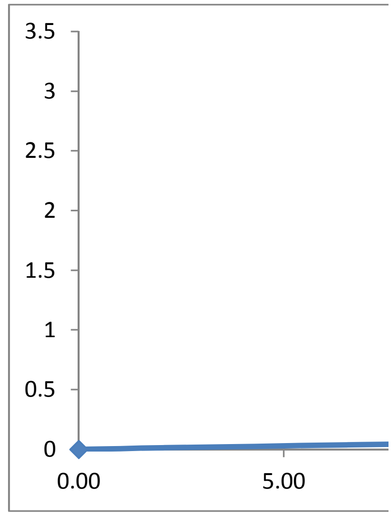

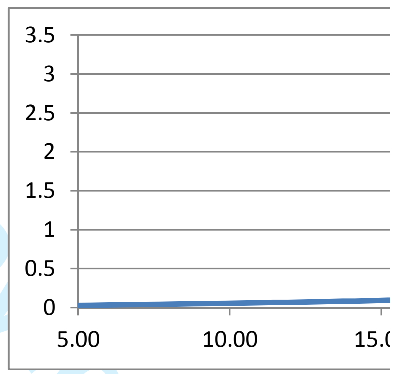

% jet 11.67

R2 0.39

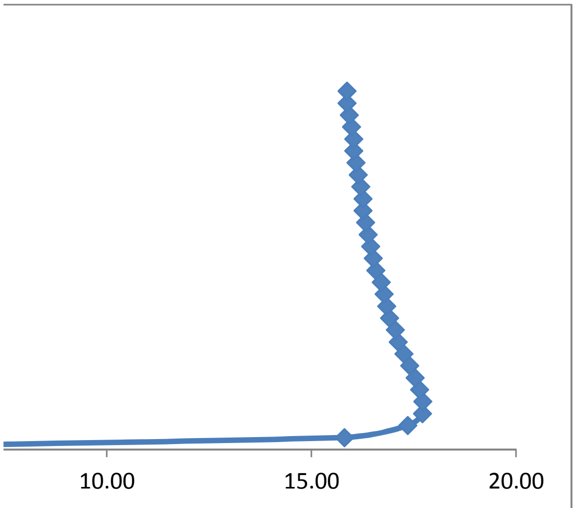
10.00
15.00
20.00

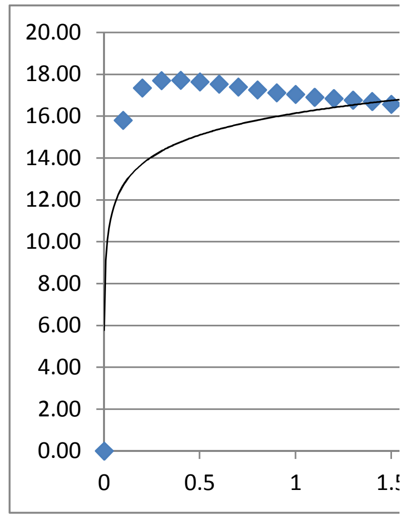
20.00
18.00
16.00
14.00
12.00
10.00
8.00
6.00
4.00
2.00
0.00
0
0.5
1

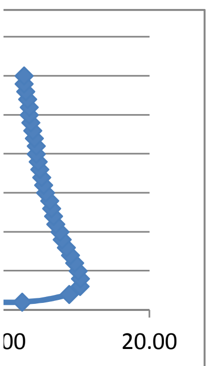
20.00

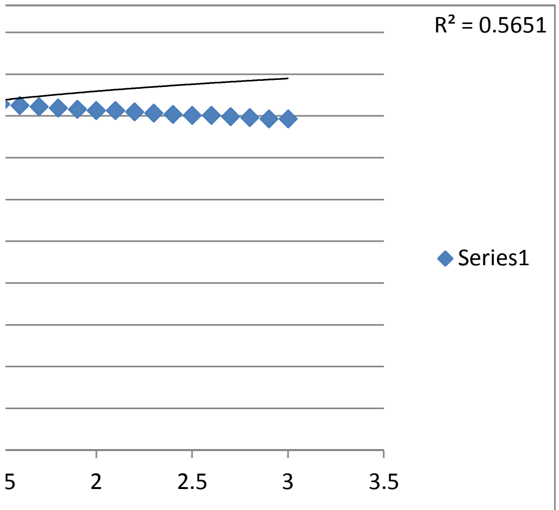
R² = 0.5651
Series1
5
2
2.5
3
3.5

conv

0.001				0.00	0.13	0.00	
0.1	12.5352	-2.37E-17	0.06349	12.54	0.55	#REF!	13.83
0.2	16.3434	1.38E-17	0.756888	16.36	1.05	17.17	16.26
0.3	16.8592	-2.18E-20	0.99848	16.89	1.87	16.97	15.68
0.4	17.1294	-3.19E-20	1.24881	17.17	3	16.62	16.34
0.5	17.1444	0	1.3613	17.20			
0.6	17.094	-5.61E-18	1.44216	17.15			
0.7	17.007	9.67E-18	1.49867	17.07			
0.8	16.9001	-4.15E-18	1.53628	16.97			
0.9	16.8425	3.94E-18	1.54932	16.91			
1	16.7232	2.66E-20	1.56599	16.80			
1.1	16.6624	2.50E-20	1.57031	16.74			
1.2	16.5406	-4.44E-20	1.57232	16.62			
1.3	16.4799	-2.60E-18	1.57047	16.55			
1.4	16.4196	1.01E-19	1.56697	16.49			
1.5	16.3598	2.45E-18	1.562	16.43			
1.6	16.2419	-4.28E-18	1.54817	16.32			
1.7	16.1839	4.90E-20	1.53955	16.26			
1.8	16.1267	1.98E-18	1.52994	16.20			
1.9	16.0702	-1.81E-18	1.51942	16.14			
2	16.0702	-1.81E-18	1.51942	16.14			
2.1	16.0146	1.70E-18	1.50808	16.09			
2.2	15.9599	5.18E-20	1.49597	16.03			
2.3	15.9061	1.55E-18	1.48318	15.98			
2.4	15.8532	-2.93E-18	1.46974	15.92			
2.5	15.8013	2.83E-18	1.45573	15.87			
2.6	15.8013	2.83E-18	1.45573	15.87			
2.7	15.7503	-2.68E-18	1.44117	15.82			
2.8	15.7005	-8.21E-21	1.42612	15.77			
2.9	15.6516	1.22E-18	1.4106	15.72			
3	15.6516	1.22E-18	1.4106	15.72			

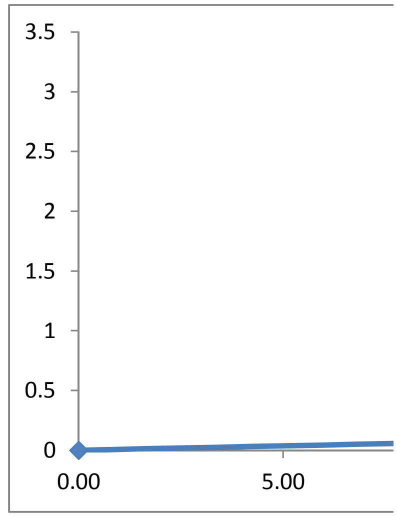

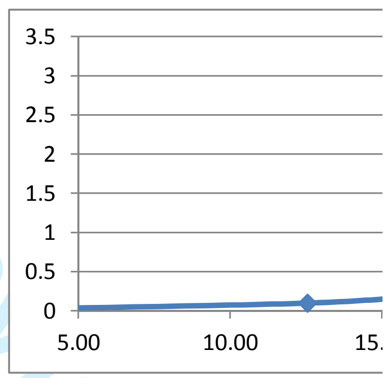

% jet 9.44

R2 0.01

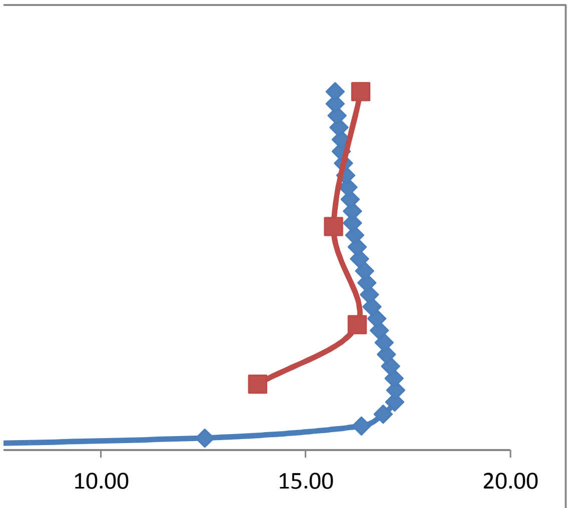
10.00
15.00
20.00

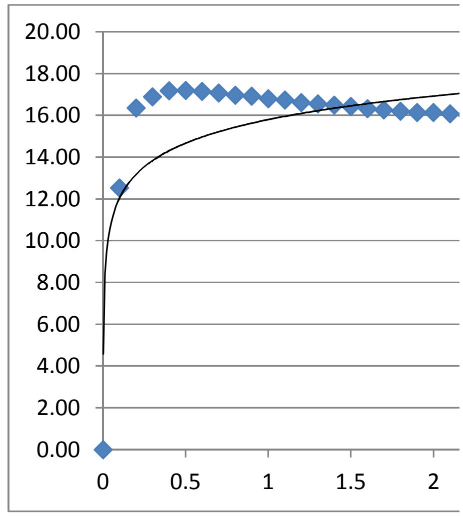
20.00
18.00
16.00
14.00
12.00
10.00
8.00
6.00
4.00
2.00
0.00
0
0.5
1
1.5
2

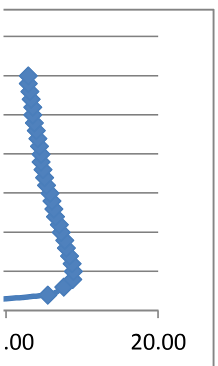
.00
20.00

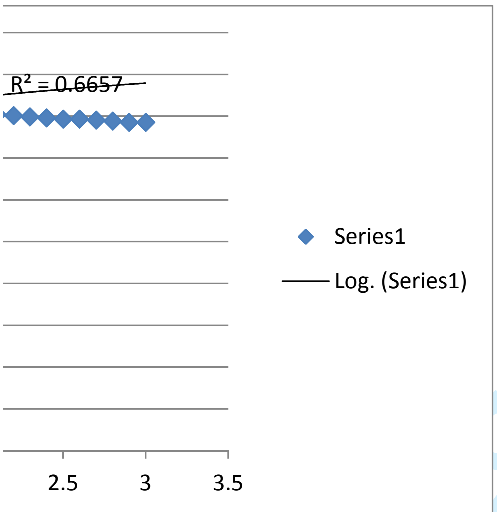
R² = 0.6657
2.5
3
3.5
Series1
Log. (Series1)

conv

0.001				0.00
0.1	12.3343	4.48E-19	0.060747	12.33
0.2	15.9056	0	0.675908	15.92
0.3	16.4285	0	0.8888	16.45
0.4	16.7488	0	1.11256	16.79
0.5	16.7977	6.48E-18	1.21448	16.84
0.6	16.7751	-5.47E-18	1.28796	16.82
0.7	16.7101	4.77E-18	1.33912	16.76
0.8	16.6207	0	1.37287	16.68
0.9	16.5707	-3.72E-18	1.38447	16.63
1	16.4649	-3.24E-18	1.39914	16.52
1.1	16.4103	3.11E-18	1.4029	16.47
1.2	16.3003	-2.68E-18	1.40464	16.36
1.3	16.2454	2.62E-18	1.40308	16.31
1.4	16.1908	-2.37E-18	1.40014	16.25
1.5	16.1367	1.80E-20	1.39597	16.20
1.6	16.03	-1.99E-18	1.3845	16.09
1.7	15.9777	0	1.37739	16.04
1.8	15.9261	-2.52E-22	1.36949	15.98
1.9	15.8752	5.37E-20	1.36087	15.93
2	15.8752	5.37E-20	1.36087	15.93
2.1	15.8251	-1.62E-18	1.35159	15.88
2.2	15.7758	1.57E-18	1.34171	15.83
2.3	15.7274	1.41E-18	1.33127	15.78
2.4	15.6798	-2.80E-18	1.32032	15.74
2.5	15.6332	1.34E-18	1.30889	15.69
2.6	15.6332	1.34E-18	1.30889	15.69
2.7	15.5875	0	1.29703	15.64
2.8	15.5427	1.18E-18	1.28475	15.60
2.9	15.4989	-1.11E-18	1.27208	15.55
3	15.4989	-1.11E-18	1.27208	15.55

0.13	0.00	
0.55	#REF!	13.83
1.05	16.79	16.26
1.87	#REF!	15.68
3	#REF!	16.34

% jet	8.30
R2	0.02

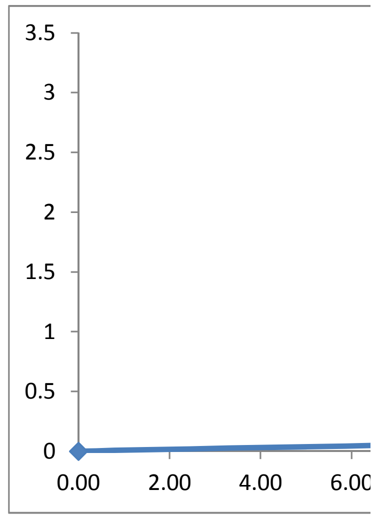

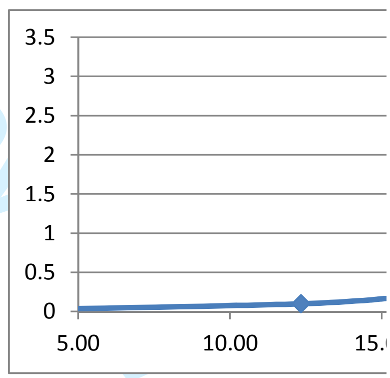

4.34
9.98
12.02
12.39
13.04

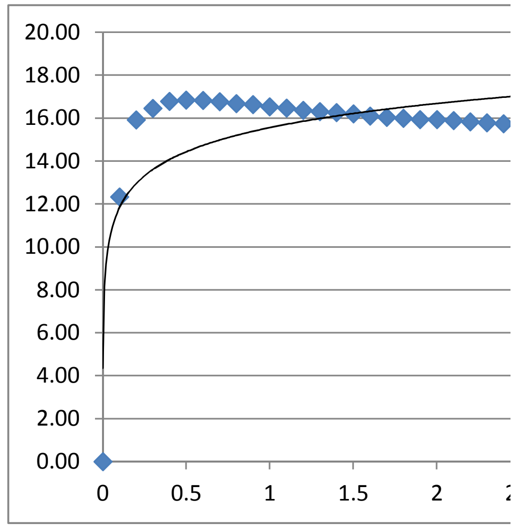

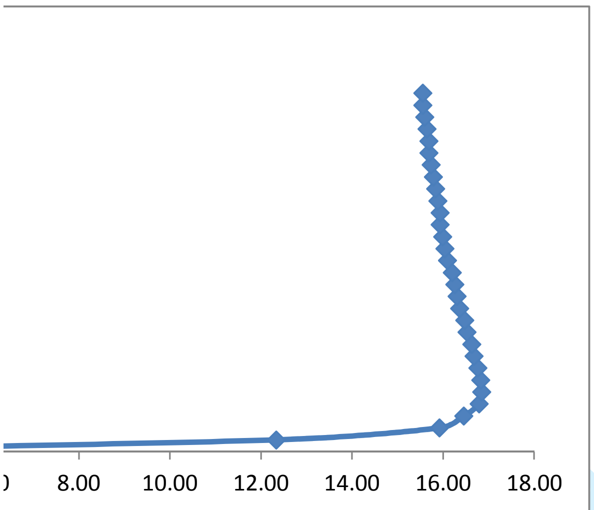

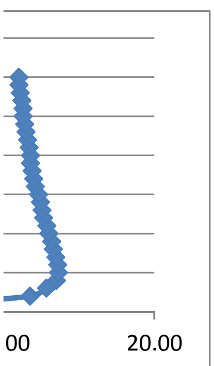

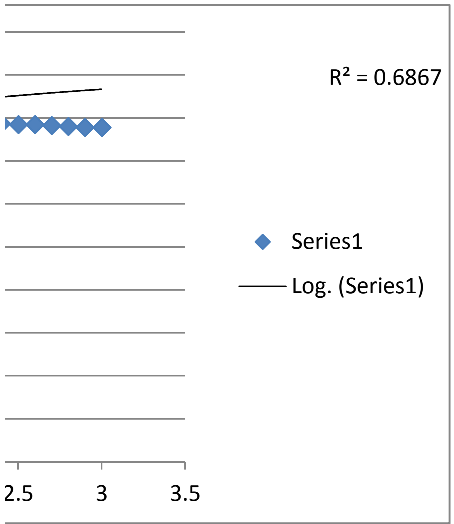
R² = 0.6867
Series1
Log. (Series1)
2.5
3
3.5

conv

0.001				0.00	0.13	0.00	
0.1	13.4618	3.35E-20	1.17927	13.51	0.55	#REF!	13.83
0.2	14.8637	1.26E-17	1.33793	14.92	1.05	15.64	16.26
0.3	15.2666	0	1.3638	15.33	1.87	#REF!	15.68
0.4	15.5842	-3.37E-20	1.36184	15.64	3	15.52	16.34
0.5	15.6785	-2.74E-20	1.34772	15.74			
0.6	15.713	-6.03E-18	1.32894	15.77			
0.7	15.7075	5.13E-18	1.30826	15.76			
0.8	15.6756	-4.38E-18	1.28721	15.73			
0.9	15.6528	4.17E-18	1.2768	15.70			
1	15.5981	0	1.25643	15.65			
1.1	15.5675	-3.25E-18	1.2465	15.62			
1.2	15.5025	5.70E-18	1.2271	15.55			
1.3	15.4688	-2.70E-18	1.21761	15.52			
1.4	15.4347	3.92E-20	1.20822	15.48			
1.5	15.4003	0	1.19892	15.45			
1.6	15.3315	-4.14E-18	1.18044	15.38			
1.7	15.2972	2.03E-18	1.17123	15.34			
1.8	15.2632	1.84E-18	1.16201	15.31			
1.9	15.2295	-1.77E-18	1.15276	15.27			
2	15.1961	-1.64E-18	1.14346	15.24			
2.1	15.1961	-1.64E-18	1.14346	15.24			
2.2	15.1631	3.38E-20	1.1341	15.21			
2.3	15.1306	1.47E-18	1.12467	15.17			
2.4	15.0985	-4.29E-20	1.11516	15.14			
2.5	15.0669	0	1.10555	15.11			
2.6	15.0669	0	1.10555	15.11			
2.7	15.0359	-3.83E-20	1.09584	15.08			
2.8	15.0054	-1.14E-18	1.08602	15.04			
2.9	14.9755	-9.39E-21	1.0761	15.01			
3	14.9755	-9.39E-21	1.0761	15.01			

% jet	5.03
R2	0.03

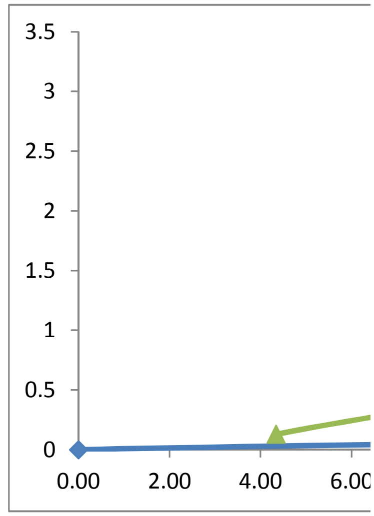

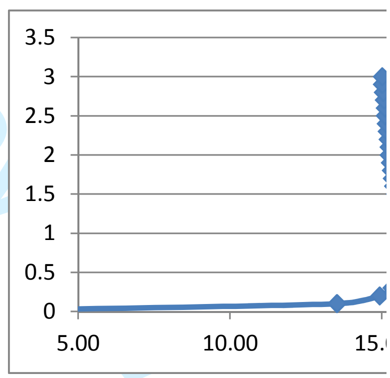

4.34
9.98
12.02
12.39
13.04

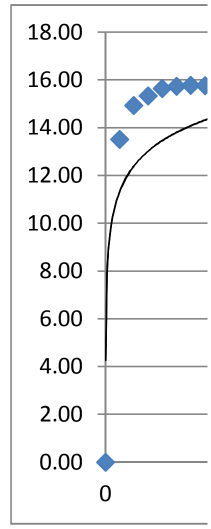

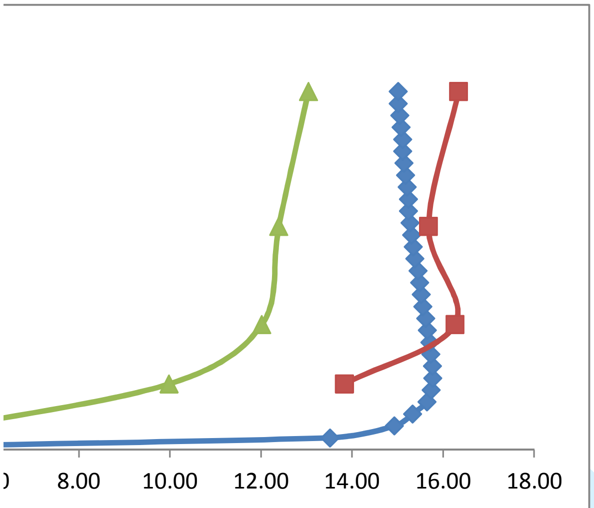

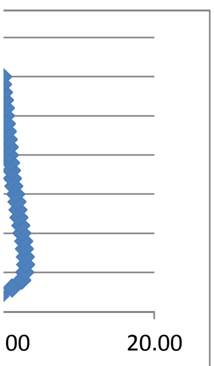

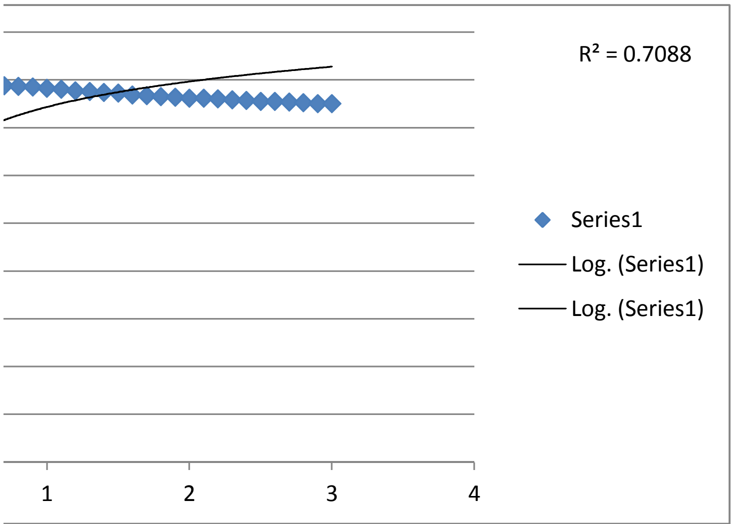
R² = 0.7088
Series1
Log. (Series1)
Log. (Series1)
1
2
3
4

conv

0.001				0.00
0.1	9.74643	-8.07E-18	0.513444	9.760
0.2	12.4328	5.82E-18	0.693156	12.452
0.3	13.4774	5.23E-20	0.751218	13.498
0.4	14.0622	3.57E-18	0.779065	14.084
0.5	14.327	-3.16E-18	0.792558	14.349
0.6	14.5189	2.16E-20	0.803443	14.541
0.7	14.6517	2.40E-18	0.812006	14.674
0.8	14.7369	2.13E-18	0.818504	14.760
0.9	14.7649	-1.96E-18	0.821059	14.788
1	14.7974	1.71E-18	0.824938	14.820
1.1	14.8041	1.57E-18	0.826322	14.827
1.2	14.8029	0	0.828109	14.826
1.3	14.7967	0	0.828553	14.820
1.4	14.7876	-1.84E-20	0.828721	14.811
1.5	14.7761	0	0.828625	14.799
1.6	14.7628	0	0.828278	14.786
1.7	14.7322	2.80E-20	0.826865	14.755
1.8	14.7154	2.62E-20	0.825813	14.739
1.9	14.698	7.09E-23	0.824536	14.721
2	14.698	7.09E-23	0.824536	14.721
2.1	14.6801	0	0.82304	14.703
2.2	14.6619	-6.68E-19	0.821325	14.685
2.3	14.6436	1.31E-18	0.819394	14.667
2.4	14.6252	-3.18E-20	0.817247	14.648
2.5	14.6069	-1.19E-20	0.814886	14.630
2.6	14.6069	-1.19E-20	0.814886	14.630
2.7	14.5887	2.29E-20	0.812309	14.611
2.8	14.5706	-1.08E-20	0.809518	14.593
2.9	14.5529	-9.70E-19	0.806513	14.575
3	14.5529	-9.70E-19	0.806513	14.575

% jet	1.73	
R2	0.57	

		60 meas
0.13	0.00	4.34
0.55	#REF!	9.98
1.05	14.08	12.02
1.87	#REF!	12.39
3	#REF!	13.04

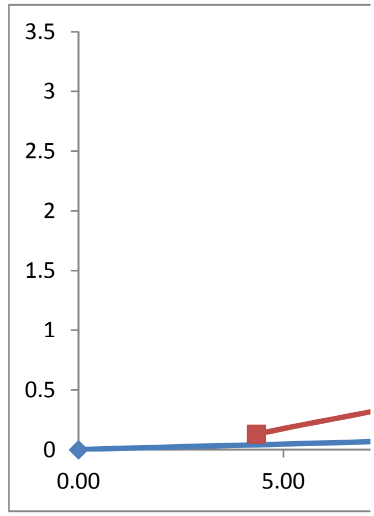

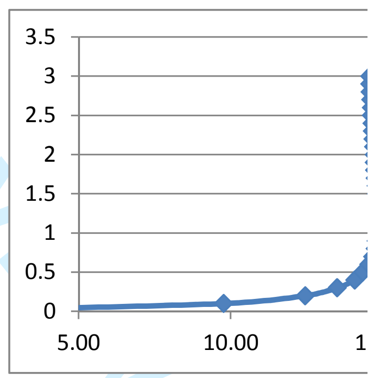

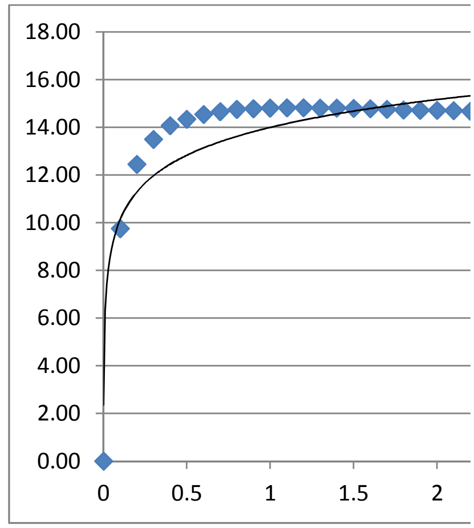
18.00
16.00
14.00
12.00
10.00
8.00
6.00
4.00
2.00
0.00
0
0.5
1
1.5
2

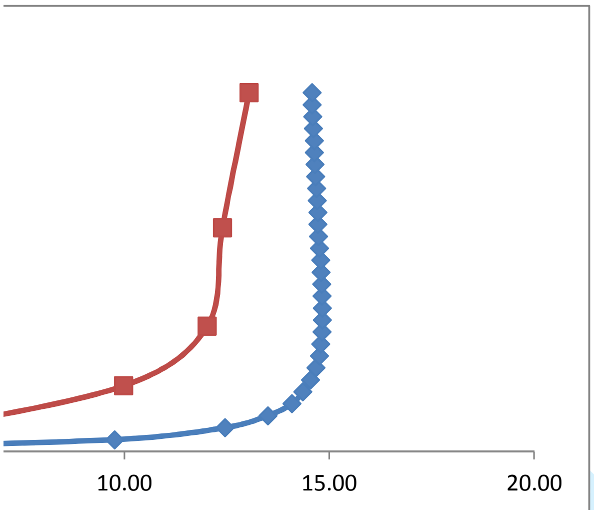
10.00
15.00
20.00

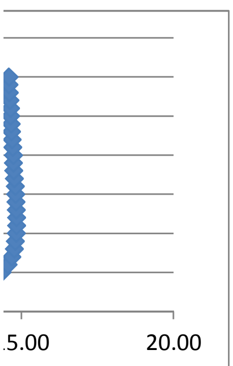
.5.00
20.00

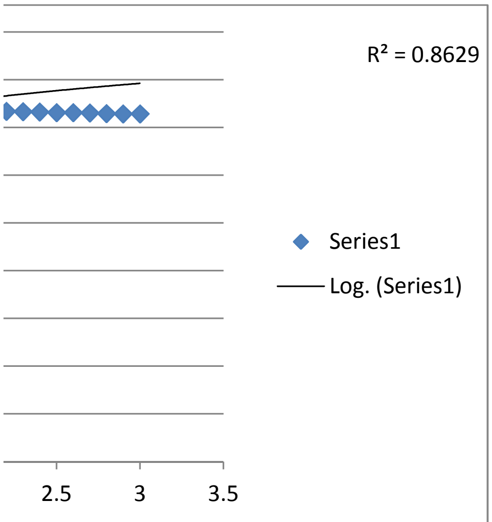
R² = 0.8629
Series1
Log. (Series1)
2.5
3
3.5

conv

0.001				0.00	0.13	0.00	4.34
0.1	7.09261	4.96E-18	0.151283	7.09	0.55	#REF!	9.98
0.2	9.65307	-3.60E-18	0.231378	9.66	1.05	11.68	12.02
0.3	10.9134	7.43E-21	0.266557	10.92	1.87	#REF!	12.39
0.4	11.6797	2.24E-18	0.288001	11.68	3	13.42	13.04
0.5	12.0673	-2.02E-18	0.302714	12.07			
0.6	12.3941	1.83E-18	0.319004	12.40			
0.7	12.6733	3.31E-21	0.336621	12.68			
0.8	12.9116	-6.09E-21	0.354926	12.92			
0.9	13.0166	5.84E-21	0.364114	13.02			
1	13.2	1.38E-18	0.38216	13.21			
1.1	13.2791	-1.30E-18	0.390885	13.28			
1.2	13.4134	4.62E-21	0.407483	13.42			
1.3	13.4694	1.74E-20	0.415284	13.48			
1.4	13.5185	1.05E-18	0.422721	13.53			
1.5	13.5611	-9.93E-19	0.429779	13.57			
1.6	13.5978	7.28E-21	0.436456	13.60			
1.7	13.6558	-1.31E-23	0.448672	13.66			
1.8	13.6782	0	0.45423	13.69			
1.9	13.6782	0	0.45423	13.69			
2	13.6969	5.61E-21	0.459438	13.70			
2.1	13.7126	-2.09E-20	0.464311	13.72			
2.2	13.7255	6.02E-19	0.468862	13.73			
2.3	13.7363	-5.81E-19	0.473107	13.74			
2.4	13.7452	5.34E-19	0.477057	13.75			
2.5	13.7526	-9.05E-21	0.480725	13.76			
2.6	13.7526	-9.05E-21	0.480725	13.76			
2.7	13.7587	-1.60E-20	0.484122	13.77			
2.8	13.7638	-8.07E-21	0.487255	13.77			
2.9	13.7681	-4.22E-19	0.490134	13.78			
3	13.7681	-4.22E-19	0.490134	13.78			

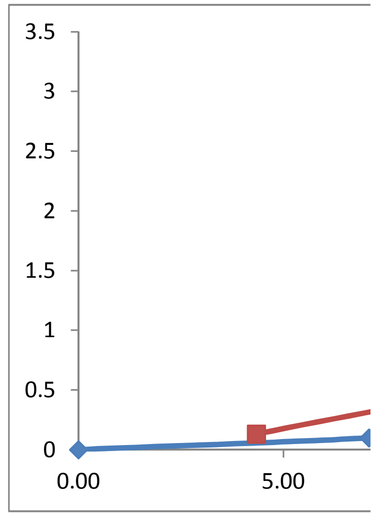

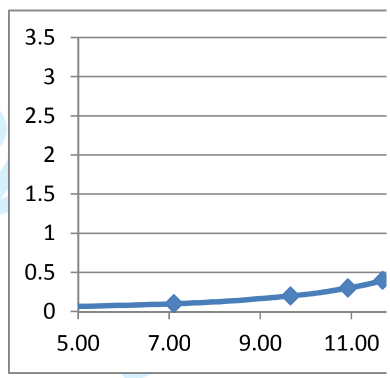

% jet	-3.57
R2	0.86

70	3.00	-8	8.54
	6.39	-6.86	9.38

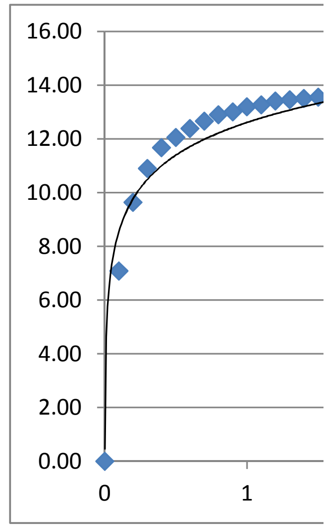

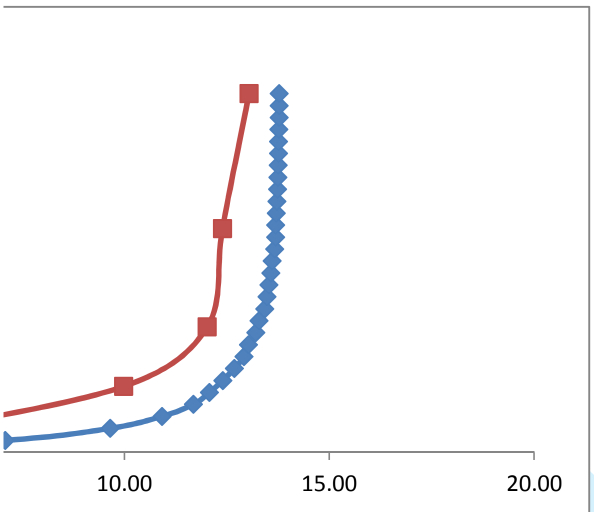

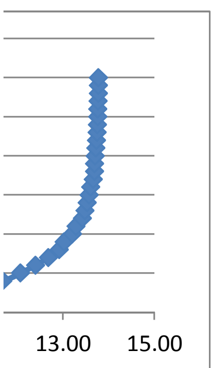

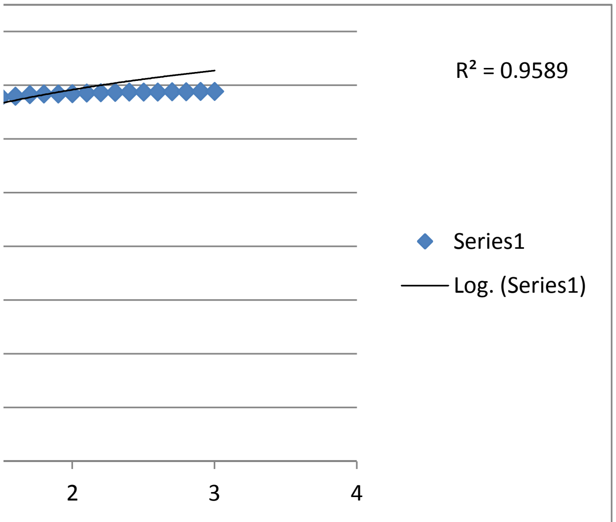
R² = 0.9589
Series1
Log. (Series1)
2
3
4

height	0°		10°		20°		30°	
0.001								
0.1	14.50	1.34	16.51	1.52	15.80	1.46	12.54	1.16
0.2	16.84	1.55	17.69	1.63	17.35	1.60	16.36	1.51
0.3	17.53	1.62	17.92	1.65	17.71	1.63	16.89	1.56
0.4	17.67	1.63	17.88	1.65	17.72	1.63	17.17	1.58
0.5	17.67	1.63	17.77	1.64	17.64	1.63	17.20	1.59
0.6	17.61	1.62	17.64	1.63	17.53	1.62	17.15	1.58
0.7	17.51	1.61	17.49	1.61	17.40	1.60	17.07	1.57
0.8	17.39	1.60	17.34	1.60	17.25	1.59	16.97	1.56
0.9	17.26	1.59	17.19	1.58	17.11	1.58	16.91	1.56
1	17.19	1.58	17.12	1.58	17.04	1.57	16.80	1.55
1.1	17.12	1.58	16.97	1.56	16.90	1.56	16.74	1.54
1.2	16.99	1.57	16.90	1.56	16.84	1.55	16.62	1.53
1.3	16.92	1.56	16.83	1.55	16.77	1.55	16.55	1.53
1.4	16.85	1.55	16.77	1.55	16.70	1.54	16.49	1.52
1.5	16.78	1.55	16.63	1.53	16.57	1.53	16.43	1.51
1.6	16.65	1.53	16.57	1.53	16.51	1.52	16.32	1.50
1.7	16.58	1.53	16.50	1.52	16.44	1.52	16.26	1.50
1.8	16.52	1.52	16.44	1.52	16.38	1.51	16.20	1.49
1.9	16.46	1.52	16.38	1.51	16.32	1.50	16.14	1.49
2	16.39	1.51	16.31	1.50	16.26	1.50	16.14	1.49
2.1	16.39	1.51	16.31	1.50	16.26	1.50	16.09	1.48
2.2	16.33	1.51	16.25	1.50	16.20	1.49	16.03	1.48
2.3	16.27	1.50	16.19	1.49	16.14	1.49	15.98	1.47
2.4	16.21	1.49	16.14	1.49	16.08	1.48	15.92	1.47
2.5	16.15	1.49	16.08	1.48	16.03	1.48	15.87	1.46
2.6	16.15	1.49	16.02	1.48	16.03	1.48	15.87	1.46
2.7	16.09	1.48	16.02	1.48	15.97	1.47	15.82	1.46
2.8	16.03	1.48	15.97	1.47	15.92	1.47	15.77	1.45
2.9	15.98	1.47	15.91	1.47	15.86	1.46	15.72	1.45
3	15.98	1.47	15.91	1.47	15.86	1.46	15.72	1.45

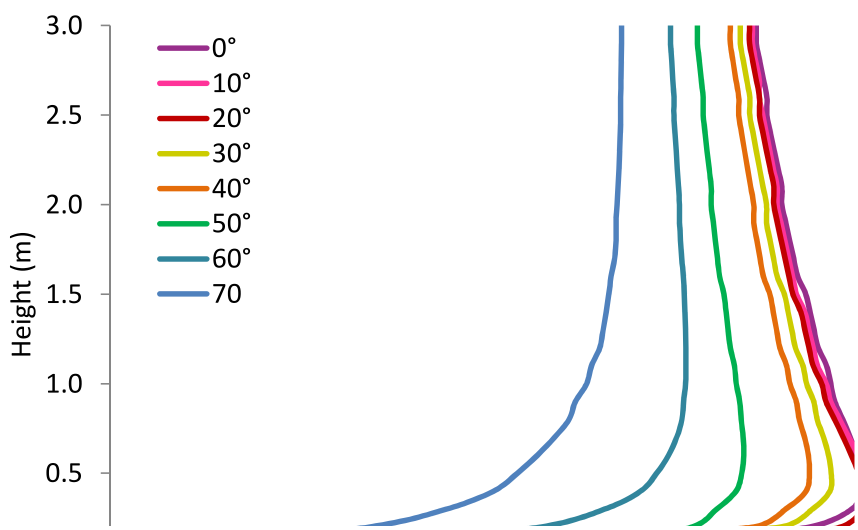

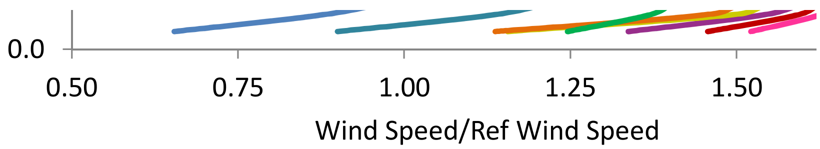
0.0
0.50
0.75
1.00
1.25
1.50
Wind Speed/Ref Wind Speed

40°	relative to 4m	50°	relative to 4m	60°	relative to 4m	70	
12.33	1.14	13.51	1.25	9.76	0.90	7.09	0.65
15.92	1.47	14.92	1.38	12.45	1.15	9.66	0.89
16.45	1.52	15.33	1.41	13.50	1.24	10.92	1.01
16.79	1.55	15.64	1.44	14.08	1.30	11.68	1.08
16.84	1.55	15.74	1.45	14.35	1.32	12.07	1.11
16.82	1.55	15.77	1.45	14.54	1.34	12.40	1.14
16.76	1.55	15.76	1.45	14.67	1.35	12.68	1.17
16.68	1.54	15.73	1.45	14.76	1.36	12.92	1.19
16.63	1.53	15.70	1.45	14.79	1.36	13.02	1.20
16.52	1.52	15.65	1.44	14.82	1.37	13.21	1.22
16.47	1.52	15.62	1.44	14.83	1.37	13.28	1.22
16.36	1.51	15.55	1.43	14.83	1.37	13.42	1.24
16.31	1.50	15.52	1.43	14.82	1.37	13.48	1.24
16.25	1.50	15.48	1.43	14.81	1.37	13.53	1.25
16.20	1.49	15.45	1.42	14.80	1.36	13.57	1.25
16.09	1.48	15.38	1.42	14.79	1.36	13.60	1.25
16.04	1.48	15.34	1.41	14.76	1.36	13.66	1.26
15.98	1.47	15.31	1.41	14.74	1.36	13.69	1.26
15.93	1.47	15.27	1.41	14.72	1.36	13.69	1.26
15.93	1.47	15.24	1.40	14.72	1.36	13.70	1.26
15.88	1.46	15.24	1.40	14.70	1.36	13.72	1.26
15.83	1.46	15.21	1.40	14.68	1.35	13.73	1.27
15.78	1.45	15.17	1.40	14.67	1.35	13.74	1.27
15.74	1.45	15.14	1.40	14.65	1.35	13.75	1.27
15.69	1.45	15.11	1.39	14.63	1.35	13.76	1.27
15.69	1.45	15.11	1.39	14.63	1.35	13.76	1.27
15.64	1.44	15.08	1.39	14.61	1.35	13.77	1.27
15.60	1.44	15.04	1.39	14.59	1.34	13.77	1.27
15.55	1.43	15.01	1.38	14.58	1.34	13.78	1.27
15.55	1.43	15.01	1.38	14.58	1.34	13.78	1.27

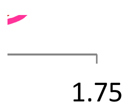
1.75

Meas46 Meas60

13.83

16.26

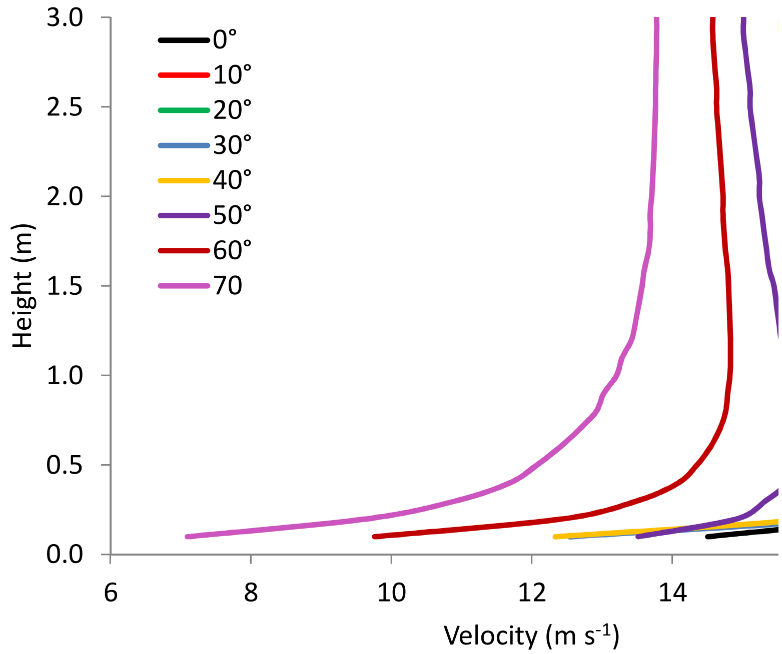

15.68

16.34 13.04

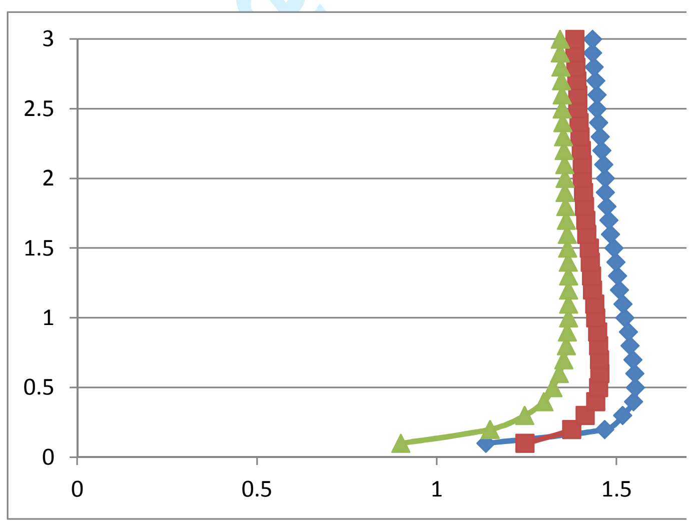


16
18

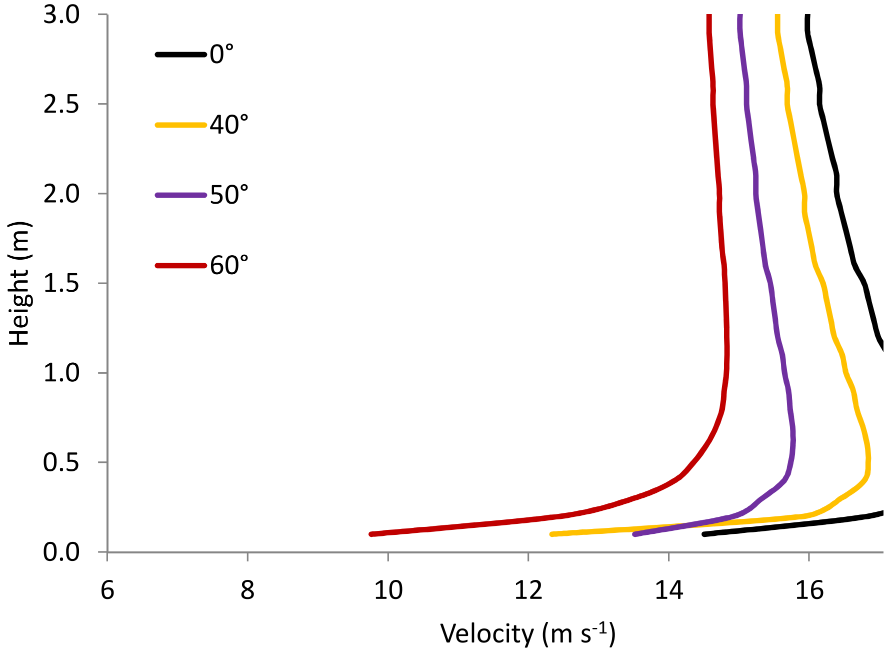
3.0
2.5
2.0
1.5
1.0
0.5
0.0
Height (m)
0°
40°
50°
60°
6
8
10
12
14
16
Velocity (m s-1)

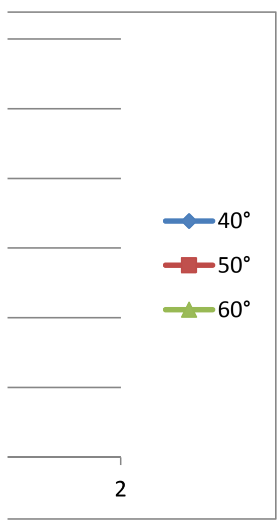
40°
50°
60°
2

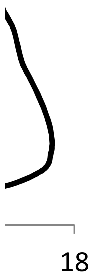
18

Dir	max jet speed	max jet height	% jet peak compared to 3m	speed @ 1m	speed @ 3m	R2
0	17.67	0.4	10.60	17.19	15.98	0.62
10	17.92	0.3	12.61	17.12	15.91	0.54
20	17.72	0.4	11.67	17.04	15.86	0.57
30	17.20	0.5	9.44	16.80	15.72	0.67
40	16.84	0.5	8.30	16.52	15.55	0.69
50	15.77	0.6	5.03	15.65	15.01	0.71
60	14.83	1.1	1.73	14.82	14.58	0.86
70	No jet			13.21	13.78	0.96

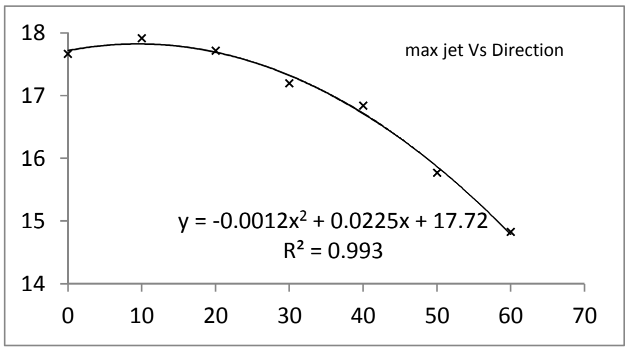

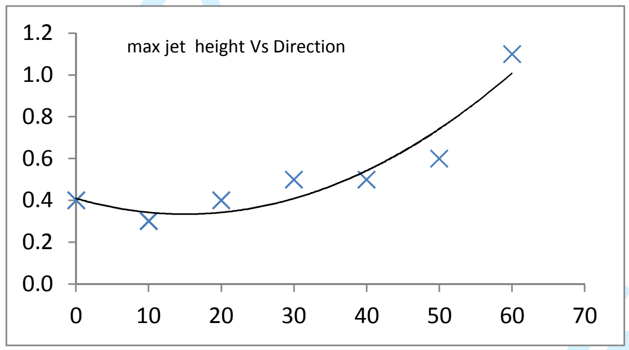

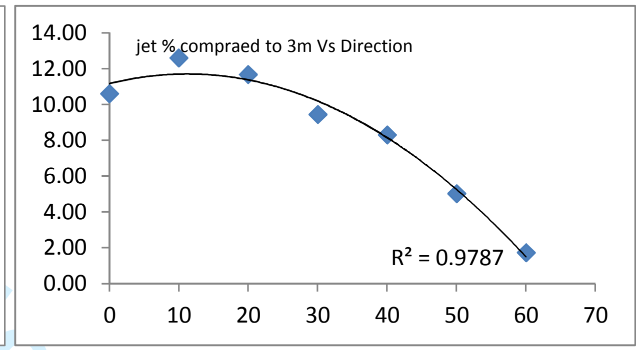

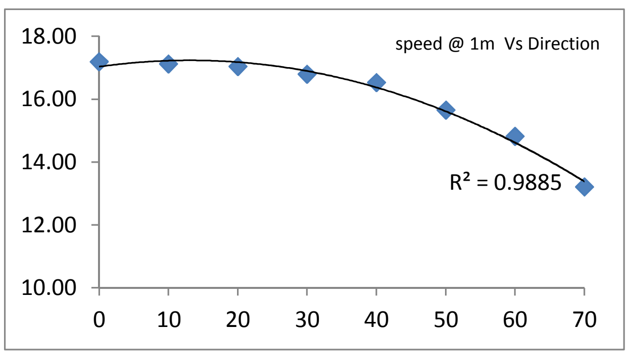

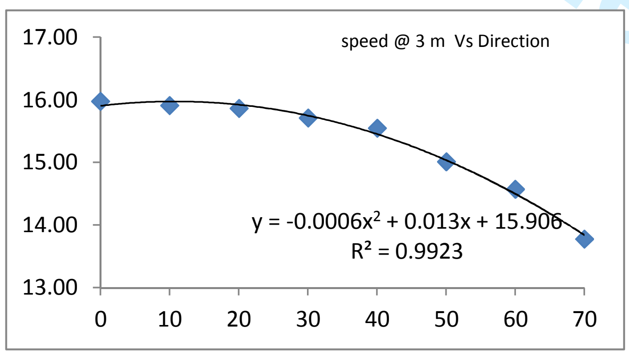

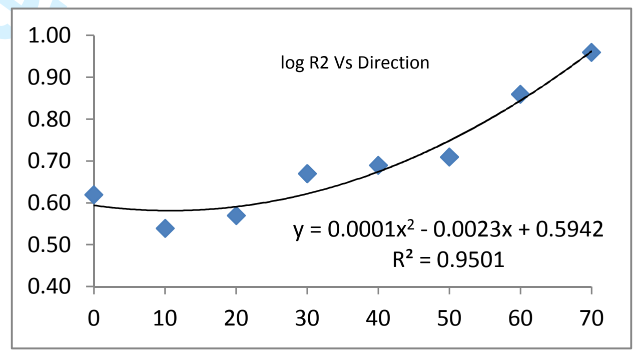

Elev	**61°**	**55°**	**46°**	**47°**	**51°**
	75	69	60.2	61	65
0.001	0	0	0	0	0
0.13	4.34			7.29	
0.55	9.98	11.12	13.83	16	14.35
1.05	12.02	13.78	16.26	18.17	16.98
1.87	12.39	13.75	15.68	17.77	16.67
3	13.04	14.63	16.34	18.22	16.99
R2	0.94	0.83	0.63	0.84	0.65

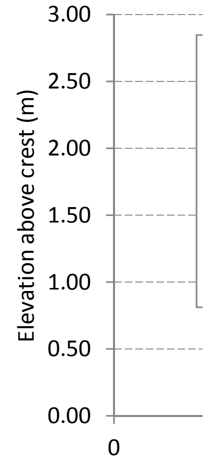

Elev	46°	51°	55°	61°
0.13				4.34
0.55	13.83	14.35	11.12	9.98
1.05	16.26	16.98	13.78	12.02
1.87	15.68	16.67	13.75	12.39
3	16.34	16.99	14.63	13.04
R2	0.63	0.65	0.83	0.94

Elev	46°	51°	55°	61°
time	0.65	14.4		
4m elev	16.10	14	12.73538	14.28
0.13				4.34
0.55	13.83	14.35	11.12	9.98
1.05	16.26	16.98	13.78	12.02
1.87	15.68	16.67	13.75	12.39
3	16.34	16.99	14.63	13.04
R2	0.63	0.65	0.83	0.94

46°		5
x	**y**	**x**
0.00	0.00	0.00
0.55	0.86	0.55
1.05	1.01	1.05
1.87	0.97	1.87
3.00	1.02	3.00

time	speed	direction	dir - 14
15:35-15:45	16.10	**61**	47
14:35-14:45	14.00	**66**	52
11:50-12:00	12.74	**71**	57
13:45-13:55	14.28	**75**	61

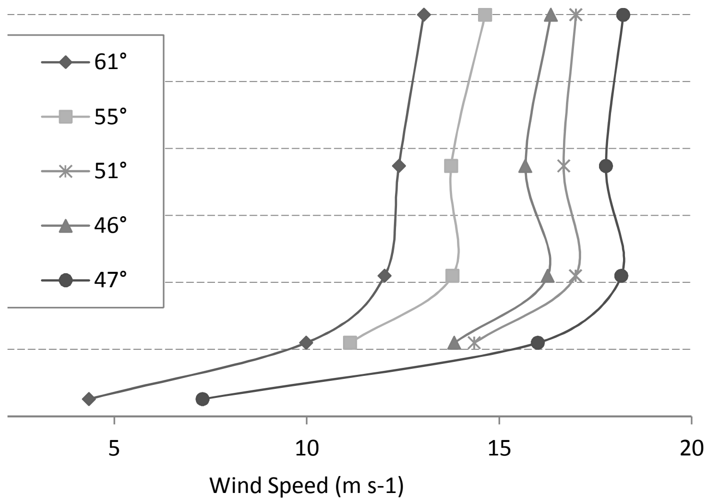

1°	55°		61°	
y	x	y	x	y
0.00	0.00	0.00	0.00	0.00
1.03	0.55	0.87	0.13	0.30
1.21	1.05	1.08	0.55	0.70
1.19	1.87	1.08	1.05	0.84
1.21	3.00	1.15	1.87	0.87
			3.00	0.91

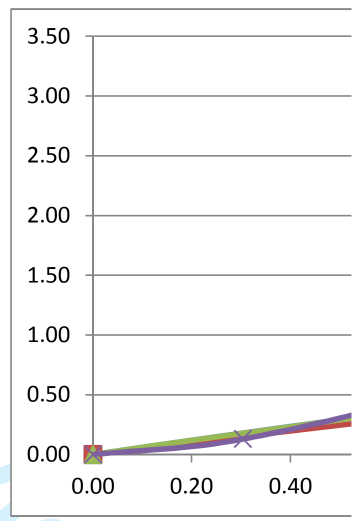

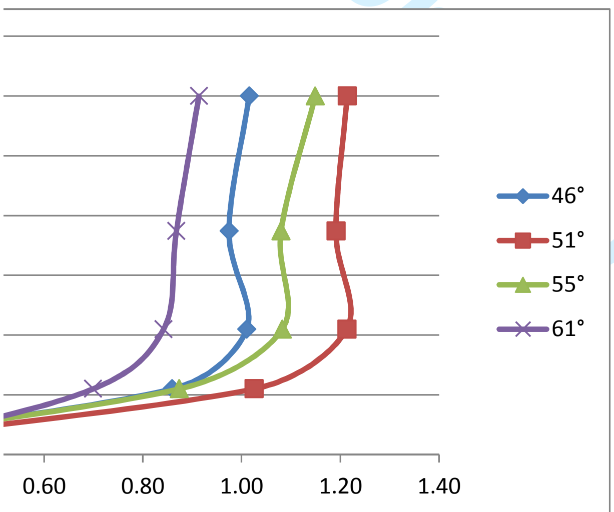
0.60
0.80
1.00
1.20
1.40
46°
51°
55°
61°

-1.50					
	u	v	w	speed	rel to 4m @ inlet
0.1	9.36767	-5.08E-17	3.51547	10.01	0.92
0.2	12.1821	3.75E-17	4.36809	12.94	1.19
0.3	13.6875	-6.19E-17	4.68943	14.47	1.33
0.4	14.5373	2.47E-17	4.73668	15.29	1.41
0.5	14.9083	0	4.68192	15.63	1.44
0.6	15.1839	0	4.58323	15.86	1.46
0.7	15.3931	-3.16E-20	4.45361	16.02	1.48
0.8	15.5533	-1.35E-17	4.30224	16.14	1.49
0.9	15.6183	-1.27E-17	4.22058	16.18	1.49
1	15.7221	-2.26E-17	4.04888	16.24	1.50
1.1	15.7621	2.14E-17	3.96006	16.25	1.50
1.2	15.8203	-9.70E-18	3.77916	16.27	1.50
1.3	15.8393	9.13E-18	3.68803	16.26	1.50
1.4	15.8521	-8.20E-20	3.59702	16.26	1.50
1.5	15.8591	-1.67E-17	3.50648	16.24	1.50
1.6	15.8606	1.60E-17	3.41675	16.22	1.50
1.7	15.857	-9.72E-20	3.32812	16.20	1.49
1.8	15.8488	-7.35E-18	3.24083	16.18	1.49
1.9	15.8364	6.92E-18	3.1551	16.15	1.49
2	15.8202	-6.66E-18	3.07109	16.12	1.49
2.1	15.8005	4.88E-20	2.98893	16.08	1.48
2.2	15.7779	5.98E-18	2.90872	16.04	1.48
2.3	15.7527	-1.16E-17	2.83053	16.00	1.48
2.4	15.7252	1.10E-17	2.75439	15.96	1.47
2.5	15.6958	-1.06E-17	2.68031	15.92	1.47
2.6	15.6958	-1.06E-17	2.68031	15.92	1.47
2.7	15.6648	6.50E-20	2.60829	15.88	1.46
2.8	15.6325	1.78E-19	2.53829	15.84	1.46
2.9	15.6325	1.78E-19	2.53829	15.84	1.46
3	15.5991	1.01E-19	2.47028	15.79	1.46
-1.25					
0.1	10.2586	5.07E-17	4.02523	11.02	1.02
0.2	12.9853	2.46E-21	4.73488	13.82	1.27
0.3	14.3919	0	4.90027	15.20	1.40
0.4	15.1667	2.36E-17	4.81521	15.91	1.47
0.5	15.4919	2.00E-17	4.68633	16.19	1.49
0.6	15.7221	0	4.52498	16.36	1.51
0.7	15.885	-1.50E-17	4.34401	16.47	1.52
0.8	15.9976	2.47E-20	4.15222	16.53	1.52
0.9	16.0384	1.24E-17	4.05432	16.54	1.52
1	16.0937	1.12E-17	3.85765	16.55	1.53
1.1	16.1098	0	3.75989	16.54	1.52
1.2	16.1217	-9.59E-18	3.56754	16.51	1.52
1.3	16.1186	-8.99E-18	3.47359	16.49	1.52
1.4	16.1102	8.72E-18	3.38146	16.46	1.52
1.5	16.097	8.20E-18	3.29133	16.43	1.51

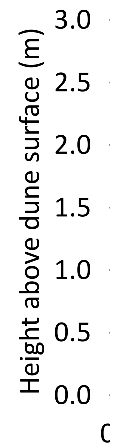

-1.50
-1.25
-1.00
-0.75
-0.50
-0.25
0.00
0.25

1.6	16.0794	-7.94E-18	3.20336	16.40	1.51
1.7	16.058	-2.99E-20	3.11765	16.36	1.51
1.8	16.033	7.15E-18	3.03428	16.32	1.50
1.9	16.0051	-6.93E-18	2.95328	16.28	1.50
2	15.9745	-6.60E-18	2.87466	16.23	1.50
2.1	15.9416	6.32E-18	2.79842	16.19	1.49
2.2	15.9069	4.60E-20	2.72451	16.14	1.49
2.3	15.8707	0	2.65289	16.09	1.48
2.4	15.8331	4.19E-20	2.5835	16.04	1.48
2.5	15.7946	-5.13E-18	2.51625	15.99	1.47
2.6	15.7946	-5.13E-18	2.51625	15.99	1.47
2.7	15.7554	1.50E-19	2.45107	15.94	1.47
2.8	15.7156	9.37E-18	2.38786	15.90	1.47
2.9	15.7156	9.37E-18	2.38786	15.90	1.47
3	15.6756	-4.53E-18	2.32654	15.85	1.46
-1.00					
0.1	14.1715	-4.14E-17	4.92271	15.00	1.38
0.2	15.3692	0	4.90896	16.13	1.49
0.3	15.8152	0	4.77941	16.52	1.52
0.4	16.1985	-2.12E-17	4.50327	16.81	1.55
0.5	16.3381	1.82E-17	4.2953	16.89	1.56
0.6	16.4177	0	4.08216	16.92	1.56
0.7	16.4538	-2.79E-20	3.87097	16.90	1.56
0.8	16.459	-2.43E-20	3.76759	16.88	1.56
0.9	16.4484	1.16E-17	3.56719	16.83	1.55
1	16.4343	-1.09E-17	3.47069	16.80	1.55
1.1	16.3917	0	3.28589	16.72	1.54
1.2	16.3642	0	3.19774	16.67	1.54
1.3	16.3333	8.76E-18	3.11245	16.63	1.53
1.4	16.2994	-8.56E-18	3.03001	16.58	1.53
1.5	16.2629	0	2.95038	16.53	1.52
1.6	16.2242	5.98E-20	2.87348	16.48	1.52
1.7	16.1836	7.21E-18	2.79923	16.42	1.51
1.8	16.1416	-7.05E-18	2.72753	16.37	1.51
1.9	16.0983	5.13E-20	2.65829	16.32	1.50
2	16.054	6.27E-18	2.59139	16.26	1.50
2.1	16.0091	-1.21E-17	2.52672	16.21	1.49
2.2	15.9636	5.88E-18	2.46417	16.15	1.49
2.3	15.9179	4.32E-20	2.40362	16.10	1.48
2.4	15.8721	0	2.34495	16.04	1.48
2.5	15.8721	0	2.34495	16.04	1.48
2.6	15.8263	0	2.28807	15.99	1.47
2.7	15.7807	3.72E-20	2.23287	15.94	1.47
2.8	15.7807	3.72E-20	2.23287	15.94	1.47
2.9	15.7354	-4.52E-18	2.17924	15.89	1.46
3	15.6905	4.03E-20	2.12709	15.83	1.46
-0.75					

0.1	13.3163	-7.22E-17	4.56481	14.08	1.30
0.2	15.537	-4.78E-17	4.79203	16.26	1.50
0.3	16.4283	-3.78E-20	4.60501	17.06	1.57
0.4	16.7908	2.72E-17	4.30027	17.33	1.60
0.5	16.8842	2.26E-17	4.08057	17.37	1.60
0.6	16.9098	0	3.86328	17.35	1.60
0.7	16.8913	0	3.6549	17.28	1.59
0.8	16.8434	2.74E-20	3.45866	17.19	1.58
0.9	16.8115	0	3.36555	17.15	1.58
1	16.7359	1.20E-17	3.18953	17.04	1.57
1.1	16.6935	-1.15E-17	3.10654	16.98	1.56
1.2	16.6019	0	2.95012	16.86	1.55
1.3	16.5535	0	2.87643	16.80	1.55
1.4	16.5038	9.14E-18	2.80557	16.74	1.54
1.5	16.453	-8.84E-18	2.73737	16.68	1.54
1.6	16.4015	0	2.6717	16.62	1.53
1.7	16.2968	0	2.54731	16.49	1.52
1.8	16.2441	0	2.48832	16.43	1.51
1.9	16.1914	0	2.43127	16.37	1.51
2	16.1914	0	2.43127	16.37	1.51
2.1	16.1388	0	2.37604	16.31	1.50
2.2	16.0864	4.86E-20	2.32252	16.25	1.50
2.3	16.0343	-4.58E-20	2.27059	16.19	1.49
2.4	15.9827	5.51E-18	2.22015	16.14	1.49
2.5	15.9317	-5.42E-18	2.17109	16.08	1.48
2.6	15.9317	-5.42E-18	2.17109	16.08	1.48
2.7	15.8812	-3.99E-20	2.12332	16.02	1.48
2.8	15.8315	-3.77E-20	2.07676	15.97	1.47
2.9	15.7825	1.44E-19	2.03133	15.91	1.47
3	15.7825	1.44E-19	2.03133	15.91	1.47

-0.50

0.1	15.8284	-8.65E-19	4.02073	16.33	1.51
0.2	17.0429	3.67E-21	3.97238	17.50	1.61
0.3	17.3375	4.13E-20	3.83087	17.76	1.64
0.4	17.4487	0	3.57742	17.81	1.64
0.5	17.4133	-2.73E-17	3.40711	17.74	1.64
0.6	17.3344	-4.80E-19	3.24446	17.64	1.63
0.7	17.2315	-3.82E-20	3.09224	17.51	1.61
0.8	17.1159	0	2.95112	17.37	1.60
0.9	17.0555	0	2.88461	17.30	1.59
1	16.9321	0	2.75912	17.16	1.58
1.1	16.8697	-2.52E-20	2.69987	17.08	1.57
1.2	16.7447	-1.15E-17	2.58764	16.94	1.56
1.3	16.6824	0	2.53437	16.87	1.56
1.4	16.6204	0	2.48282	16.80	1.55
1.5	16.5588	0	2.43285	16.74	1.54
1.6	16.437	-8.72E-18	2.33724	16.60	1.53

1.7	16.377	0	2.29138	16.54	1.52
1.8	16.3176	-6.12E-20	2.2467	16.47	1.52
1.9	16.2589	-5.82E-20	2.20311	16.41	1.51
2	16.201	-6.96E-18	2.16054	16.34	1.51
2.1	16.201	-6.96E-18	2.16054	16.34	1.51
2.2	16.1439	6.68E-18	2.11891	16.28	1.50
2.3	16.0877	6.29E-18	2.07816	16.22	1.50
2.4	16.0324	-6.13E-18	2.03823	16.16	1.49
2.5	15.978	0	1.99907	16.10	1.48
2.6	15.978	0	1.99907	16.10	1.48
2.7	15.9245	4.25E-20	1.96062	16.04	1.48
2.8	15.8721	0	1.92284	15.99	1.47
2.9	15.8206	-7.66E-20	1.88567	15.93	1.47
3	15.8206	-7.66E-20	1.88567	15.93	1.47
-0.25					
0.1	16.3406	4.85E-17	2.35563	16.51	1.52
0.2	17.574	-1.71E-17	2.60924	17.77	1.64
0.3	17.7813	-3.51E-19	2.64327	17.98	1.66
0.4	17.7749	0	2.61543	17.97	1.66
0.5	17.6776	8.06E-18	2.5718	17.86	1.65
0.6	17.5492	0	2.51882	17.73	1.63
0.7	17.4075	-5.63E-18	2.46107	17.58	1.62
0.8	17.2616	3.81E-20	2.40113	17.43	1.61
0.9	17.1887	0	2.37079	17.35	1.60
1	17.0444	3.10E-20	2.30986	17.20	1.59
1.1	16.9734	2.86E-20	2.27937	17.13	1.58
1.2	16.8338	8.02E-20	2.21852	16.98	1.56
1.3	16.7654	3.17E-18	2.18817	16.91	1.56
1.4	16.6978	0	2.1579	16.84	1.55
1.5	16.6312	0	2.1277	16.77	1.55
1.6	16.5008	-2.47E-18	2.06756	16.63	1.53
1.7	16.437	5.74E-20	2.03761	16.56	1.53
1.8	16.3742	2.31E-18	2.00777	16.50	1.52
1.9	16.3124	2.14E-18	1.97801	16.43	1.51
2	16.2517	-2.08E-18	1.94836	16.37	1.51
2.1	16.2517	-2.08E-18	1.94836	16.37	1.51
2.2	16.1919	-4.93E-22	1.91881	16.31	1.50
2.3	16.1333	-1.72E-18	1.88935	16.24	1.50
2.4	16.0757	1.72E-18	1.86	16.18	1.49
2.5	16.0192	-5.07E-20	1.83075	16.12	1.49
2.6	16.0192	-5.07E-20	1.83075	16.12	1.49
2.7	15.9638	0	1.8016	16.07	1.48
2.8	15.9095	-9.11E-20	1.77255	16.01	1.48
2.9	15.8564	-8.62E-20	1.74358	15.95	1.47
3	15.8564	-8.62E-20	1.74358	15.95	1.47

Crest

0.1	14.5014	0	0.223057	14.50	1.34
0.2	16.8127	-2.61E-20	0.867985	16.84	1.55
0.3	17.4847	1.01E-17	1.3074	17.53	1.62
0.4	17.6015	7.94E-18	1.5023	17.67	1.63
0.5	17.5952	-6.74E-18	1.63917	17.67	1.63
0.6	17.523	-1.69E-19	1.7325	17.61	1.62
0.7	17.4157	-3.69E-20	1.79345	17.51	1.61
0.8	17.2906	-3.19E-20	1.83023	17.39	1.60
0.9	17.1572	0	1.84887	17.26	1.59
1	17.0893	2.77E-22	1.8528	17.19	1.58
1.1	17.021	0	1.85374	17.12	1.58
1.2	16.8847	-4.45E-20	1.848	16.99	1.57
1.3	16.817	-2.69E-18	1.84191	16.92	1.56
1.4	16.7498	2.57E-18	1.83398	16.85	1.55
1.5	16.6832	3.78E-20	1.8244	16.78	1.55
1.6	16.5519	0	1.80099	16.65	1.53
1.7	16.4874	2.03E-18	1.78743	16.58	1.53
1.8	16.4237	-3.91E-18	1.7728	16.52	1.52
1.9	16.3608	1.88E-18	1.75718	16.45	1.52
2	16.2989	1.80E-18	1.74068	16.39	1.51
2.1	16.2989	1.80E-18	1.74068	16.39	1.51
2.2	16.238	-4.27E-20	1.72339	16.33	1.50
2.3	16.1781	-9.00E-20	1.70536	16.27	1.50
2.4	16.1192	-1.54E-18	1.68667	16.21	1.49
2.5	16.0615	-1.39E-18	1.66738	16.15	1.49
2.6	16.0615	-1.39E-18	1.66738	16.15	1.49
2.7	16.0048	1.35E-18	1.64755	16.09	1.48
2.8	15.9492	8.14E-20	1.62721	16.03	1.48
2.9	15.8947	7.73E-20	1.60641	15.98	1.47
3	15.8947	7.73E-20	1.60641	15.98	1.47
0.25					
0.1	8.3593	4.26E-20	-0.75755	8.39	0.77
0.2	13.4699	2.44E-20	-0.50362	13.48	1.24
0.3	15.7741	1.99E-17	0.031626	15.77	1.45
0.4	16.7641	2.99E-20	0.510601	16.77	1.55
0.5	17.0561	1.29E-17	0.764498	17.07	1.57
0.6	17.1829	2.10E-20	0.96771	17.21	1.59
0.7	17.2084	-1.82E-17	1.12712	17.25	1.59
0.8	17.172	-3.03E-20	1.25037	17.22	1.59
0.9	17.1385	-7.14E-18	1.30062	17.19	1.58
1	17.0515	-2.47E-20	1.38202	17.11	1.58
1.1	17.0009	0	1.4144	17.06	1.57
1.2	16.8906	-5.36E-18	1.46505	16.95	1.56
1.3	16.8323	-4.94E-18	1.48418	16.90	1.56
1.4	16.7726	1.52E-19	1.49968	16.84	1.55
1.5	16.7119	4.54E-18	1.51186	16.78	1.55
1.6	16.6506	-3.34E-20	1.52101	16.72	1.54
1.7	16.589	3.18E-20	1.5274	16.66	1.54

1.8	16.5272	0	1.53126	16.60	1.53
1.9	16.4656	-3.61E-18	1.53281	16.54	1.52
2	16.4042	8.60E-20	1.53224	16.48	1.52
2.1	16.3432	3.35E-18	1.52973	16.41	1.51
2.2	16.2827	-7.21E-22	1.52543	16.35	1.51
2.3	16.2229	0	1.51951	16.29	1.50
2.4	16.1638	0	1.51208	16.23	1.50
2.5	16.1056	4.27E-20	1.50329	16.18	1.49
2.6	16.1056	4.27E-20	1.50329	16.18	1.49
2.7	16.0483	4.01E-20	1.49323	16.12	1.49
2.8	15.9919	0	1.48202	16.06	1.48
2.9	15.9919	0	1.48202	16.06	1.48
3	15.9366	-7.35E-20	1.46974	16.00	1.48

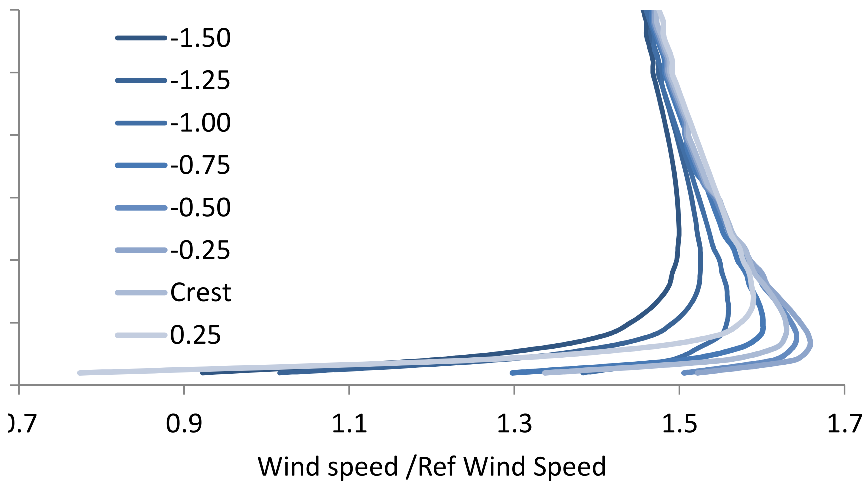

65.2	8.35
65.45	8.45
65.7	8.56
65.95	8.66
66.2	8.75
66.45	8.80
66.7	8.81
66.95	8.76

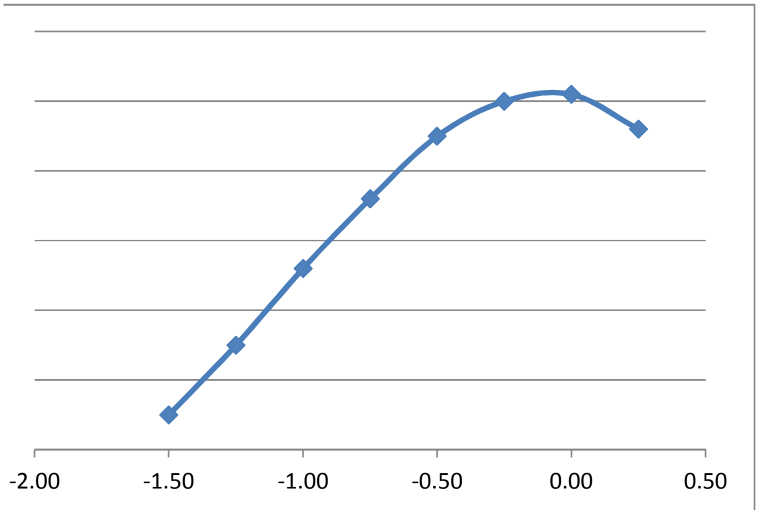
-2.00
-1.50
-1.00
-0.50
0.00
0.50

x	y	
0	0.53	-30
0.25	0.53	-29.75
0.5	0.54	-29.5
0.75	0.54	-29.25
1	0.55	-29
1.25	0.55	-28.75
1.5	0.56	-28.5
1.75	0.56	-28.25
2	0.57	-28
2.25	0.57	-27.75
2.5	0.58	-27.5
2.75	0.58	-27.25
3	0.59	-27
3.25	0.59	-26.75
3.5	0.6	-26.5
3.75	0.6	-26.25
4	0.61	-26
4.25	0.61	-25.75
4.5	0.62	-25.5
4.75	0.62	-25.25
5	0.62	-25
5.25	0.63	-24.75
5.5	0.63	-24.5
5.75	0.64	-24.25
6	0.64	-24
6.25	0.65	-23.75
6.49	0.65	-23.51
6.74	0.66	-23.26
6.99	0.66	-23.01
7.24	0.67	-22.76
7.49	0.67	-22.51
7.74	0.68	-22.26
7.99	0.68	-22.01
8.24	0.69	-21.76
8.49	0.69	-21.51
8.74	0.7	-21.26
8.99	0.7	-21.01
9.24	0.71	-20.76
9.49	0.71	-20.51
9.74	0.72	-20.26
9.99	0.72	-20.01
10.24	0.73	-19.76
10.49	0.73	-19.51
10.74	0.74	-19.26
10.99	0.74	-19.01
11.24	0.75	-18.76
11.49	0.75	-18.51
11.74	0.76	-18.26
11.99	0.76	-18.01

UA height	Dist		Rel Height
0.13	66.5	36.5	8.94
0.55	66.5	36.5	9.36
1.05	66.5	36.5	9.86
1.87	66.5	36.5	10.68
3	66.5	36.5	11.81
4.25	38	8	5.98

12.24	0.77	-17.76
12.49	0.77	-17.51
12.74	0.78	-17.26
12.99	0.78	-17.01
13.24	0.79	-16.76
13.49	0.79	-16.51
13.74	0.79	-16.26
13.99	0.8	-16.01
14.24	0.8	-15.76
14.49	0.81	-15.51
14.74	0.81	-15.26
14.99	0.82	-15.01
15.24	0.82	-14.76
15.49	0.83	-14.51
15.74	0.83	-14.26
15.99	0.84	-14.01
16.24	0.84	-13.76
16.49	0.85	-13.51
16.74	0.85	-13.26
16.99	0.86	-13.01
17.24	0.86	-12.76
17.49	0.87	-12.51
17.74	0.87	-12.26
17.99	0.88	-12.01
18.24	0.88	-11.76
18.49	0.89	-11.51
18.74	0.89	-11.26
18.98	0.9	-11.02
19.23	0.9	-10.77
19.48	0.91	-10.52
19.73	0.91	-10.27
19.98	0.92	-10.02
20.23	0.92	-9.77
20.48	0.93	-9.52
20.73	0.93	-9.27
20.98	0.94	-9.02
21.23	0.94	-8.77
21.48	0.95	-8.52
21.73	0.95	-8.27
21.98	0.96	-8.02
22.23	0.96	-7.77
22.48	0.97	-7.52
22.73	0.97	-7.27
22.98	0.98	-7.02
23.23	0.98	-6.77
23.48	0.98	-6.52
23.73	0.99	-6.27
23.98	0.99	-6.02
24.23	1	-5.77
24.48	1	-5.52

24.73	1.01	-5.27
24.98	1.01	-5.02
25.23	1.02	-4.77
25.48	1.02	-4.52
25.73	1.03	-4.27
25.98	1.04	-4.02
26.23	1.05	-3.77
26.48	1.06	-3.52
26.73	1.07	-3.27
26.98	1.08	-3.02
27.23	1.09	-2.77
27.48	1.1	-2.52
27.73	1.11	-2.27
27.98	1.12	-2.02
28.23	1.12	-1.77
28.48	1.13	-1.52
28.73	1.14	-1.27
28.98	1.15	-1.02
29.23	1.16	-0.77
29.48	1.17	-0.52
29.73	1.17	-0.27
29.98	1.18	-0.02
30.23	1.19	0.23
30.48	1.18	0.48
30.73	1.18	0.73
30.98	1.19	0.98
31.23	1.21	1.23
31.48	1.22	1.48
31.72	1.23	1.72
31.97	1.24	1.97
32.22	1.25	2.22
32.47	1.26	2.47
32.72	1.26	2.72
32.97	1.27	2.97
33.22	1.28	3.22
33.47	1.29	3.47
33.72	1.3	3.72
33.97	1.31	3.97
34.22	1.32	4.22
34.47	1.34	4.47
34.72	1.35	4.72
34.97	1.36	4.97
35.22	1.38	5.22
35.47	1.39	5.47
35.72	1.41	5.72
35.97	1.42	5.97
36.22	1.44	6.22
36.47	1.46	6.47
36.72	1.47	6.72
36.97	1.49	6.97

37.22	1.5	7.22
37.47	1.52	7.47
37.72	1.53	7.72
37.97	1.55	7.97
38.22	1.57	8.22
38.47	1.58	8.47
38.72	1.6	8.72
38.97	1.62	8.97
39.22	1.64	9.22
39.47	1.66	9.47
39.72	1.68	9.72
39.97	1.7	9.97
40.22	1.72	10.22
40.47	1.73	10.47
40.72	1.75	10.72
40.97	1.77	10.97
41.22	1.79	11.22
41.47	1.81	11.47
41.72	1.83	11.72
41.97	1.85	11.97
42.22	1.86	12.22
42.47	1.88	12.47
42.72	1.9	12.72
42.97	1.92	12.97
43.22	1.94	13.22
43.47	1.96	13.47
43.72	1.98	13.72
43.97	2	13.97
44.22	2.01	14.22
44.46	2.03	14.46
44.71	2.04	14.71
44.96	2.06	14.96
45.21	2.08	15.21
45.46	2.1	15.46
45.71	2.12	15.71
45.96	2.15	15.96
46.21	2.18	16.21
46.46	2.22	16.46
46.71	2.25	16.71
46.96	2.29	16.96
47.21	2.33	17.21
47.46	2.37	17.46
47.71	2.41	17.71
47.96	2.47	17.96
48.21	2.53	18.21
48.46	2.59	18.46
48.71	2.65	18.71
48.96	2.71	18.96
49.21	2.76	19.21
49.46	2.81	19.46

49.71	2.87	19.71
49.96	2.96	19.96
50.21	3.1	20.21
50.46	3.29	20.46
50.71	3.46	20.71
50.96	3.57	20.96
51.21	3.63	21.21
51.46	3.68	21.46
51.71	3.74	21.71
51.96	3.81	21.96
52.21	3.89	22.21
52.46	3.97	22.46
52.71	4.05	22.71
52.96	4.14	22.96
53.21	4.23	23.21
53.46	4.32	23.46
53.71	4.4	23.71
53.96	4.49	23.96
54.21	4.57	24.21
54.46	4.64	24.46
54.71	4.72	24.71
54.96	4.8	24.96
55.21	4.87	25.21
55.46	4.95	25.46
55.71	5.02	25.71
55.96	5.08	25.96
56.21	5.14	26.21
56.46	5.22	26.46
56.71	5.3	26.71
56.96	5.38	26.96
57.2	5.46	27.2
57.45	5.55	27.45
57.7	5.64	27.7
57.95	5.73	27.95
58.2	5.82	28.2
58.45	5.92	28.45
58.7	6.01	28.7
58.95	6.1	28.95
59.2	6.19	29.2
59.45	6.28	29.45
59.7	6.37	29.7
59.95	6.46	29.95
60.2	6.55	30.2
60.45	6.65	30.45
60.7	6.74	30.7
60.95	6.83	30.95
61.2	6.92	31.2
61.45	7	31.45
61.7	7.07	31.7
61.95	7.14	31.95

62.2	7.24	32.2
62.45	7.36	32.45
62.7	7.48	32.7
62.95	7.58	32.95
63.2	7.66	33.2
63.45	7.74	33.45
63.7	7.83	33.7
63.95	7.9	33.95
64.2	7.98	34.2
64.45	8.06	34.45
64.7	8.16	34.7
64.95	8.26	34.95
65.2	8.35	35.2
65.45	8.45	35.45
65.7	8.56	35.7
65.95	8.66	35.95
66.2	8.75	36.2
66.45	8.8	36.45
66.7	8.81	36.7
66.95	8.76	36.95
67.2	8.69	37.2
67.45	8.61	37.45
67.7	8.54	37.7
67.95	8.49	37.95
68.2	8.46	38.2
68.45	8.45	38.45
68.7	8.43	38.7
68.95	8.41	38.95
69.2	8.38	39.2
69.45	8.34	39.45
69.69	8.31	39.69
69.94	8.28	39.94
70.19	8.25	40.19
70.44	8.2	40.44
70.69	8.16	40.69
70.94	8.12	40.94
71.19	8.08	41.19
71.44	8.04	41.44
71.69	8	41.69
71.94	7.93	41.94
72.19	7.84	42.19
72.44	7.76	42.44
72.69	7.73	42.69
72.94	7.75	42.94
73.19	7.78	43.19
73.44	7.79	43.44
73.69	7.78	43.69
73.94	7.77	43.94
74.19	7.76	44.19
74.44	7.76	44.44

74.69	7.75	44.69
74.94	7.75	44.94
75.19	7.75	45.19
75.44	7.75	45.44
75.69	7.75	45.69
75.94	7.75	45.94
76.19	7.75	46.19
76.44	7.75	46.44
76.69	7.74	46.69
76.94	7.73	46.94
77.19	7.73	47.19
77.44	7.72	47.44
77.69	7.72	47.69
77.94	7.71	47.94
78.19	7.7	48.19
78.44	7.69	48.44
78.69	7.65	48.69
78.94	7.58	48.94
79.19	7.49	49.19
79.44	7.39	49.44
79.69	7.28	49.69
79.94	7.18	49.94
80.19	7.06	50.19
80.44	6.96	50.44
80.69	6.86	50.69
80.94	6.79	50.94
81.19	6.74	51.19
81.44	6.7	51.44
81.69	6.66	51.69
81.94	6.62	51.94
82.18	6.58	52.18
82.43	6.54	52.43
82.68	6.49	52.68
82.93	6.44	52.93
83.18	6.39	53.18
83.43	6.34	53.43
83.68	6.3	53.68
83.93	6.25	53.93
84.18	6.2	54.18
84.43	6.15	54.43
84.68	6.12	54.68
84.93	6.08	54.93
85.18	6.02	55.18
85.43	5.97	55.43
85.68	5.91	55.68
85.93	5.85	55.93
86.18	5.79	56.18
86.43	5.72	56.43
86.68	5.66	56.68
86.93	5.59	56.93

87.18	5.52	57.18
87.43	5.47	57.43
87.68	5.43	57.68
87.93	5.4	57.93
88.18	5.36	58.18
88.43	5.31	58.43
88.68	5.26	58.68
88.93	5.19	58.93
89.18	5.13	59.18
89.43	5.1	59.43
89.68	5.06	59.68
89.93	5.01	59.93
90.18	4.96	60.18
90.43	4.9	60.43
90.68	4.85	60.68
90.93	4.8	60.93
91.18	4.75	61.18
91.43	4.69	61.43
91.68	4.64	61.68
91.93	4.59	61.93
92.18	4.54	62.18
92.43	4.49	62.43
92.68	4.44	62.68
92.93	4.39	62.93
93.18	4.34	63.18
93.43	4.29	63.43
93.68	4.24	63.68
93.93	4.19	63.93
94.18	4.14	64.18
94.43	4.09	64.43
94.67	4.04	64.67
94.92	3.99	64.92
95.17	3.94	65.17
95.42	3.89	65.42
95.67	3.84	65.67
95.92	3.79	65.92
96.17	3.74	66.17
96.42	3.69	66.42
96.67	3.64	66.67
96.92	3.59	66.92
97.17	3.54	67.17
97.42	3.49	67.42
97.67	3.44	67.67
97.92	3.4	67.92
98.17	3.36	68.17
98.42	3.32	68.42
98.67	3.29	68.67
98.92	3.26	68.92
99.17	3.23	69.17
99.42	3.19	69.42

99.67	3.16	69.67
99.92	3.13	69.92
100.17	3.09	70.17
100.42	3.06	70.42
100.67	3.03	70.67
100.92	2.99	70.92
101.17	2.96	71.17
101.42	2.93	71.42
101.67	2.89	71.67
101.92	2.86	71.92
102.17	2.83	72.17
102.42	2.81	72.42
102.67	2.79	72.67
102.92	2.77	72.92
103.17	2.76	73.17
103.42	2.75	73.42
103.67	2.74	73.67
103.92	2.73	73.92
104.17	2.72	74.17
104.42	2.71	74.42
104.67	2.71	74.67
104.92	2.72	74.92
105.17	2.74	75.17
105.42	2.75	75.42
105.67	2.77	75.67
105.92	2.79	75.92
106.17	2.81	76.17
106.42	2.83	76.42
106.67	2.84	76.67
106.92	2.86	76.92
107.17	2.88	77.17
107.41	2.89	77.41
107.66	2.91	77.66
107.91	2.92	77.91
108.16	2.94	78.16
108.41	2.95	78.41
108.66	2.96	78.66
108.91	2.97	78.91
109.16	2.96	79.16
109.41	2.95	79.41
109.66	2.92	79.66
109.91	2.9	79.91
110.16	2.87	80.16
110.41	2.85	80.41
110.66	2.83	80.66
110.91	2.8	80.91
111.16	2.78	81.16
111.41	2.77	81.41
111.66	2.77	81.66
111.91	2.76	81.91

112.16	2.76	82.16
112.41	2.75	82.41
112.66	2.75	82.66
112.91	2.75	82.91
113.16	2.74	83.16
113.41	2.74	83.41
113.66	2.74	83.66
113.91	2.74	83.91
114.16	2.74	84.16
114.41	2.74	84.41
114.66	2.74	84.66
114.91	2.74	84.91
115.16	2.73	85.16
115.41	2.73	85.41
115.66	2.73	85.66
115.91	2.73	85.91
116.16	2.73	86.16
116.41	2.73	86.41
116.66	2.73	86.66
116.91	2.72	86.91
117.16	2.72	87.16
117.41	2.72	87.41
117.66	2.72	87.66
117.91	2.72	87.91
118.16	2.72	88.16
118.41	2.72	88.41
118.66	2.71	88.66
118.91	2.71	88.91
119.16	2.71	89.16
119.41	2.71	89.41
119.66	2.71	89.66
119.91	2.71	89.91
120.15	2.71	90.15
120.4	2.71	90.4
120.65	2.7	90.65
120.9	2.7	90.9
121.15	2.7	91.15
121.4	2.7	91.4
121.65	2.7	91.65
121.9	2.7	91.9
122.15	2.7	92.15
122.4	2.69	92.4
122.65	2.69	92.65
122.9	2.69	92.9
123.15	2.69	93.15
123.4	2.69	93.4
123.65	2.69	93.65
123.9	2.69	93.9
124.15	2.69	94.15
124.4	2.68	94.4

124.65	2.68	94.65
124.9	2.68	94.9
125.15	2.68	95.15
125.4	2.68	95.4
125.65	2.68	95.65
125.9	2.68	95.9
126.15	2.67	96.15
126.4	2.67	96.4
126.65	2.67	96.65
126.9	2.67	96.9
127.15	2.67	97.15
127.4	2.67	97.4
127.65	2.67	97.65
127.9	2.67	97.9
128.15	2.66	98.15
128.4	2.66	98.4
128.65	2.66	98.65
128.9	2.66	98.9
129.15	2.66	99.15
129.4	2.66	99.4
129.65	2.66	99.65
129.9	2.65	99.9
130.15	2.65	100.15
130.4	2.65	100.4
130.65	2.65	100.65
130.9	2.65	100.9
131.15	2.65	101.15
131.4	2.65	101.4
131.65	2.65	101.65
131.9	2.64	101.9
132.15	2.64	102.15
132.4	2.64	102.4
132.65	2.64	102.65
132.89	2.64	102.89
133.14	2.64	103.14
133.39	2.64	103.39
133.64	2.63	103.64
133.89	2.63	103.89
134.14	2.63	104.14
134.39	2.63	104.39
134.64	2.63	104.64
134.89	2.63	104.89
135.14	2.63	105.14
135.39	2.62	105.39
135.64	2.62	105.64
135.89	2.62	105.89
136.14	2.62	106.14
136.39	2.62	106.39
136.64	2.62	106.64
136.89	2.62	106.89

137.14	2.62	107.14
137.39	2.61	107.39
137.64	2.61	107.64
137.89	2.61	107.89
138.14	2.61	108.14
138.39	2.61	108.39
138.64	2.61	108.64
138.89	2.61	108.89
139.14	2.6	109.14
139.39	2.6	109.39
139.64	2.6	109.64
139.89	2.6	109.89
140.14	2.6	110.14
140.39	2.6	110.39
140.64	2.6	110.64
140.89	2.6	110.89
141.14	2.59	111.14
141.39	2.59	111.39
141.64	2.59	111.64
141.89	2.59	111.89
142.14	2.59	112.14
142.39	2.59	112.39
142.64	2.59	112.64
142.89	2.58	112.89
143.14	2.58	113.14
143.39	2.58	113.39
143.64	2.58	113.64
143.89	2.58	113.89
144.14	2.58	114.14
144.39	2.58	114.39
144.64	2.58	114.64
144.89	2.57	114.89
145.14	2.57	115.14
145.39	2.57	115.39
145.63	2.57	115.63
145.88	2.57	115.88
146.13	2.57	116.13
146.38	2.57	116.38
146.63	2.56	116.63
146.88	2.56	116.88
147.13	2.56	117.13
147.38	2.56	117.38
147.63	2.56	117.63
147.88	2.56	117.88
148.13	2.56	118.13
148.38	2.55	118.38
148.63	2.55	118.63
148.88	2.55	118.88
149.13	2.55	119.13
149.38	2.55	119.38

149.63	2.55	119.63
149.88	2.55	119.88
150.13	2.55	120.13
150.38	2.54	120.38
150.63	2.54	120.63
150.88	2.54	120.88
151.13	2.54	121.13
151.38	2.54	121.38
151.63	2.54	121.63
151.88	2.54	121.88
152.13	2.53	122.13
152.38	2.53	122.38
152.63	2.53	122.63
152.88	2.53	122.88
153.13	2.53	123.13
153.38	2.53	123.38
153.63	2.53	123.63
153.88	2.53	123.88
154.13	2.52	124.13
154.38	2.52	124.38
154.63	2.52	124.63
154.88	2.52	124.88
155.13	2.52	125.13
155.38	2.52	125.38
155.63	2.52	125.63
155.88	2.51	125.88

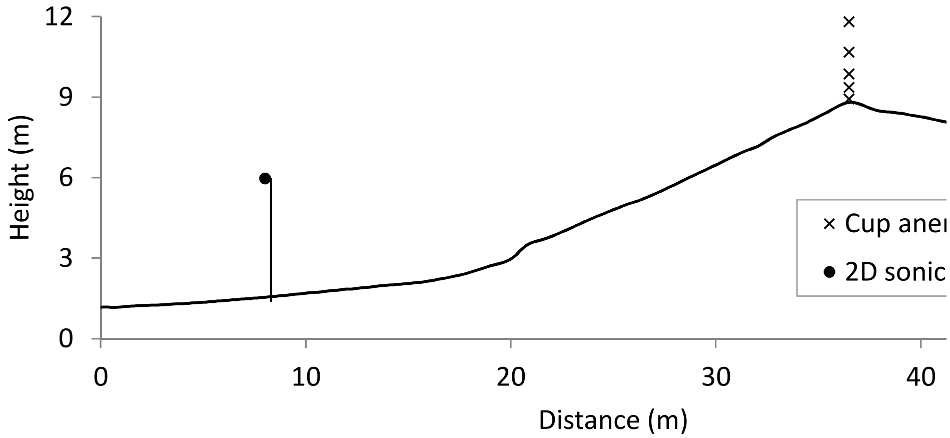

12
9
6
3
0
Height (m)
0
10
20
30
40
Distance (m)
× Cup aner
● 2D sonic

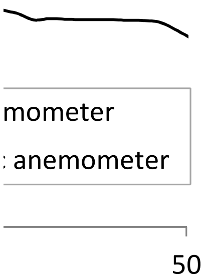
mometer
anemometer
50

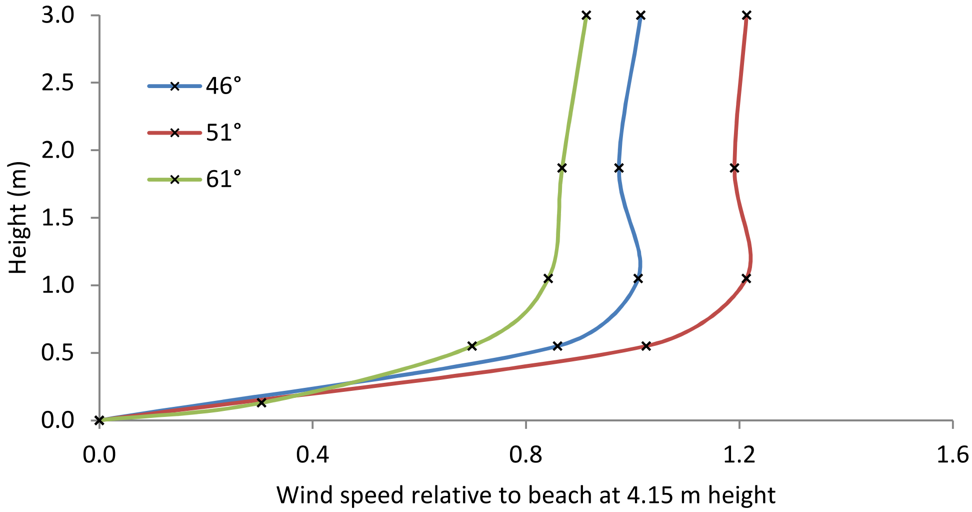
3.0
2.5
2.0
1.5
1.0
0.5
0.0
Height (m)
46°
51°
61°
0.0
0.4
0.8
1.2
1.6
Wind speed relative to beach at 4.15 m height

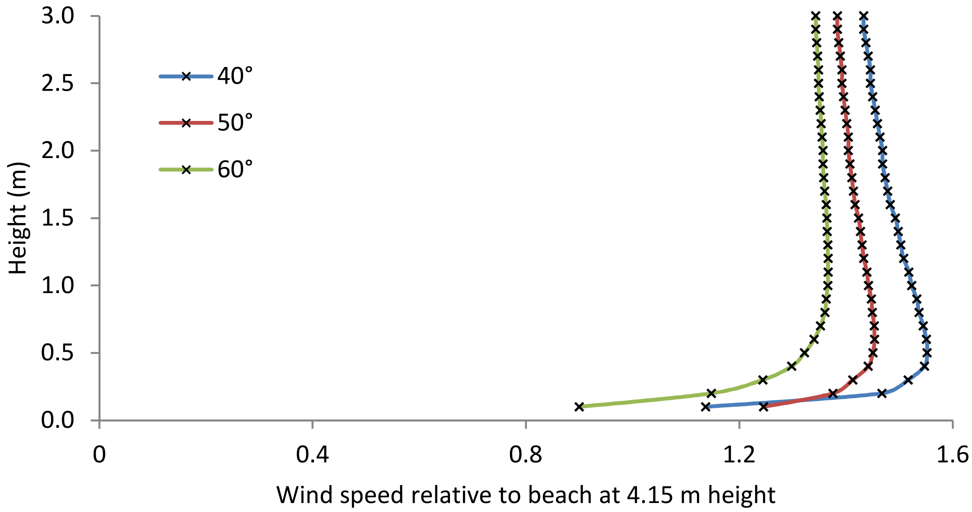
3.0
2.5
2.0
1.5
1.0
0.5
0.0
Height (m)
40°
50°
60°
0
0.4
0.8
1.2
1.6
Wind speed relative to beach at 4.15 m height

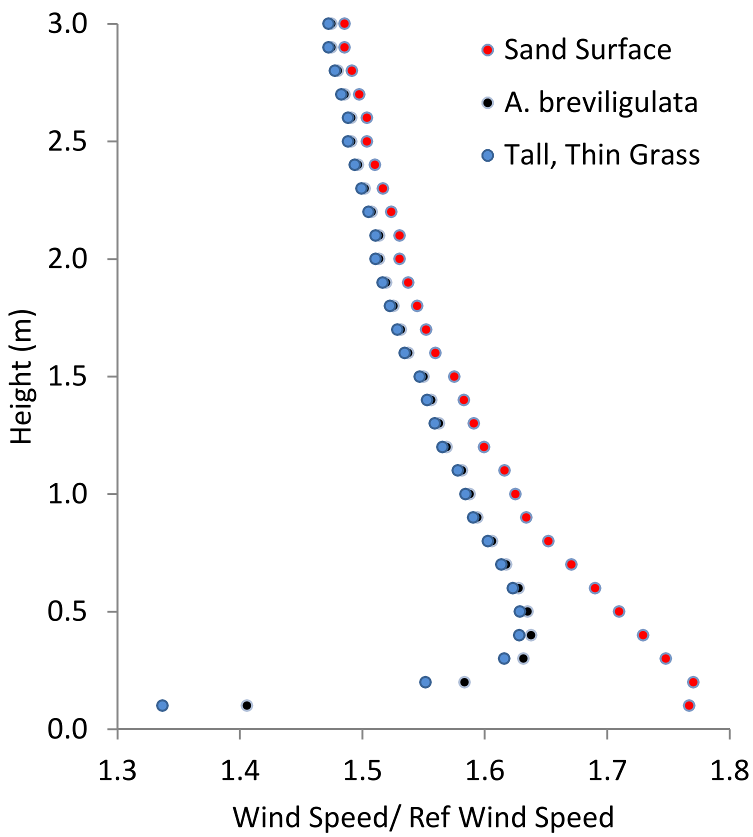
Sand Surface
A. breviligulata
Tall, Thin Grass
Height (m)
3.0
2.5
2.0
1.5
1.0
0.5
0.0
1.3
1.4
1.5
1.6
1.7
1.8
Wind Speed/ Ref Wind Speed

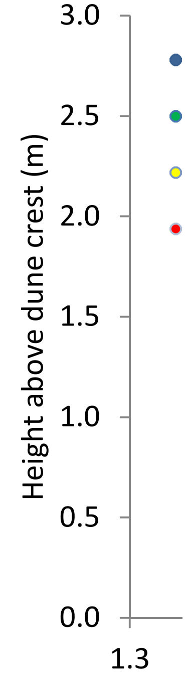
Height above dune crest (m)
3.0
2.5
2.0
1.5
1.0
0.5
0.0
1.3

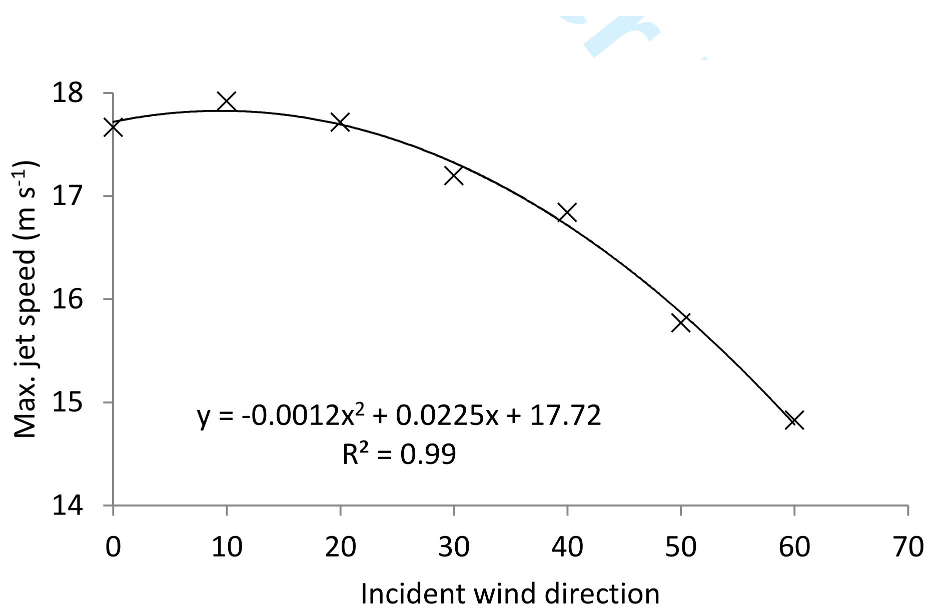
Max. jet speed (m s-1)
18
17
16
15
14
y = -0.0012x2 + 0.0225x + 17.72
R2 = 0.99
0
10
20
30
40
50
60
70
Incident wind direction

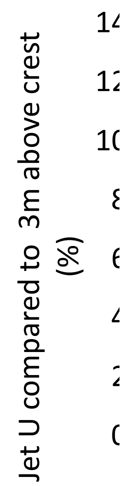
Jet U compared to 3m above crest
(%)

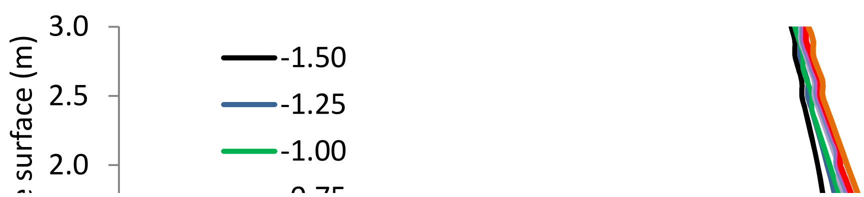
3.0
2.5
2.0
-1.50
-1.25
-1.00

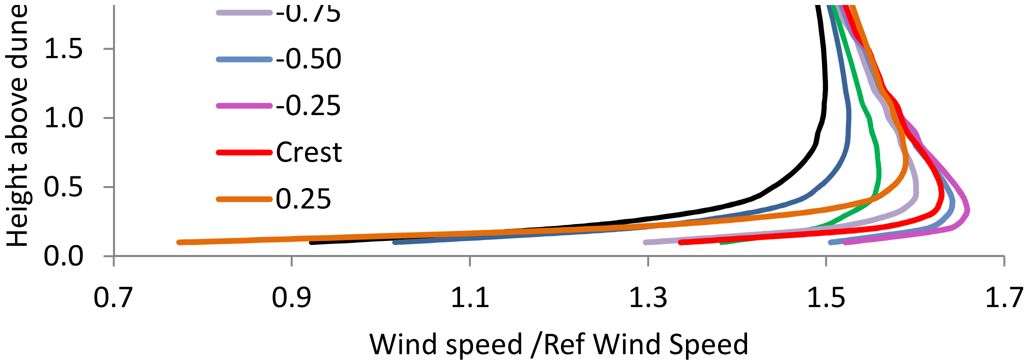
-0.75
-0.50
-0.25
Crest
0.25
Height above dune
1.5
1.0
0.5
0.0
0.7
0.9
1.1
1.3
1.5
1.7
Wind speed /Ref Wind Speed

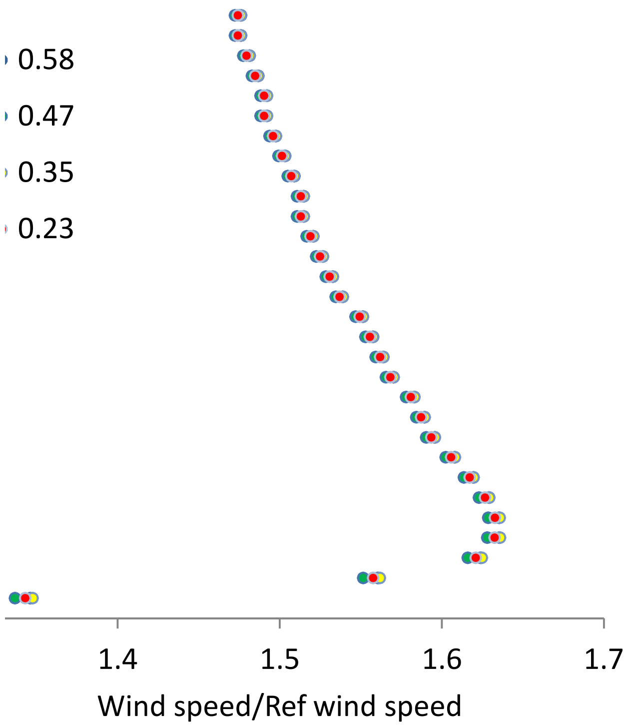
0.58
0.47
0.35
0.23
1.4
1.5
1.6
1.7
Wind speed/Ref wind speed

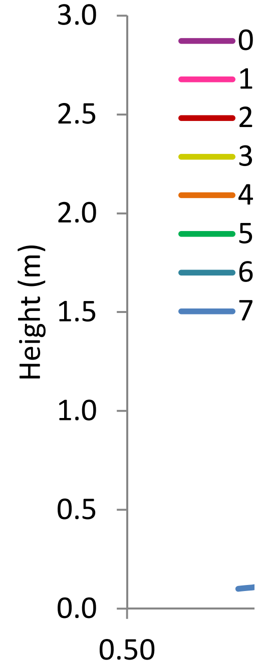
3.0
2.5
2.0
1.5
1.0
0.5
0.0
Height (m)
0.50
0
1
2
3
4
5
6
7

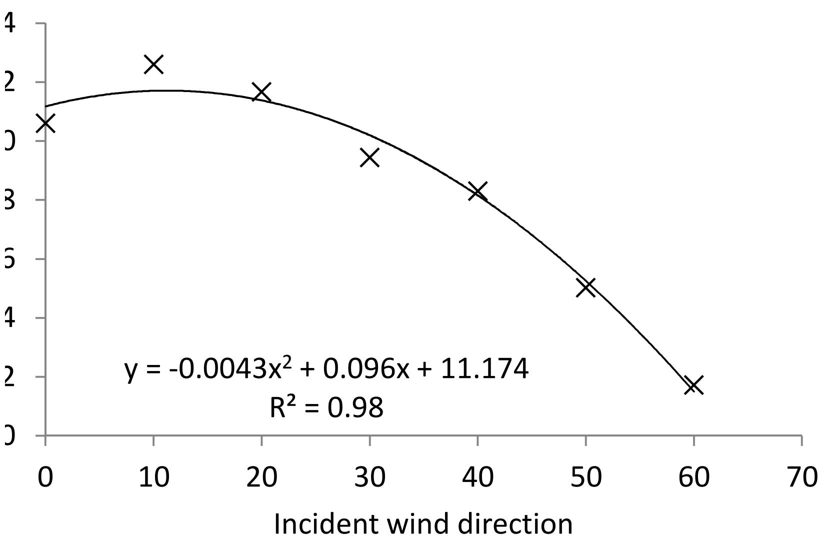
y = -0.0043x² + 0.096x + 11.174
R² = 0.98
0
10
20
30
40
50
60
70
Incident wind direction

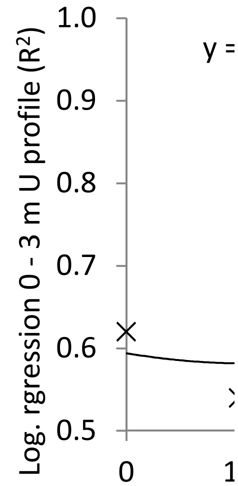
1.0
0.9
0.8
0.7
0.6
0.5
Log. rgression 0 - 3 m U profile (R²)
y =
0
1

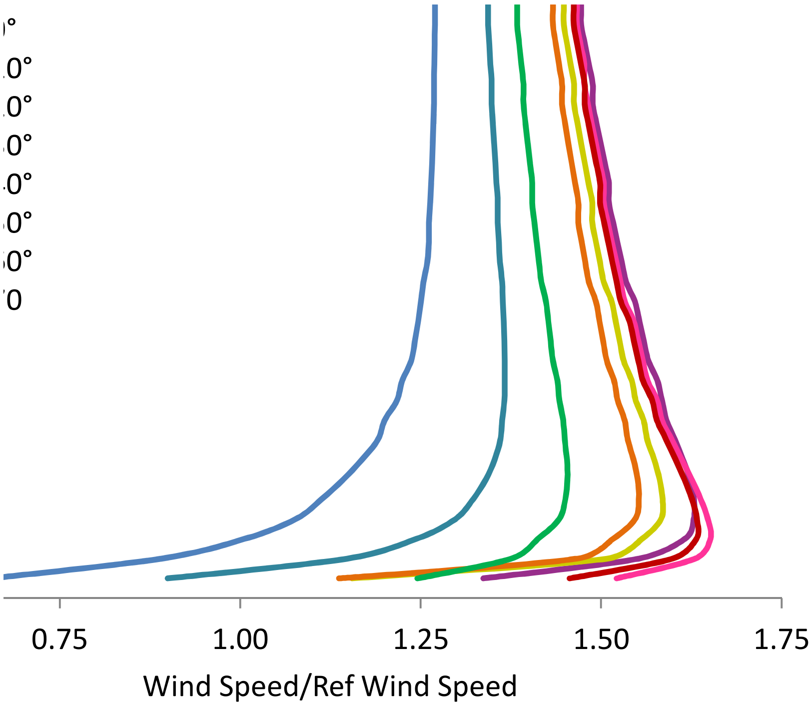
0.75
1.00
1.25
1.50
1.75
Wind Speed/Ref Wind Speed

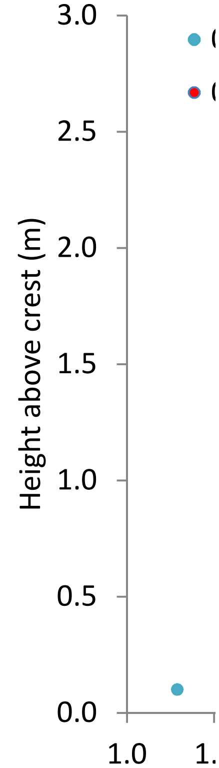
3.0
2.5
2.0
1.5
1.0
0.5
0.0
Height above crest (m)
1.0

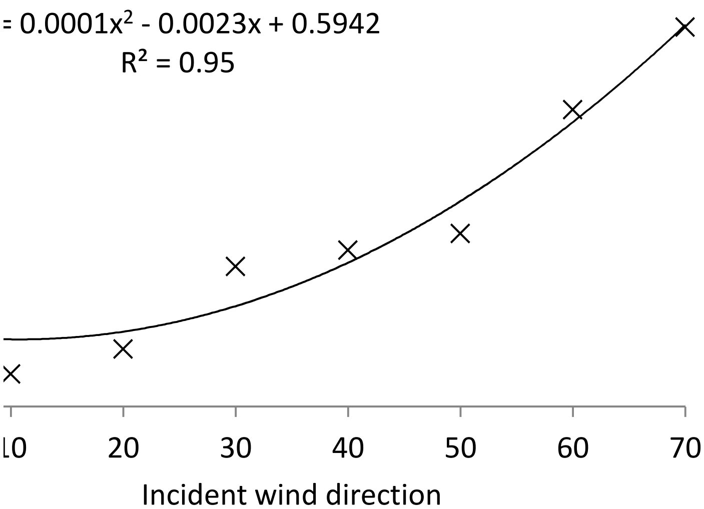
= 0.0001x² - 0.0023x + 0.5942
R² = 0.95
20
30
40
50
60
70
Incident wind direction

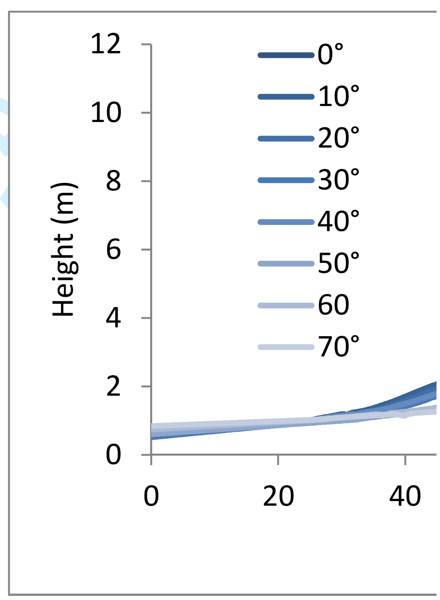
0°
10°
20°
30°
40°
50°
60
70°
12
10
8
6
4
2
0
Height (m)
0
20
40


8
-2.00
-1.50
Dis

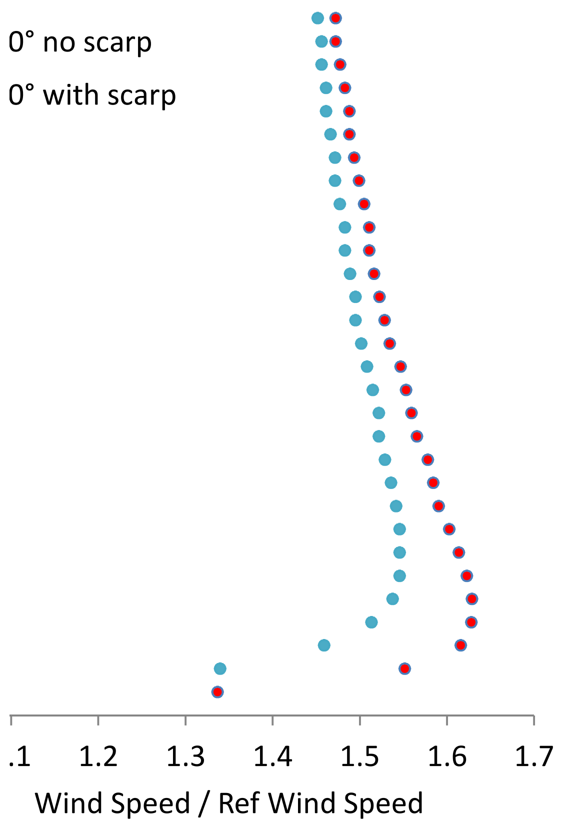
0° no scarp
0° with scarp
.1
1.2
1.3
1.4
1.5
1.6
1.7
Wind Speed / Ref Wind Speed

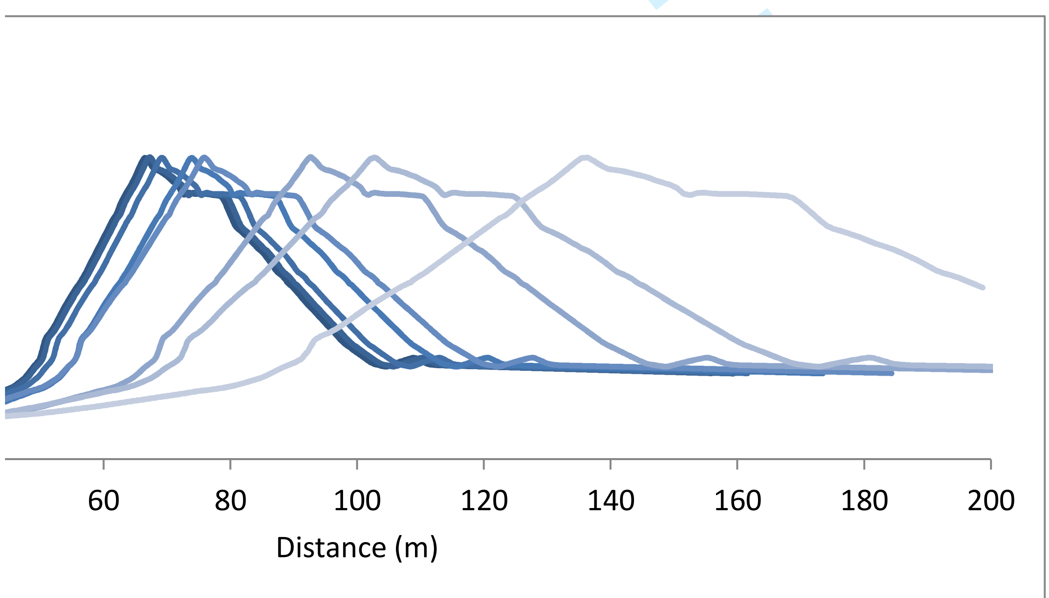
60
80
100
120
140
160
180
200
Distance (m)

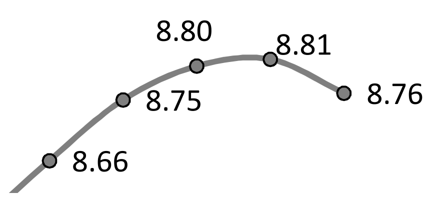
8.80
8.81
8.75
8.76
8.66

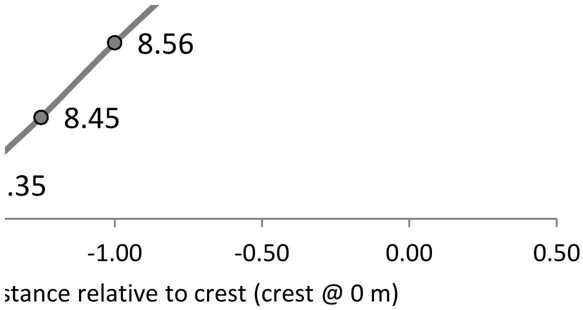
8.56
8.45
.35
-1.00
-0.50
0.00
0.50
stance relative to crest (crest @ 0 m)

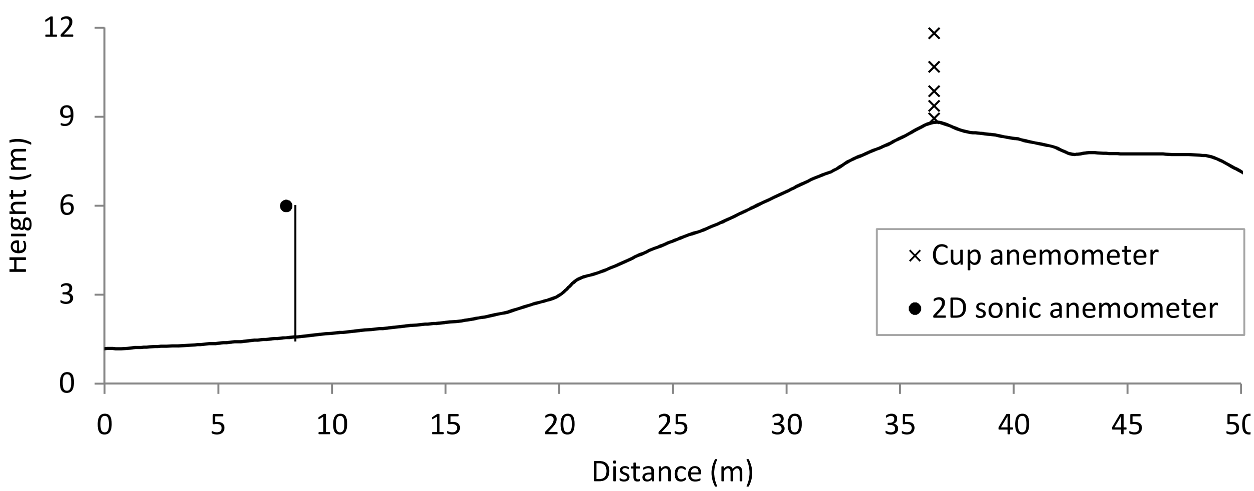

12
9
6
3
0
Height (m)
0
5
10
15
20
25
30
35
40
45
50
Distance (m)
× Cup anemometer
● 2D sonic anemometer

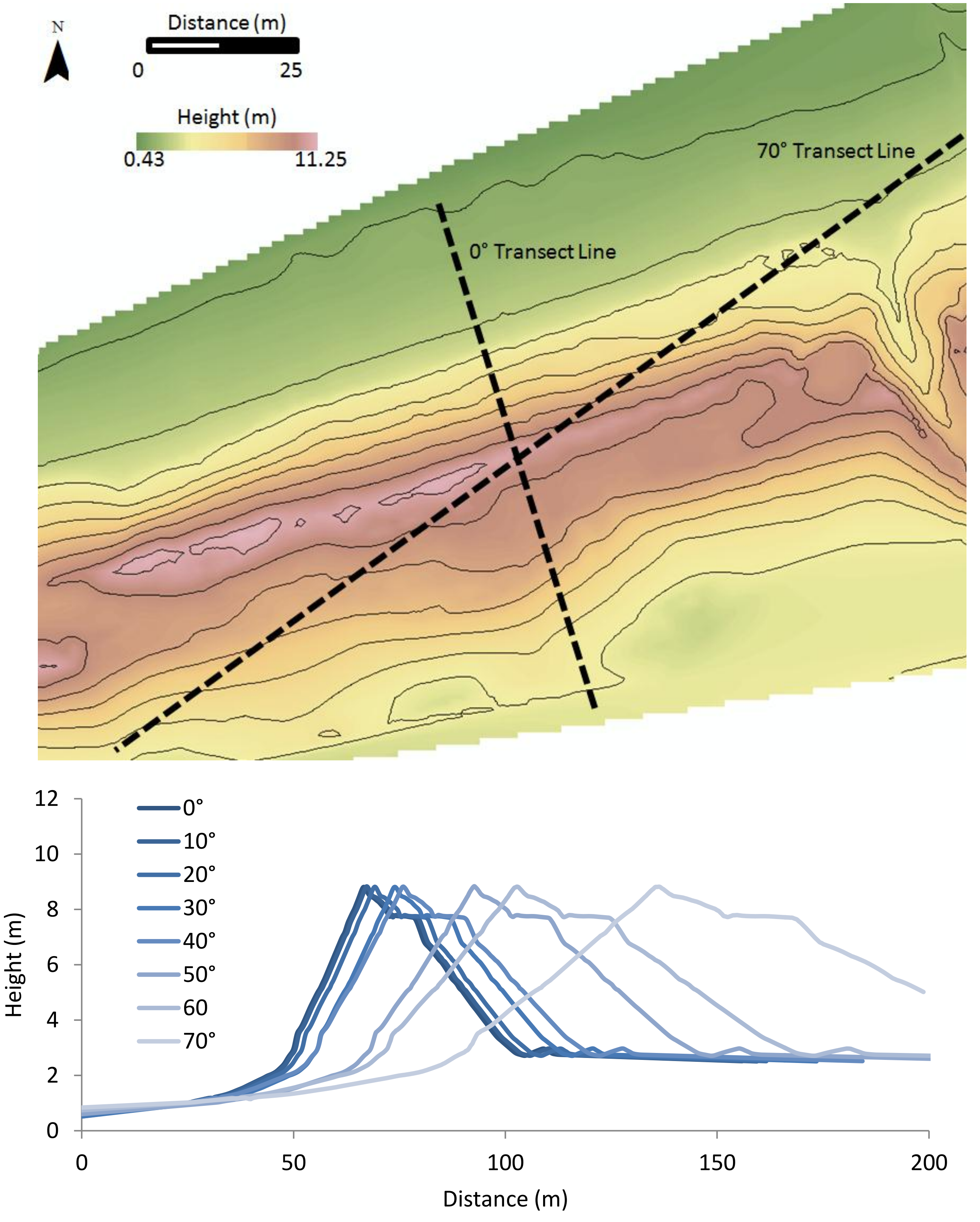
N
Distance (m)
0
25
Height (m)
0.43
11.25
70° Transect Line
0° Transect Line
12
10
8
6
4
2
0
Height (m)
0°
10°
20°
30°
40°
50°
60
70°
0
50
100
150
200
Distance (m)

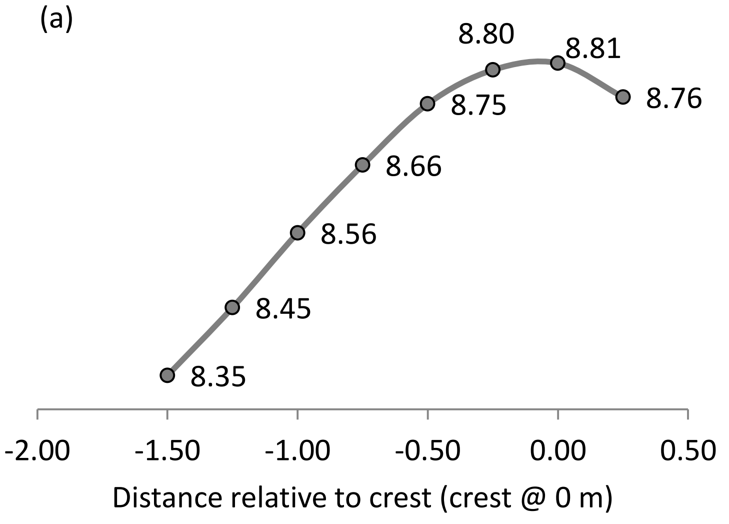
(a)
8.80
8.81
8.76
8.75
8.66
8.56
8.45
8.35
-2.00
-1.50
-1.00
-0.50
0.00
0.50
Distance relative to crest (crest @ 0 m)

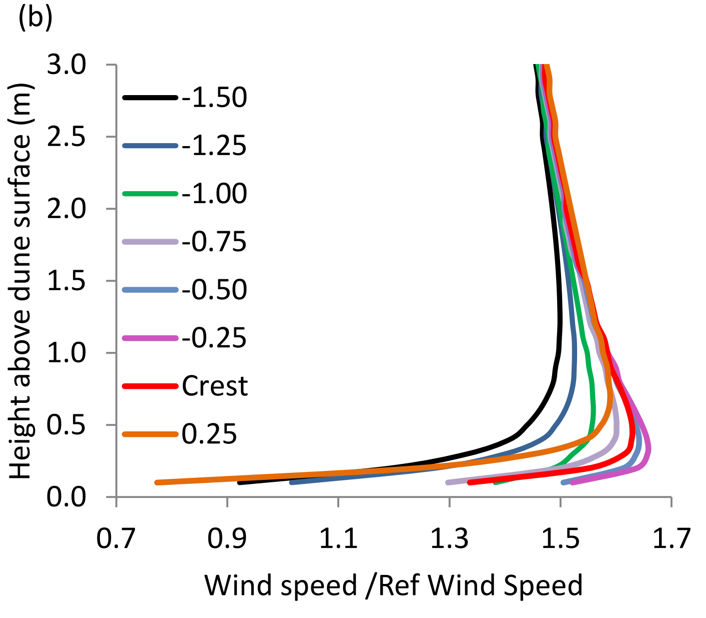
(b)
Height above dune surface (m)
3.0
2.5
2.0
1.5
1.0
0.5
0.0
-1.50
-1.25
-1.00
-0.75
-0.50
-0.25
Crest
0.25
0.7
0.9
1.1
1.3
1.5
1.7
Wind speed /Ref Wind Speed

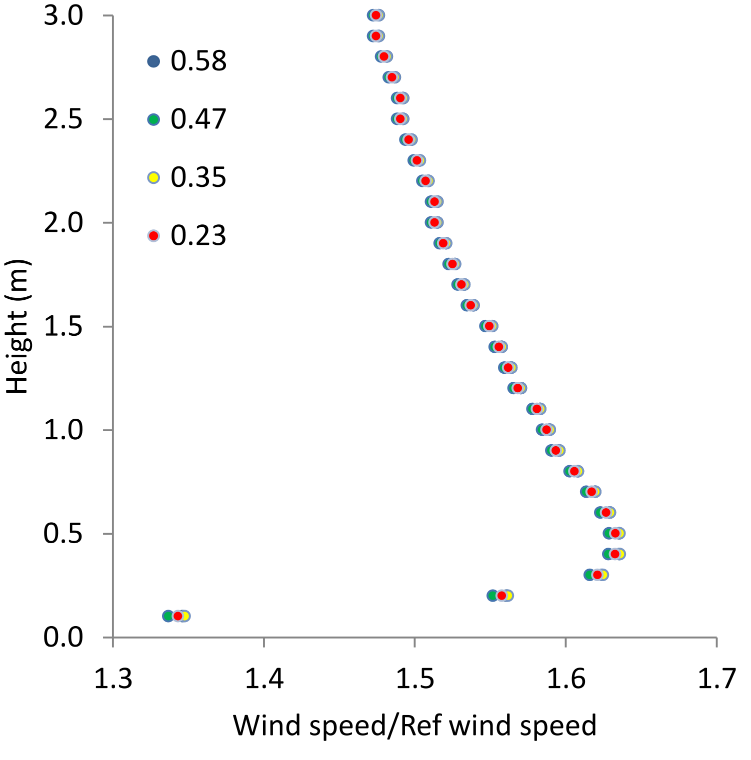
3.0
2.5
2.0
1.5
1.0
0.5
0.0
Height (m)
0.58
0.47
0.35
0.23
1.3
1.4
1.5
1.6
1.7
Wind speed/Ref wind speed

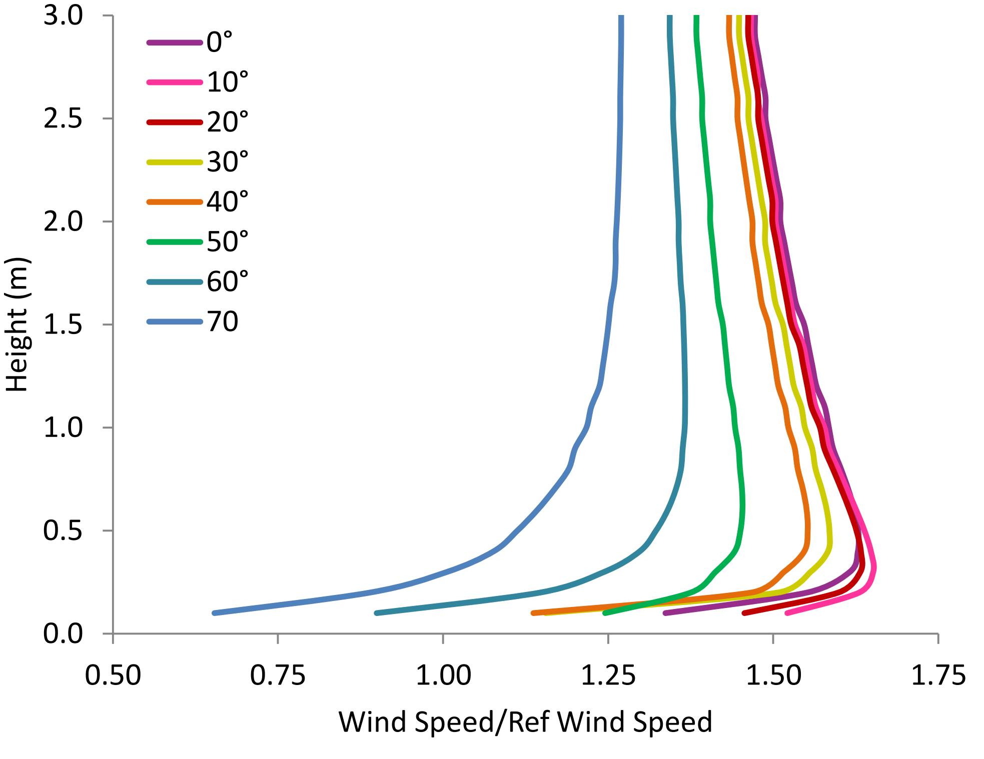

3.0
2.5
2.0
1.5
1.0
0.5
0.0
Height (m)
0.50
0.75
1.00
1.25
1.50
1.75
Wind Speed/Ref Wind Speed
0°
10°
20°
30°
40°
50°
60°
70

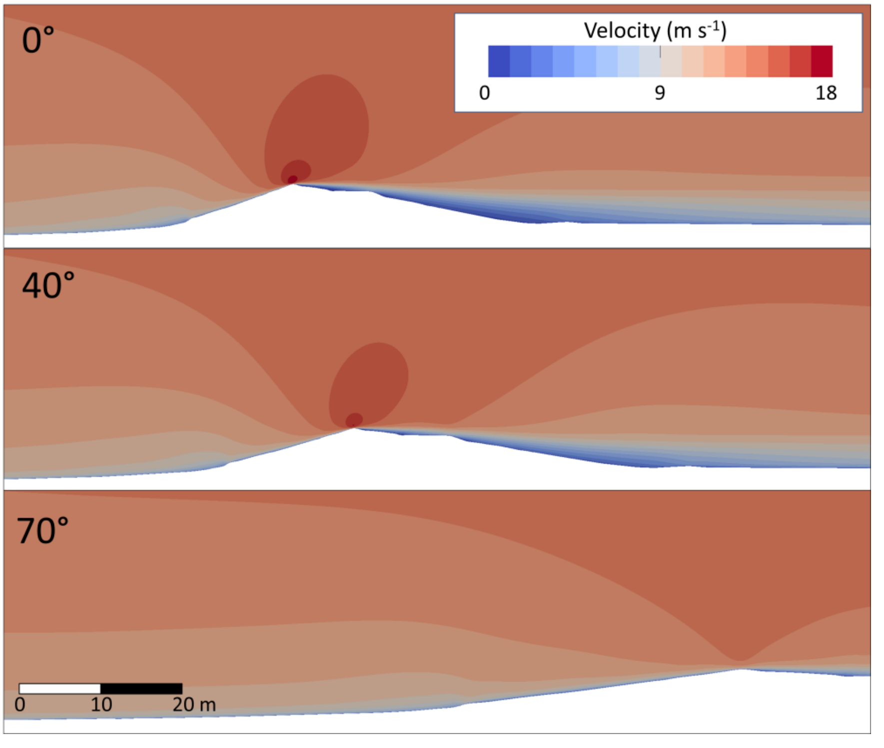
Velocity (m s-1)
0
9
18
0°
40°
70°
0
10
20 m

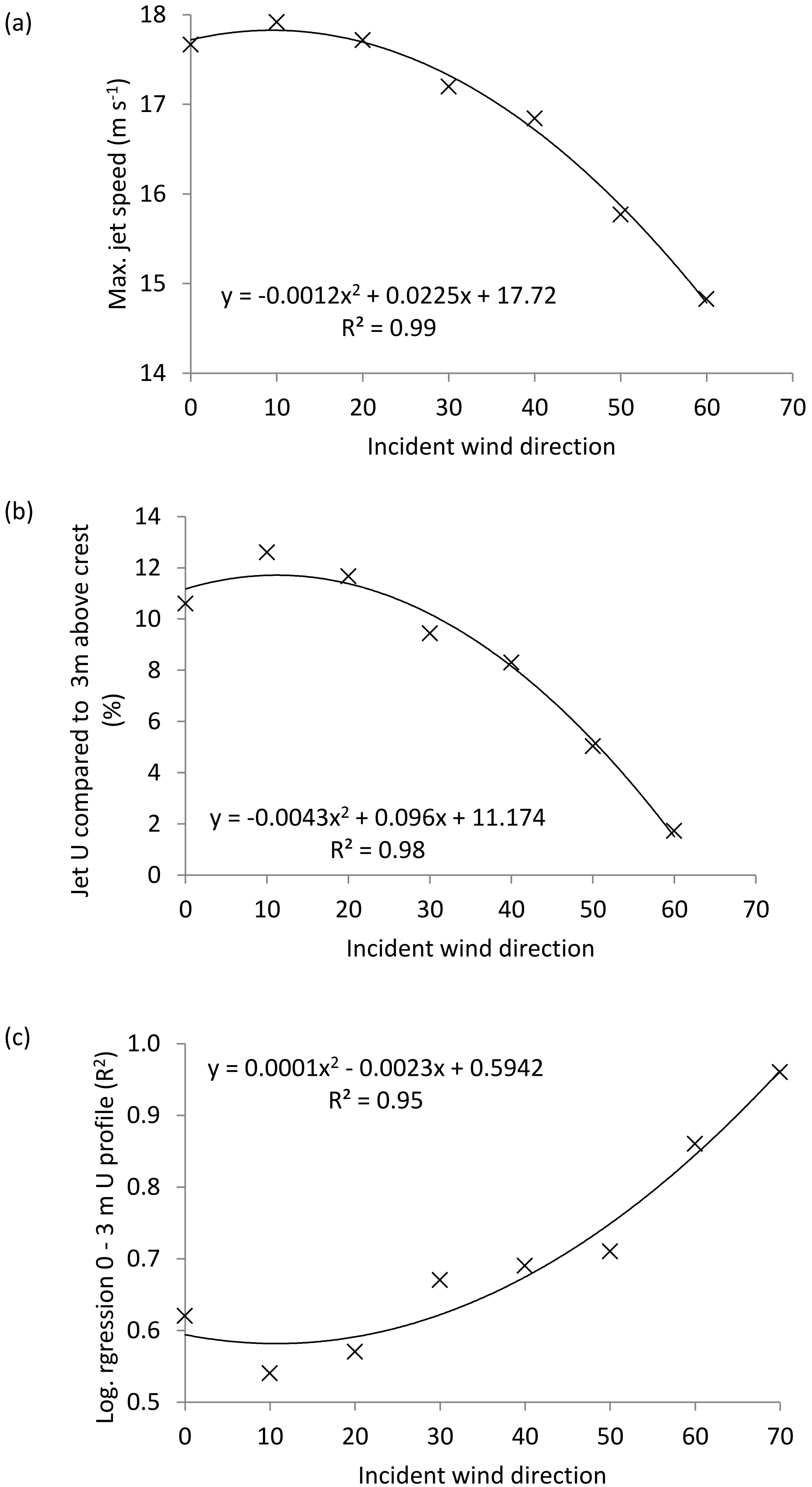
(a)
Max. jet speed (m s-1)
18
17
16
15
14
y = -0.0012x2 + 0.0225x + 17.72
R² = 0.99
0
10
20
30
40
50
60
70
Incident wind direction
(b)
Jet U compared to 3m above crest (%)
14
12
10
8
6
4
2
0
y = -0.0043x2 + 0.096x + 11.174
R² = 0.98
Incident wind direction
(c)
Log. rgression 0 - 3 m U profile (R2)
1.0
0.9
0.8
0.7
0.6
0.5
y = 0.0001x2 - 0.0023x + 0.5942
R² = 0.95
Incident wind direction

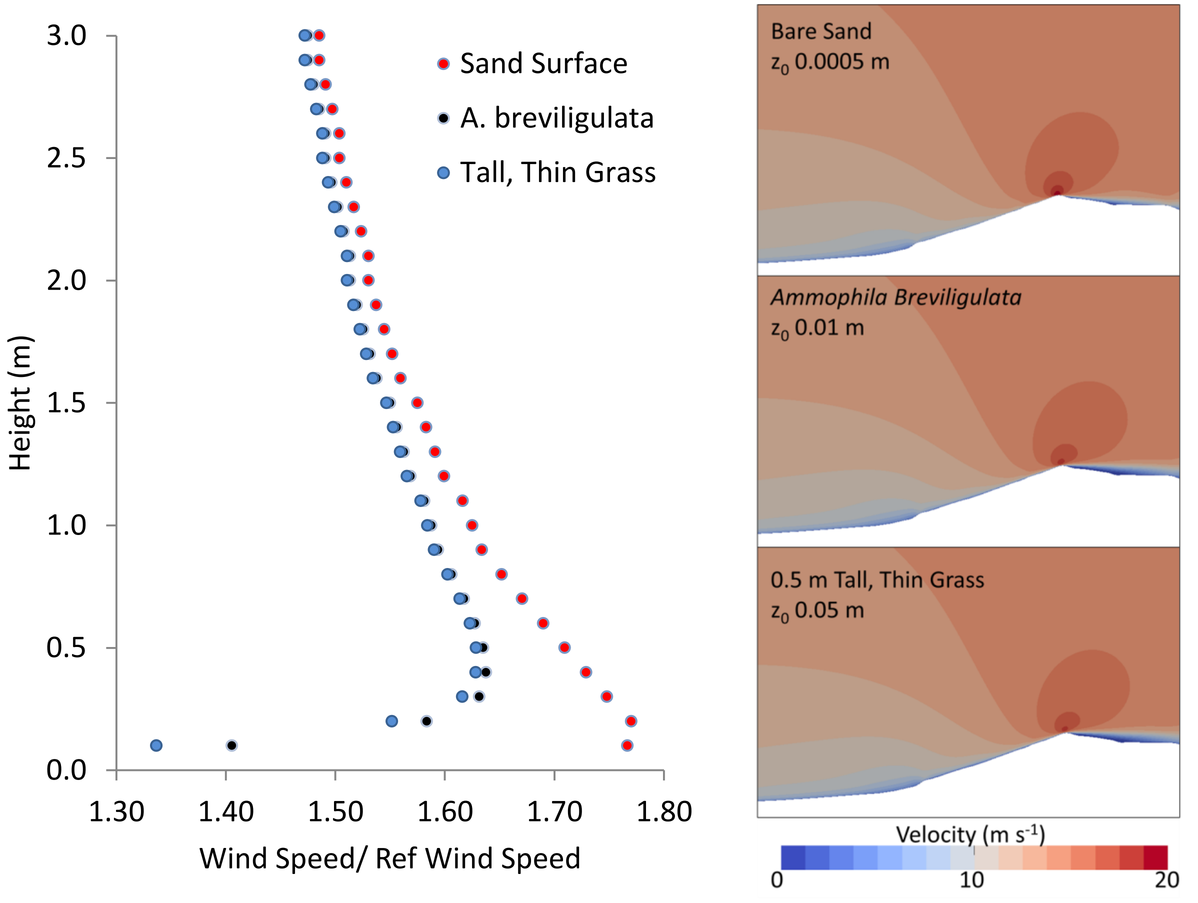
Sand Surface
A. breviligulata
Tall, Thin Grass
Height (m)
Wind Speed/ Ref Wind Speed
3.0
2.5
2.0
1.5
1.0
0.5
0.0
1.30
1.40
1.50
1.60
1.70
1.80
Bare Sand
z_0 0.0005 m
Ammophila Breviligulata
z_0 0.01 m
0.5 m Tall, Thin Grass
z_0 0.05 m
Velocity (m s^{-1})
0
10
20

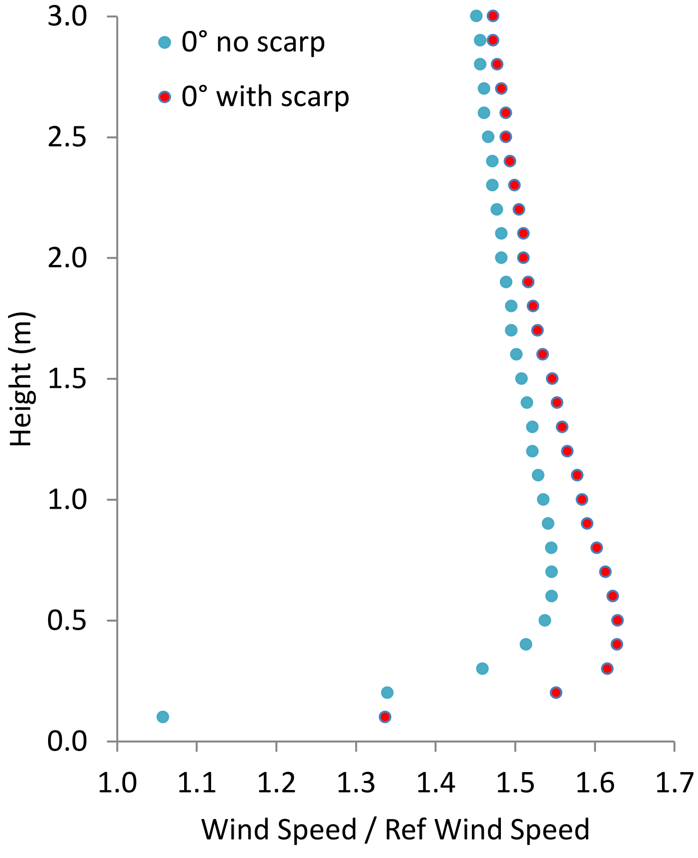

0° no scarp
0° with scarp
Height (m)
3.0
2.5
2.0
1.5
1.0
0.5
0.0
1.0
1.1
1.2
1.3
1.4
1.5
1.6
1.7
Wind Speed / Ref Wind Speed

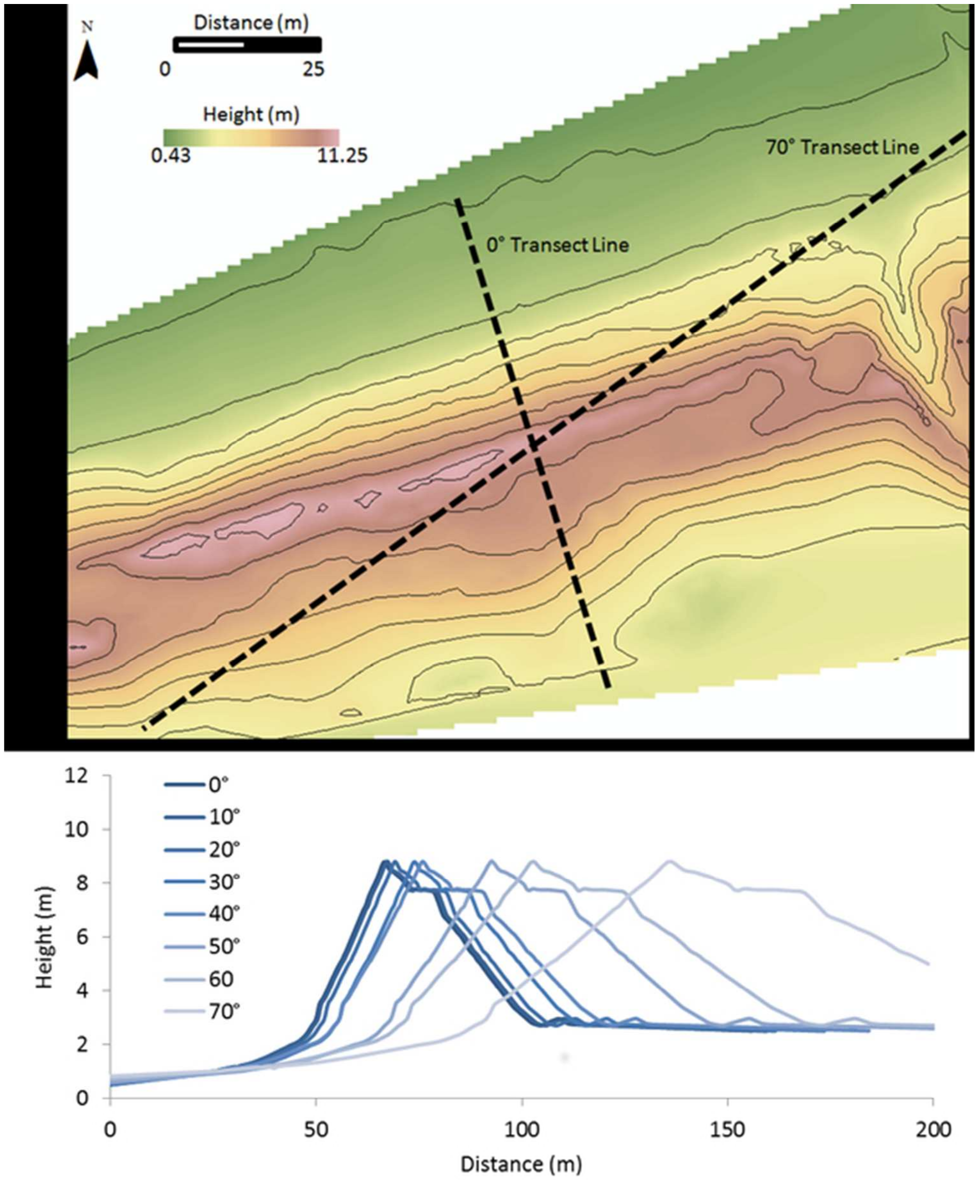

52x65mm (300 x 300 DPI)

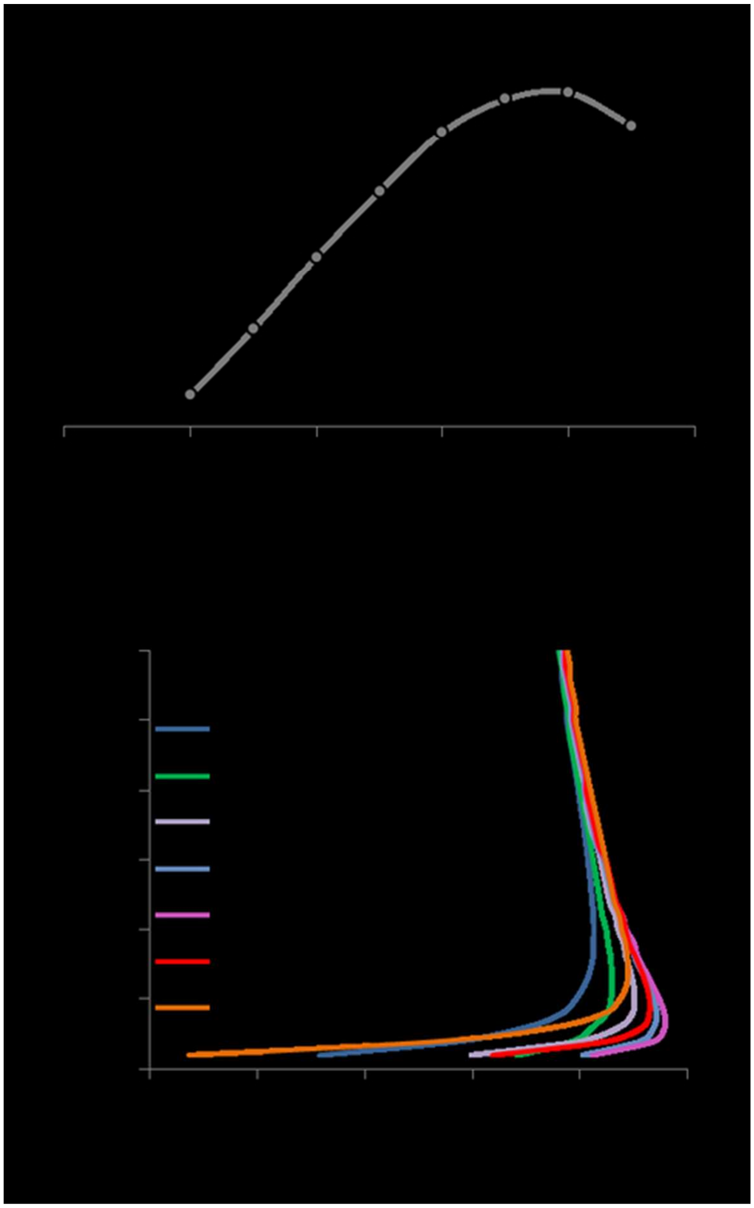

40x65mm (300 x 300 DPI)

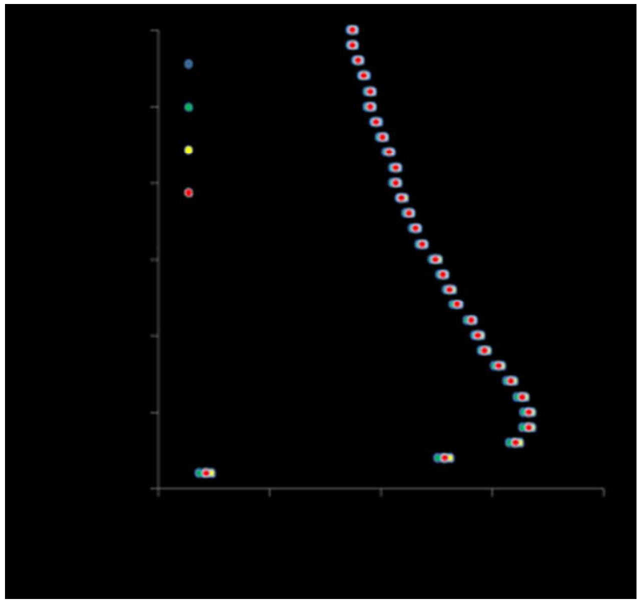

26x25mm (300 x 300 DPI)